DISPERSIVE SHOCK WAVE INTERACTIONS AND TWO-DIMENSIONAL OCEAN-WAVE SOLITON INTERACTIONS

by

DOUGLAS EUGENE BALDWIN

B.S., Colorado School of Mines, 2003

M.S., Colorado School of Mines, 2004

A thesis submitted to the

Faculty of the Graduate School of the

University of Colorado in partial fullfillment

of the requirement for the degree of

Doctor of Philosophy

Department of Applied Mathematics

2013

This dissertation entitled:

Dispersive shock wave interactions and two-dimensional ocean-wave soliton interactions

written by Douglas Eugene Baldwin

has been approved for the Department of Applied Mathematics

Mark J. Ablowitz

Keith Julien

The final copy of this thesis has been examined by the signatories, and we Find that both the content and the form meet acceptable presentation standards Of scholarly work in the above mentioned discipline.

Baldwin, Douglas Eugene (Ph.D., Applied Mathematics)

Dispersive shock wave interactions and two-dimensional ocean-wave soliton interactions

Dissertation directed by Professor Mark J. Ablowitz

Many physical phenomena are understood and modeled with nonlinear partial differential equations (PDEs). Unfortunately, nonlinear PDEs rarely have analytic solutions. But perturbation theory can lead to PDEs that asymptotically approximate the phenomena and have analytic solutions. A special subclass of these nonlinear PDEs have stable localized waves—called solitons—with important applications in engineering and physics. This dissertation looks at two such applications: dispersive shock waves and shallow ocean-wave soliton interactions.

Dispersive shock waves (DSWs) are physically important phenomena that occur in systems dominated by weak dispersion and weak nonlinearity. The Korteweg–de Vries (KdV) equation is the universal model for phenomena with weak dispersion and weak quadratic nonlinearity. Here we show that the long-time asymptotic solution of the KdV equation for general step-like data is a single-phase DSW; this DSW is the 'largest' possible DSW based on the boundary data. We find this asymptotic solution using the inverse scattering transform (IST) and matched-asymptotic expansions; we also compare it with a numerically computed solution. While multi-step data evolve to have multiphase dynamics at intermediate times, these interacting DSWs eventually merge to form a single-phase DSW at large time. We then use IST and matched-asymptotic expansions to find the modified KdV equation's long-time-asymptotic DSW solutions.

Ocean waves are complex and often turbulent. While most ocean-wave interactions are essentially linear, sometimes two or more waves interact in a nonlinear

way. For example, two or more waves can interact and yield waves that are much taller than the sum of the original wave heights. Most of these nonlinear interactions look like an X or a Y or two connected Ys; much less frequently, several lines appear on each side of the interaction region. It was thought that such nonlinear interactions are rare events: they are not. This dissertation reports that such interactions occur every day, close to low tide, on two flat beaches that are about 2,000 km apart. These interactions are related to the analytic, soliton solutions of the Kadomtsev–Petviashvili equation. On a much larger scale, tsunami waves can merge in similar ways.

Dedicated to my parents

Acknowledgements

I wish to acknowledge my adviser Mark J. Ablowitz's invaluable help: thank you for leading me out of all those blind alleys.

I also wish to acknowledge support from

- the National Science Foundation under grant nos. DMS-0604151, DMS-0803074, and DMS-0905779,
- the Air Force Office of Scientific Research under grant no. FA9550-09-1-0250,
- a National Defense Science and Engineering Graduate Fellowship, and
- a Dean's Graduate Student Research Grant.

Contents

List of Figures

Chapter 1

Introduction

Many physical phenomena are understood and modeled with nonlinear partial differential equations (PDEs). Unfortunately, nonlinear PDEs rarely have analytic solutions. But perturbation theory can lead to PDEs that asymptotically approximate the phenomena and lead to analytic understanding. A special subclass of these nonlinear PDEs have stable localized waves—called solitons—with important applications in engineering and physics. This dissertation looks at two such applications: dispersive shock waves and shallow ocean-wave soliton interactions.

J. S. Russell, a naval architect, made the first recorded observation of a solitary wave in the Union Canal, Edinburgh in 1834: a stopping barge set off a solitary wave that went along the canal for one or two miles without changing its speed or its shape (Russell, 1844). He did experiments and found, among other things, that the wave's speed depends on its height; so he concluded that it must be a nonlinear effect. Boussinesq (1877) and Korteweg and de Vries (1895) derived approximate nonlinear equations for shallow water waves. They found both solitary and periodic nonlinear wave solutions to these equations; they also found that the speed is proportional to its amplitude — bigger waves move faster. So Russell's observations were quantitatively confirmed.

Between 1895 and 1960, solitary waves were mostly studied by water wave scientists, mathematicians, and coastal engineers. In the 1960s, applied mathematicians developed robust approximation techniques and found that the Korteweg–de Vries (KdV) equation appears universally when there is weak quadratic nonlinearity and weak dispersion (Ablowitz, 2011). In 1965, Zabusky and Kruskal (1965) found that the solitary waves of the KdV equation have remarkable elastic interaction properties and termed them solitons. Gardner et al. (1967) then developed a method for solving the KdV equation with rapidly decaying initial data; this method has been extended to many other nonlinear equations and is called the inverse scattering transform (IST) (see Ablowitz and Segur, 1981b; Novikov et al., 1984) — such equations are often called integrable.

The IST method is the nonlinear analog of the Fourier transform method: the initial data are transformed into scattering data; this scattering data are evolved in time; and then the solution is recovered from this evolved scattering data. To get the scattering data, the nonlinear PDE is associated with a linear Lax pair, a scattering equation and an evolution equation. When we assume that the scattering equation is isospectral (the eigenvalue doesn't depend on time), then the compatibility condition is the original nonlinear PDE. The scattering equation of the Lax pair transforms the initial data into scattering data. Then the other linear equation of the Lax pair evolves the scattering data. Finally, the solution is recovered using a linear integral equation, the Gel'fand–Levitan–Marchenko (GLM) integral equation, at any time. There are also elegant and powerful asymptotic methods based on Riemann–Hilbert problems for recovering the solution, but using GLM integral equations are sufficient for our purposes. We use the IST method to investigate dispersive shock waves along with the dynamics of slowly varying waves, which is often referred to as Whitham theory, and numerical simulations.

Dispersive shock waves (DSWs) are physically important phenomena that occur

in systems dominated by weak dispersion and weak nonlinearity. The KdV equation is the universal model for phenomena with weak dispersion and weak quadratic nonlinearity. First we investigate the interactions of two DSWs, then a DSW and an expansion or rarefaction wave (RW), and two RWs. The interaction of two DSWs lead to transient two-phase dynamics; this suggests that the multiphase dynamics of general step-like initial data will also be transient. To show that multiphase dynamics are transient for general step-like initial data, we find the long-time asymptotic solution using IST and matched-asymptotic expansions. We find that general step-like data go to a single-phase DSW in the large-time limit for the KdV equation; this DSW's shape is determined by the boundary data and its position by the initial data. We also compare our asymptotic solution with a numerically computed solution.

To investigate the interaction of DSWs and RWs, we evolved the two-step data

$$u(x<0,t=0)=h_0, \quad u(0<x<L,t=0)=h_1, \quad u(x>0,t=0)=h_2$$

and find six canonical cases:

- one is the interaction of two DSWs which exhibit a transient two-phase solution, but evolve to a single phase DSW for large time;
- two tend to a DSW with either a small-amplitude wave train or a finite number of solitons, which can be determined analytically;
- two tend to a RW with either a small-amplitude wave train or a finite number of solitons; and
- one tends to a pure RW.

There is a similar merging of shock waves for classical or viscous shock waves (VSWs), but VSWs neither exhibit multiphase dynamics nor do they form solitons.

The small-amplitude wave train and the transient two-phase dynamics can be understood using Whitham theory. Whitham theory consists of looking for a fully nonlinear single- or multi-phase solution whose parameters (amplitude, wave number, and frequency) are slowly varying with respect to the phase(s) and then deriving new equations for the evolution of the slowly varying wave properties.

Whitham theory alone cannot give the number of solitons because solitons are solitary waves and Whitham theory describes periodic waves. We determine the number, speed, and location of the solitons using IST theory: the solitons correspond to the scattering data's discrete spectra, which are the simple poles of the transmission coefficient. For two-step data, the scattering data can be determined exactly for all time, and so we can determine the exact number and speed of the solitons.

The IST theory for general, step-like initial data is more complicated. First, we need that the initial data decay to the boundary data sufficiently rapidly. If we have sufficiently rapid decay to the boundary data, then we can formulate GLM integral equations to recover the solution from the evolved scattering data. The GLM integral equations for step-like data for the KdV equation were found previously, but we derived them in a different way. The GLM integral equation formulated from x to $+\infty$ has a kernel with three terms: one that depends on the reflection coefficient, one that depends on the transmission coefficient, and one that depends on the simple poles of the transmission coefficient. The simple poles of the transmission coefficient correspond to the solitons that form from the initial data; they are also present for vanishing boundary data. The term that depends on the reflection coefficient leads to a decaying oscillatory structure; similar to that for vanishing boundary data. The term that depends on the transmission coefficient does not have an analogue for vanishing boundary data: it corresponds to the dispersive shock wave and comes from a branch cut in the scattering data. The scattering data for vanishing boundary data do not have a branch cut.

To the DSW's right, we can asymptotically solve this GLM integral equation for

large time. In this large-time limit, we can asymptotically approximate the kernel and then solve the GLM integral equation with a Neumann series. Far to the DSW's right, the reflection-coefficient term in the kernel dominates and gives an exponentially small solution. Near the right-edge of the DSW, the transmission-coefficient term in the kernel dominates and we can again sum the Neumann series; summing the Neumann series gives a soliton-like train at the DSW's front. When our asymptotic approximation becomes disordered, we use the asymptotic form at the DSW's right-edge to suggest a variable change in the KdV equation. Introducing fast and slow variables in this transformed KdV equation gives a multiple-scales perturbation problem; this perturbation problem leads to a slowly varying cnoidal wave solution with three parameters that are determined by three conservation equations. After a variable change, these conservation equations reduce to Whitham's equation for a single-phase DSW. So while multi-step data evolve to have multiphase dynamics at intermediate times, these interacting DSWs eventually merge to form a single-phase DSW at large time. Finally, we use WKB-theory to find the small-amplitude tail left of the DSW.

This IST-matched-asymptotic method is then applied to the modified KdV (mKdV) equation. For the mKdV equation, the GLM integral equations needed to be found; while the scattering data for the KdV equation with step-like data has one branch cut, the scattering data for the mKdV equation typically has two branch cuts — this makes finding the GLM integral equations more complicated. The branch cut structure of the scattering data for the mKdV equation, if we take $\lim_{x\to-\infty} u > \lim_{x\to+\infty} u$, naturally divides into seven cases; of these seven cases, three are dominated by DSWs, three are dominated by RWs, and one is the boundary between these. The matched-asymptotic solution in the long-time limit is found for classes of initial data that are dominated by DSWs. As with the KdV equation, the long-time asymptotic solution is a single-phase DSW in these cases despite multiphase dynamics at intermediate times.

In addition to studying dispersive shock waves, ocean-wave observations were

also carried out. Ocean waves are complex and often turbulent. While most ocean-wave interactions are essentially linear, sometimes two or more waves interact in a nonlinear, but coherent, way; for example, two or more waves can interact and yield waves that are much taller than the sum of the original wave heights. Most of these nonlinear interactions look like an X or a Y or two connected Ys; much less frequently, several lines appear on each side of the interaction region. It was thought that such nonlinear interactions are rare events: they are not. These interactions occur every day, close to low tide, on two flat beaches that are about 2,000 km apart. These interactions are related to the analytic, soliton solutions of the Kadomtsev–Petviashvili equation.

Kadomtsev and Petviashvili (1970) (KP) extended the KdV equation to include transverse effects; this multi-dimensional equation, like the KdV equation, is integrable (Ablowitz and Clarkson, 1991a). Our observations are related to soliton solutions of the KP equation that do not decay at large distances; these interacting, multi-dimensional line-soliton solutions can be found analytically (see Ablowitz and Segur, 1981b). Before our observations, it was thought that such interactions are rare events because there was only one well-known photograph of an interacting line-soliton in the ocean; it was taken in the 1970s in Oregon (see Ablowitz and Segur, 1981b, fig. 4.7b). Since the KP equation has other and more complex line-soliton solutions, which we refer to as X, Y, and H type solutions, M. J. Ablowitz and D.B. sought and found ocean waves with similar behavior at two relatively flat beaches, some 2,000 km apart. Surprisingly, these X, Y, H, and more complex types of line-solitons appear frequently on these shallow water beaches. Such freely propagating, interacting line-solitons are remarkably robust. While these interactions are not stationary, and so only last a few seconds, a casual observer will be able to see them if they know when and where to look. On a much larger scale, tsunami waves can merge in similar ways.

In this dissertation: Chapter 2 discusses the interactions of DSWs and RWs for the KdV equation and was published in *Physical Review E* with M. J. Ablowitz and M.

Hoefer (Ablowitz et al., 2009). Chapter 3 looks at the long-time asymptotics of the KdV equation's solutions for general step-like data using IST theory and matched asymptotics; these results were published with Mark J. Ablowitz in *Physics Letters A* (Ablowitz and Baldwin, 2013b) and *Physical Review E* (Ablowitz and Baldwin, 2013a). Chapter 4 first derives the GLM integral equations for the mKdV equation for general step-like data, which is new, and then looks at the long-time asymptotics for general step-like data with $\lim_{x\to-\infty} q = q_\ell > 0$ and $\lim_{x\to+\infty} q = 0$, which is new and leads to a DSW — these results have not been submitted for publication yet. Chapter 5 discusses our observations of shallow ocean-wave soliton interactions on two flat beaches; these results were published with M. J. Ablowitz in *Physical Review E* (Ablowitz and Baldwin, 2012). Finally, chapter 6 draws some conclusions.

Part I

Dispersive shock wave interactions

Chapter 2

Soliton generation and multiple phases in dispersive shock and rarefaction wave interaction

Many physical processes are dominated by weak dispersion and weak nonlinearity. Shock waves in such processes have been experimentally observed in plasmas (Taylor et al., 1970), fluids (e.g., undular bores) (Smyth and Holloway, 1988; Lighthill, 1978), superfluids (e.g., Bose-Einstein condensates) (Dutton et al., 2001; Simula et al., 2005; Hoefer et al., 2006; Chang et al., 2008), and optics (Wan et al., 2007; Jia et al., 2007; Ghofraniha et al., 2007; Conti et al., 2009). These shock waves are called dispersive shock waves (DSWs) and have yielded novel dynamics and interesting interactions. These dynamics and interactions have only just begun to be studied theoretically (see El and Grimshaw, 2002; Hoefer and Ablowitz, 2007) and there is still much to explore: the first part of this dissertation looks at DSW interactions that are modeled by either the Korteweg–de Vries (KdV) equation or the modified KdV equation, usually in the large-time limit. In this chapter, we characterize the KdV equation's solution for

large-time when the initial condition is

$$u(x,t=0) = \begin{cases} h_0, & x < 0 \\ h_1, & 0 < x < L \\ h_2, & x > L \end{cases}$$

and find six canonical cases: one is the interaction of two DSWs which exhibit a transient two-phase solution, but evolve to a single phase DSW for large time; two tend to a DSW with either a small amplitude wave train or a finite number of solitons, which can be determined analytically; two tend to a rarefaction or expansion wave (RW) with either a small wave train or a finite number of solitons; and, finally, one tends to a pure RW. There is a similar merging of shock waves for classical or viscous shock waves (VSWs), but VSWs neither exhibit multiphase dynamics nor do they form solitons. To better understand this transient multiphase behavior, the KdV equation's long-time asymptotics solution for general, step-like data is explored in the next chapter using the inverse scattering transform (IST) (see Ablowitz and Clarkson, 1991b) and matched-asymptotic expansions.

A version of this chapter was published in *Physical Review E* with Mark J. Ablowitz and Mark Hoefer (Ablowitz et al., 2009).

2.1 Background

Here we consider DSWs which are described by the Korteweg-de Vries (KdV) equation,

$$u_t + uu_x + \varepsilon^2 u_{xxx} = 0, \qquad 0 < \varepsilon \ll 1. \tag{2.1}$$

Individual DSWs are characterized by a soliton train front with an expanding oscillatory wave at its trailing edge; these waves have been well-studied (see Gurevich and

Pitaevskii, 1974; Kamchatnov, 2000; El, 2005) using wave averaging techniques, often referred to as Whitham theory (Whitham, 1965, 1974).

When illustrative, we contrast DSW interaction with classical or viscous shock waves (VSWs), which are dominated by weak *dissipation* and nonlinearity, using Burgers' equation

$$u_t + uu_x - \nu u_{xx} = 0, \qquad 0 < \nu \ll 1. \tag{2.2}$$

The interaction of VSWs is an entire field and has been extensively studied (see Courant and Friedrichs, 1948; Lax, 1973), while little is known about DSW interactions.

In this chapter, we use analytic, asymptotic, and numeric methods to investigate (2.1) and (2.2) using the step-like initial data

$$u(x,0) = u_0(x) = \begin{cases} h_0, & x < 0, \\ h_1, & 0 < x < L, \\ h_2, & x > L, \end{cases} \tag{2.3}$$

where h_0, h_1 and h_2 are distinct, real and non-negative. This gives six canonical cases, which we denote:

$$\begin{aligned} \text{I } (\urcorner\!\llcorner\!\lrcorner)\text{: } h_0 > h_1 > h_2, \qquad & \text{II } (\urcorner\!\lrcorner\!\ulcorner)\text{: } h_0 > h_2 > h_1, \\ \text{III } (\ulcorner\!\urcorner\!\lrcorner)\text{: } h_1 > h_0 > h_2, \qquad & \text{IV } (\llcorner\!\lrcorner\!\ulcorner)\text{: } h_2 > h_0 > h_1, \\ \text{V } (\lrcorner\!\ulcorner\!\llcorner)\text{: } h_1 > h_2 > h_0, \qquad & \text{VI } (\lrcorner\!\ulcorner\!\urcorner)\text{: } h_2 > h_1 > h_0, \end{aligned}$$

where a symbol of the initial step data is shown in parentheses. When convenient, we take h_i to be 0, $0 < h_* < 1$, or 1; we can do this without loss of generality because both (2.1) and (2.2) are Galilean invariant. El and Grimshaw (2002) studied the well (e.g., $h_0 = h_2 = 0 > h_1$) and the box (e.g., $h_0 = h_2 = 0 < h_1$) with vanishing boundaries and constructed the asymptotic solution analytically.

This chapter is organized as follows: First we briefly discuss the methods we will use. Then we discuss each of the six cases: Case I (⌐¬_), where two DSWs interact and exhibit a two-phase region that evolves into a one-phase solution for large time. A DSW with a small amplitude wave train develops in Case II (⌐_⌐). In Case III (¬⌐_), the interaction produces a DSW with a finite number of solitons. Cases IV (¬_⌐), V (_⌐¬), and VI (_⌐⌐) lead to RWs.

2.2 Methods

In this chapter we use Whitham theory, IST theory, and a fourth-order numerical scheme. In this section, we give a very brief discussion of each method.

2.2.1 Whitham theory

One-phase Whitham theory

Whitham theory consists of looking for a fully nonlinear single- or multi-phase solution whose parameters (amplitude, wave number, and frequency) are slowing varying with respect to the phase(s) and then deriving new equations for the evolution of the slowly varying wave properties. The one-phase Whitham equations for (2.1) are

$$\frac{\partial r_i}{\partial t} + v_i(r_1, r_2, r_3)\frac{\partial r_i}{\partial x} = 0, \qquad i = 1, 2, 3, \tag{2.4a}$$

where

$$\begin{aligned} v_1 &= V - \frac{2}{3}(r_2 - r_1)\frac{K(k)}{K(k) - E(k)}, \\ v_2 &= V - \frac{2}{3}(r_2 - r_1)\frac{(1-k^2)K(k)}{E(k) - (1-k^2)K(k)}, \\ v_3 &= V + \frac{2}{3}(r_3 - r_1)\frac{(1-k^2)K(k)}{E(k)}, \end{aligned} \tag{2.4b}$$

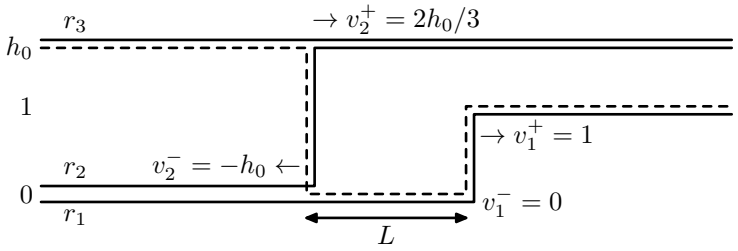

Figure 2.1: The initial data regularization of Case II (⌝⌟⌜) for $h_0 > 1$, $h_1 = 0$ and $h_2 = 1$; the dashed line is the initial condition, $u_0(x)$, and the solid lines are r_1, r_2, and r_3. The figure also gives the speed of the front and back of the DSW and RW at $t = 0$.

$V = (r_1 + r_2 + r_3)/3$, $k^2 = (r_2 - r_1)/(r_3 - r_1)$ (Gurevich and Pitaevskii, 1974). Here, $K(k)$ is the complete elliptic integral of the first kind and $E(k)$ is the complete elliptic integral of the second kind (see, for example, Olver et al., 2010). Then, the asymptotic solution is

$$u_a(x,t) \sim r_1 + r_2 - r_3 + 2(r_3 - r_1)\,\mathrm{dn}^2\left(\theta - \theta_0, k\right),$$

where $\theta_x = \kappa$, $\theta_t = -\omega = -\kappa V$, $\kappa = \sqrt{(r_3 - r_1)/(6\varepsilon^2)}$, and r_i are slowly varying functions of x and t. We can make a global dispersive regularization for the initial value problem (2.1) and (2.3) by choosing appropriate initial data for the r_i that result in a global solution (Hoefer et al., 2006; Kodama, 1999; Biondini and Kodama, 2006). A global dispersive regularization of Case II (⌝⌟⌜) is shown in figure 2.1; the r_i are taken to be nondecreasing, $r_i(x,0) < r_{i+1}(x,0)$ and $\bar{u}_a(x,0) = u(x,0)$ for all $x \in \mathbb{R}$.

In order to study the interaction we evolve the r_i numerically. A simple and effective method for evolving the r_i is to discretize the initial data regularization along the dependent variable, r_i, and then compute the shift in x of each data point using (2.4). Figure 2.2 compares a numerically evolved Whitham approximation with direct numerics for Case II (⌝⌟⌜); the Whitham approximation does not capture the small quasi-periodic modulations in the tail.

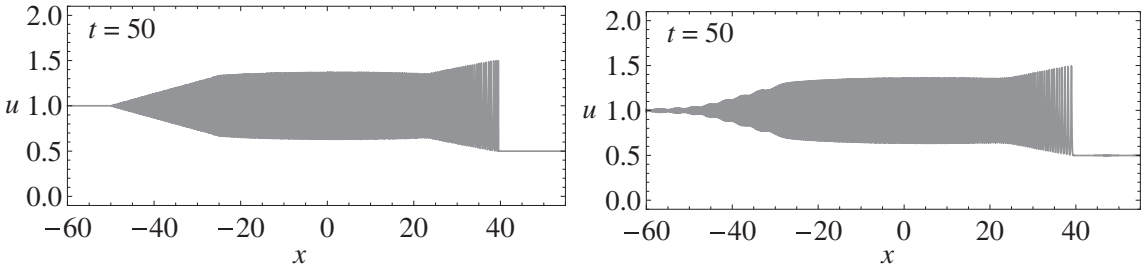

(a) (b)

Figure 2.2: Plot (a) shows the Whitham approximation and (b) direct numerics of the solution of (2.1) for Case II (⌐└⌐) with the same initial condition as in figure 2.4.

Multiphase Whitham theory

Multiphase Whitham theory is more complicated than one-phase Whitham theory and dates back to 1970 (Ablowitz and Benny, 1970); multiphase Whitham equations were developed for the KdV equation in (Flaschka et al., 1980). The interaction of two DSWs from certain step-like data was recently analyzed in (Hoefer and Ablowitz, 2007) for the nonlinear Schrödinger equation. The one- and two-phase regions and the averaged solution in Case I (⌐└┘) are found by numerically evolving the two-phase Whitham equations for the KdV (see Levermore, 1988),

$$\frac{\partial r_i}{\partial t} + v_i(r_1, \ldots, r_5)\frac{\partial r_i}{\partial x} = 0, \qquad i = 1, 2, \ldots, 5, \tag{2.5}$$

where $v_i = (2r_i^3 - \chi r_i^2 - \beta_1 r_i - \beta_2)/(r_i^2 - \alpha_1 r_i - \alpha_2)$, $\chi = \sum_{j=1}^{5} r_j$, and α_1, α_2, β_1 and β_2 are solutions of

$$\begin{bmatrix} I_1^1 & I_1^0 \\ I_2^1 & I_2^0 \end{bmatrix} \begin{bmatrix} \alpha_1 \\ \alpha_2 \end{bmatrix} = \begin{bmatrix} I_1^2 \\ I_2^2 \end{bmatrix}, \quad \begin{bmatrix} I_1^1 & I_1^0 \\ I_2^1 & I_2^0 \end{bmatrix} \begin{bmatrix} \beta_1 \\ \beta_2 \end{bmatrix} = \begin{bmatrix} 2I_1^3 - \chi I_1^2 \\ 2I_2^3 - \chi I_2^2 \end{bmatrix},$$

with

$$I_j^k = \int_{r_{2j-1}}^{r_{2j}} \frac{\xi^k}{\sqrt{\prod_{i=1}^{5}(\xi - r_i)}}\, d\xi. \tag{2.6}$$

2.2.2 IST theory

In this chapter, we use IST theory to determine the number of solitons that correspond to the time-independent number of zeroes of $a(k)$ (which is the number of poles of the reflection coefficient $R \equiv b(k)/a(k)$) in the upper half k-plane. Associated with (2.1), the data $a(k)$ is defined by

$$\phi(x;k) \equiv a(k)\bar{\psi}(x;k) + b(k)\psi(x;k),$$
$$\bar{\phi}(x;k) \equiv \bar{a}(k)\psi(x;k) + \bar{b}(k)\bar{\psi}(x;k),$$

corresponding to the eigenfunctions,

$$\phi(x;k) \sim e^{-ik_0x}, \qquad \bar{\phi}(x;k) \sim e^{ik_0x}, \qquad \text{as } x \to -\infty,$$
$$\psi(x;k) \sim e^{ik_2x}, \qquad \bar{\psi}(x;k) \sim e^{-ik_2x}, \qquad \text{as } x \to +\infty,$$

which satisfy the Schrödinger scattering problem,

$$w_{xx} + w\{u/6 + k^2\}/\varepsilon^2 = 0. \tag{2.7}$$

The solution of (2.7), at $t = 0$, is

$$w(x) = \begin{cases} Ae^{ik_0x} + Be^{-ik_0x}, & x < 0, \\ Ce^{ik_1x} + De^{-ik_1x}, & 0 < x < L, \\ Ee^{ik_2x} + Fe^{-ik_2x}, & x > L, \end{cases}$$

where $k_0 = \sqrt{h_0/6 + k^2}/\varepsilon$, $k_1 = \sqrt{h_1/6 + k^2}/\varepsilon$, and $k_2 = \sqrt{h_2/6 + k^2}/\varepsilon$. The eigenfunctions, ϕ, $\bar{\phi}$, ψ and $\bar{\psi}$ are determined by requiring that w and w' are continuous across $x = 0$ and $x = L$. Indeed, ϕ is found by taking $A = 0$ and $B = 1$ and then solving

for C, D, $E \equiv b(k)$, $F \equiv a(k)$, so that

$$a(k) = e^{ik_2 L}\frac{k_0+k_2}{2k_2}\left\{\cos(k_1 L) - i\frac{k_1^2+k_0k_2}{k_1(k_0+k_2)}\sin(k_1 L)\right\}.$$

Note that the branch cut in $a(k)$ corresponds to the DSW in Case III (⌐¬) and the RW in Case V (¬⌐). Since $e^{ik_2 L}(k_0+k_2)/(2k_2) \neq 0$, the zeroes of $a(k)$ occur when $\tan(k_1 L) = ik_1(k_0+k_2)/(k_1^2+k_0k_2)$. It can be shown that the zeroes of $a(k)$ are purely imaginary; thus, we let $k = i\kappa$ (where $\kappa \in \mathbb{R}$ and $\kappa > 0$).

2.2.3 Numerical scheme

We numerically solve (2.1) and (2.2) using an adaptation of the modified exponential-time-differencing fourth-order Runge-Kutta (ETDRK4) method (see Cox and Matthews, 2002; Kassam and Trefethen, 2005). We use this (sophisticated) numerical method because (2.1) is stiff and standard numerical methods require the time step to be $O(\varepsilon^3)$, while for ETDRK4 the time step need only be $O(\varepsilon)$ (since the period in the oscillatory tail is $O(\varepsilon)$). When this numerical scheme was used to evolve a multi-soliton initial condition where the analytic solution was known, it was accurate to more than six decimal digits when compared with the analytic solution. We do not expect or require such accuracy in our numerically computed DSW solutions, since we are interested in the solution's qualitative rather than quantitative behavior. A significant source of error when numerically computing DSW solutions is the small-amplitude linear-wave tail to the DSW's left: while small-amplitude, it is much larger than the machine-epsilon and we apply reflectionless dampening at the computational domain's left edge to keep it from affecting the DSW's shock-front. To mitigate the effects of dampening this small-amplitude linear-wave tail near the computational domain's edge, we use a domain that is four times the DSW region's width. Most of our calculations only took a few minutes on a desktop computer, and we typically used five times the Nyquist rate of

the linear-wave tail and a time step of 10^{-3} to 10^{-4}.

For spectral accuracy in space when using the ETDRK4 method, the initial data must be both smooth and periodic. Therefore, we differentiate (2.1) with respect to x and define $v \equiv u_x$ to get

$$v_t + (uv)_x + \varepsilon^2 v_{xxx} = 0.$$

Transforming to Fourier space gives

$$\hat{v}_t = i\varepsilon^2 k^3 \hat{v} - ik\widehat{uv} \equiv \mathbf{L}\hat{v} + \mathbf{N}(\hat{v}, t),$$

where we define $(\mathbf{L}\hat{v})(k) \equiv i\varepsilon^2 k^3 \hat{v}$ and

$$\mathbf{N}(\hat{v}, t) = \mathbf{N}(\hat{v}) \equiv -ik\mathcal{F}\left\{\left[h_0 + \int_{-\infty}^{x} \mathcal{F}^{-1}(\hat{v})dx'\right]\mathcal{F}^{-1}(\hat{v})\right\}.$$

It is important that the integral in $\mathbf{N}$ is computed using a spectrally accurate method. Moreover, we approximate the initial step data with the analytic function

$$v(x,0) = \frac{h_2 - h_1}{2w}\operatorname{sech}^2[(x-L)/w] + \frac{h_1 - h_0}{2w}\operatorname{sech}^2(x/w),$$

where w is small. See (Cox and Matthews, 2002; Kassam and Trefethen, 2005) for details about how this $\mathbf{L}$ and $\mathbf{N}$ are used to numerically compute the solution of (2.1).

2.3 The dispersive shock wave cases

2.3.1 Two-phase DSW case

In Case I (⌐¬_), two one-phase DSWs form and propagate to the right (see fig. 2.3a). When the shock front of the left DSW reaches the expanding oscillatory tail of the right DSW, they interact and form a quasi-periodic two-phase solution (see fig. 2.3b). The

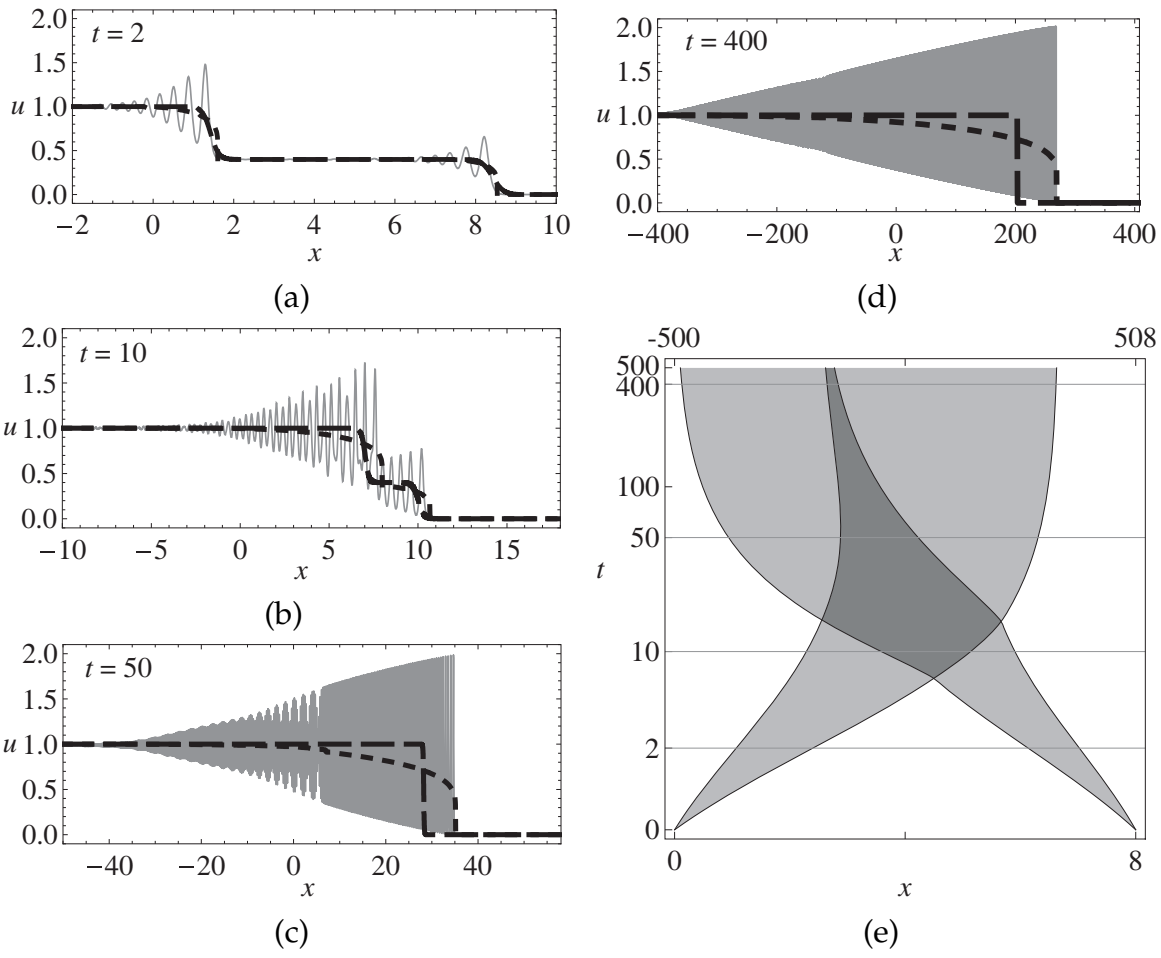

Figure 2.3: Plots (a)–(d) show the numerically computed solution of (2.1) and (e) the boundary of the one- (light gray) and two-phase (dark gray) regions computed using Whitham theory. The averaged solution, $\bar{u}$, is computed using Whitham averaging (see Levermore, 1988) and shown as dotted lines in (a)–(d); the solution of (2.2) is shown as dashed lines in (a)–(d). In all plots, $\varepsilon^2 = 0.001$, $h_0 = 1$, $h_1 = 0.4$, $h_2 = 0$ and $L = 8$. The vertical axis in (e) is log-time and the horizontal axis is $-t \leq x \leq t + 8$ (and matches the domain in (a)–(d)).

shock front of the left DSW subsequently overtakes the shock front of the right DSW and forms a one-phase solution to the right of the two-phase region (see fig. 2.3c). To the left of the two-phase solution, an essentially one-phase DSW tail emerges (see fig. 2.3c); although the tail is weakly modulated by a quasi-periodic wave, its behavior is essentially one-phase. For large time, the two-phase region closes and a one-phase DSW remains (see fig. 2.3d–e); Whitham theory indicates that the amplitude of the two-phase modulations decrease with time and result in an effectively one-phase DSW. This closing of the two phase region is suggested by the rigorous (Whitham theory) results in Grava and Tian (2002), though the authors studied smooth initial data. The computation of the boundaries of the one- and two-phase regions using multiphase Whitham theory is discussed later in this chapter.

Although the (initial) shock front speed is different for DSWs and VSWs ($2h_0/3$ and $h_0/2$, respectively), the averaged DSWs are similar in behavior to VSWs (see fig. 2.3a–d); in both, two shock waves merge to form a single shock wave.

2.3.2 DSW with oscillatory tail

For Case II (⌝⌟⌜), a large DSW forms on the left and a small RW forms on the right (see fig. 2.4a). The front of the DSW then interacts with the trailing edge of the RW; the interaction decreases the DSW's speed and height (see fig. 2.4b). The front of the DSW is faster than the front of the RW and overtakes it (see fig. 2.4c). The size of the interaction region continues to expand with a DSW emerging in front with a small amplitude wave train behind, whose amplitude is proportional to $t^{-1/2}$ (see fig. 2.4d). As in Case I (⌝⌞⌟), the averaged DSW and the VSW (see fig. 2.4) both tend to a single DSW (VSW) once the front of the DSW (VSW) passes the front of the RW.

We can use the one-phase Whitham equations to characterize the interaction of the DSW and RW in Case II (⌝⌟⌜) (figs. 2.1 and 2.2). Both direct numerics and the Whitham approximation agree and show that for large enough time, the amplitude of

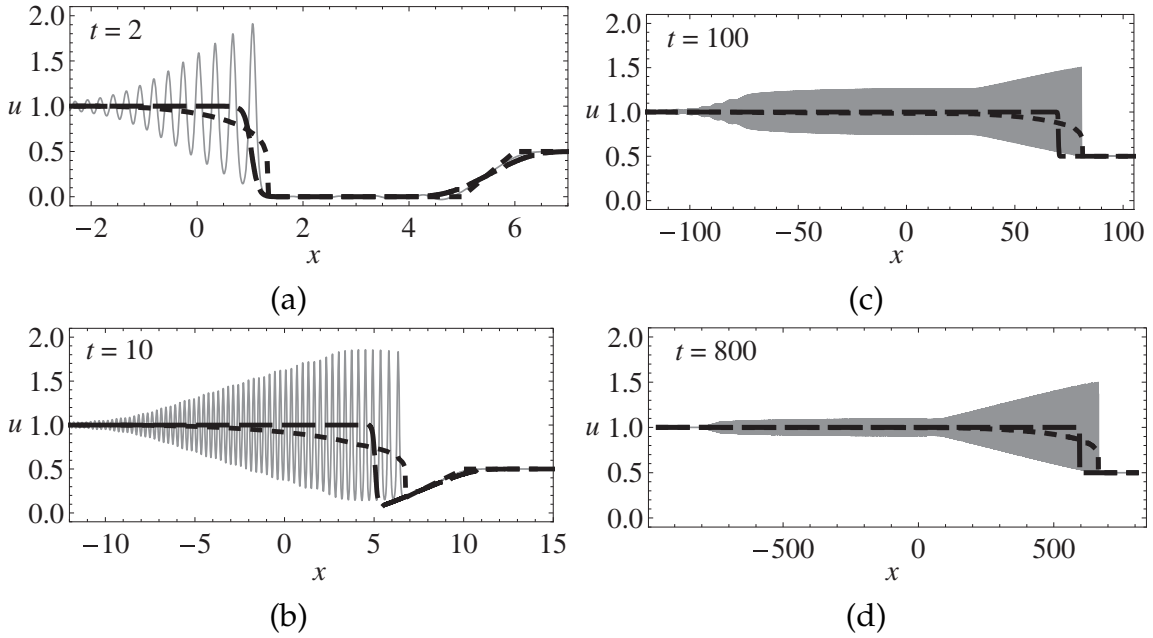

Figure 2.4: Plots of the numerical and averaged Whitham solutions of (2.1) for Case II (⌝⌟⌜) where $\varepsilon^2 = 0.001$, $h_0 = 1$, $h_1 = 0$, $h_2 = 0.5$ and $L = 5$.

the tail in Cases II (⌝⌟⌜) is proportional to $t^{-1/2}$; this is typical of a uniform linear wave train when the total energy remains constant (see Whitham, 1965) and was observed by El and Grimshaw (2002) in the context of a well with vanishing boundaries (e.g., $h_0 = h_2 = 0 > h_1$).

2.3.3 Using IST to find the number of solitons

In Case III (⌜⌝⌟), a small RW forms on the left and a large DSW forms on the right. The front of the RW then interacts with the tail of the DSW and reduces the amplitude of the waves—essentially cutting off the top of the box. Since the front speed of the RW is less than the front speed of the initial DSW, a finite number of solitons can escape the interaction (see fig. 2.5). These solitons have no analogue in the VSW solution of Case III (⌜⌝⌟). We can compute the precise number, height, and speed of these escaping solitons for all time using IST theory.

For Case III (⌜⌝⌟), where $h_1 = 1 > h_0 = h_* $ and $h_2 = 0$, the zeroes of $a(i\kappa)$ occur

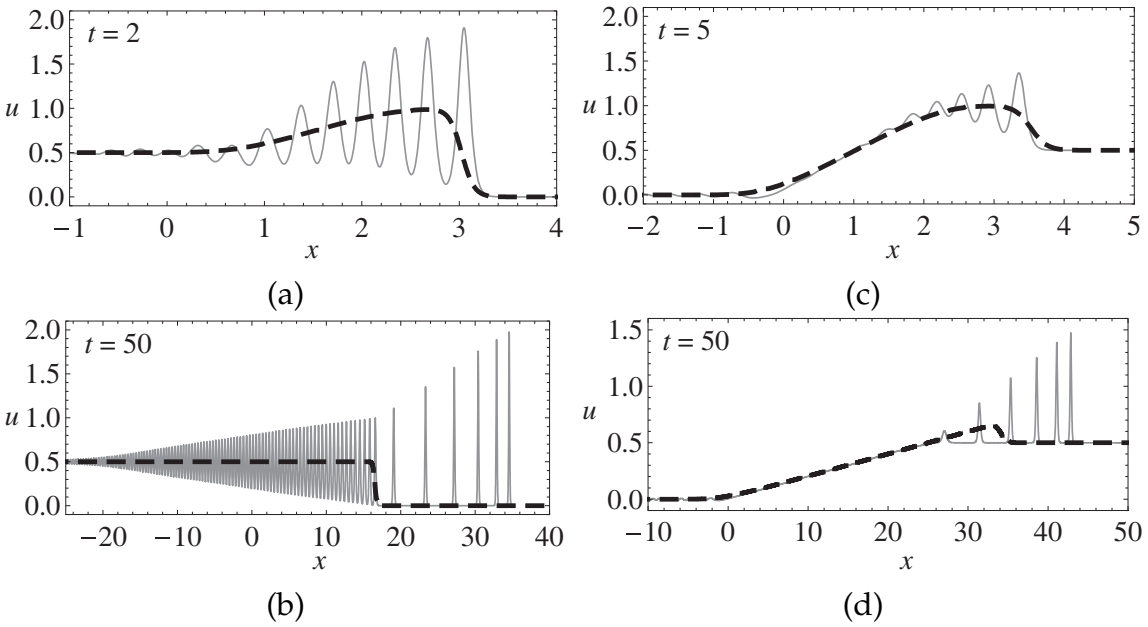

Figure 2.5: Plots of Cases (a) & (b) III (⌐⌐) with $h_0 = 0.5$, $h_1 = 1$, $h_2 = 0$ and (c) & (d) V (⌐⌐) with $h_0 = 0$, $h_1 = 1$, $h_2 = 0.5$, where $\varepsilon^2 = 0.001$ and $L = 2$. There are six solitons in both cases, see (2.8).

when

$$\tan\left(\sqrt{1/6-\kappa^2}L/\varepsilon\right) = \frac{\sqrt{1/6-\kappa^2}\left(\sqrt{\kappa^2-h_*/6}+\kappa\right)}{1/6-\kappa^2-\kappa\sqrt{\kappa^2-h_*/6}}. \tag{2.8}$$

If we denote the zeros determined using (2.8) as $\kappa_1, \kappa_2, \ldots, \kappa_N$, then the corresponding solitions in Case III (⌐⌐) have height $12\kappa_i^2$ and speed $4\kappa_i^2$. The number of periods for $\sqrt{h_*/6} \le \kappa \le \sqrt{1/6}$ of the RHS of (2.8), $L\sqrt{1-h_*}/(\varepsilon\pi\sqrt{6})$, is an estimate of the number of solitons. The number, height and speed of the solitons determined using (2.8) exactly corresponds to the solitons observed using direct numerics (for various values of h_*, L and ε).

2.4 The expansion wave cases

In Case IV (¬⌐), a small DSW forms on the left and a large RW forms on the right (see fig. 2.6a). As in Case II (⌐¬), the front of the DSW interacts with the trailing edge of the RW and decreases the DSW's amplitude and speed. Unlike Case II (⌐¬), the front of the

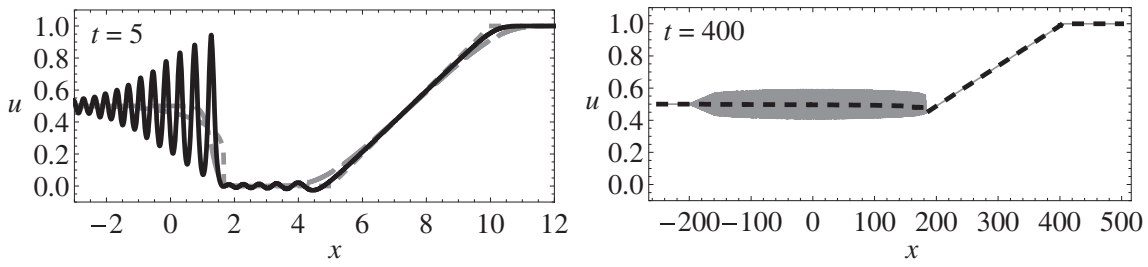

(a) (b)

Figure 2.6: Plots of the solution of (2.1) for Case IV (⌐⌐) where $\varepsilon^2 = 0.001$, $h_0 = 0.5$, $h_1 = 0$, $h_2 = 1$ and $L = 5$.

DSW does not overtake the front of the RW. The DSW becomes a small amplitude tail on the left of the RW and decreases in amplitude proportional to $t^{-1/2}$ (see fig. 2.6b).

For Case V (⌐¬), a large RW forms on the left and a small DSW forms on the right; the front of the RW interacts with the tail of the DSW and results in a RW and a finite number of solitons. The solitons corresponds to the number of zeroes of (2.8) where where $h_0 = 0$ and $h_1 = 1 > h_2 = h_*$.

In Case VI (⌐⌐), two rarefaction waves form; the small amplitude oscillatory tail (see for instance the RW in fig. 2.6a) of the right RW interacts with the front of left RW; the tail of the right and left RWs then interact to form a small amplitude, modulated, quasi-periodic tail; this modulation decreases with time and Case VI (⌐⌐) tends to a pure RW for large time.

2.5 Conclusion

For large time Case I (¬¬) and II (¬⌐) go to a single DSW, while Case IV (⌐⌐) and VI (⌐⌐) go to a single RW; this is consistent with VSW theory. However, unlike VSW theory, Case III (⌐¬) and V (⌐¬) form a finite number of solitons in addition to the DSW or RW, respectively. Moreover, unlike VSW theory, Case I (¬¬) exhibits a transient two-phase region and Case II (¬⌐) and IV (⌐⌐) have a small amplitude tail that decays at a rate proportional to $t^{-1/2}$.

Chapter 3

Dispersive shock wave interactions and asymptotics — the Korteweg–de Vries equation

Dispersive shock waves (DSWs) have been seen in plasmas (Taylor et al., 1970), fluids (e.g., undular bores) (Smyth and Holloway, 1988; Lighthill, 1978), superfluids (Dutton et al., 2001; Simula et al., 2005; Hoefer et al., 2006; Chang et al., 2008), and optics (Wan et al., 2007; Jia et al., 2007; Ghofraniha et al., 2007; Conti et al., 2009). DSWs occur when weak nonlinearity and weak dispersion dominate the physics and there is step-like data. For many weakly dispersive, weakly nonlinear systems, the Korteweg–de Vries (KdV) equation is the leading-order asymptotic equation (Ablowitz, 2011). Here we find the long-time-asymptotic behavior of the KdV equation with general, step-like data using the inverse scattering transform (IST) and matched-asymptotic expansions. We show that general, step-like data go to a single-phase DSW for the KdV equation in the long-time, fixed-dispersion limit. Our results show that while multi-step data evolve to have multiphase dynamics at intermediate times, these interacting DSWs eventually merge to form a single-phase DSW: each sub-step in well-separated, multi-step data

forms its own DSW (fig. 3.1a); these DSWs then interact and develop multiphase dynamics at intermediate times (figs. 3.1b and 3.1c); and, in the long-time limit, these DSWs merge to form a single-phase DSW (fig. 3.1d). The boundary data determine this single-phase DSW's form; the initial data determine its position. This is similar to interacting viscous shock waves (VSW), where only the single, largest possible VSW remains after a long time (Ablowitz and Baldwin, 2013a). Grava and Tian (2002) and Ablowitz et al. (2009) suggested this merging of multiphase to single-phase by their two-phase to one-phase results — they used Whitham theory, which applies to slowly varying periodic wavetrains. We apply this IST and matched-asymptotic procedure to another important, nonlinear integrable system — the modified KdV (mKdV) equation — for general, step-like data in chapter 4; we anticipate that this procedure will also be applied to the nonlinear Schrödinger (NLS) equation.

A version of this chapter was published with Mark J. Ablowitz in *Physics Letters A* (Ablowitz and Baldwin, 2013b) and *Physical Review E* (Ablowitz and Baldwin, 2013a).

3.1 Introduction

A shock wave is an abrupt change in the medium that propagates; it often moves faster than the local wave speed. If dissipation and dispersion are ignored, then breaking occurs in finite time; since this is not usually physical, most models include weak dissipation or weak dispersion. When dissipation dominates dispersion, a VSW forms that is smooth but changes rapidly from one value to another; VSWs form in compressible gases and other classical fluids. When dispersion dominates dissipation, a DSW forms that is smooth but has an additional modulated wavetrain that allows transitions from one value to another; DSWs form in cold plasmas, superfluids (like Bose–Einstein condensates), and nonlinear electromagnetic waves in suitable optical materials.

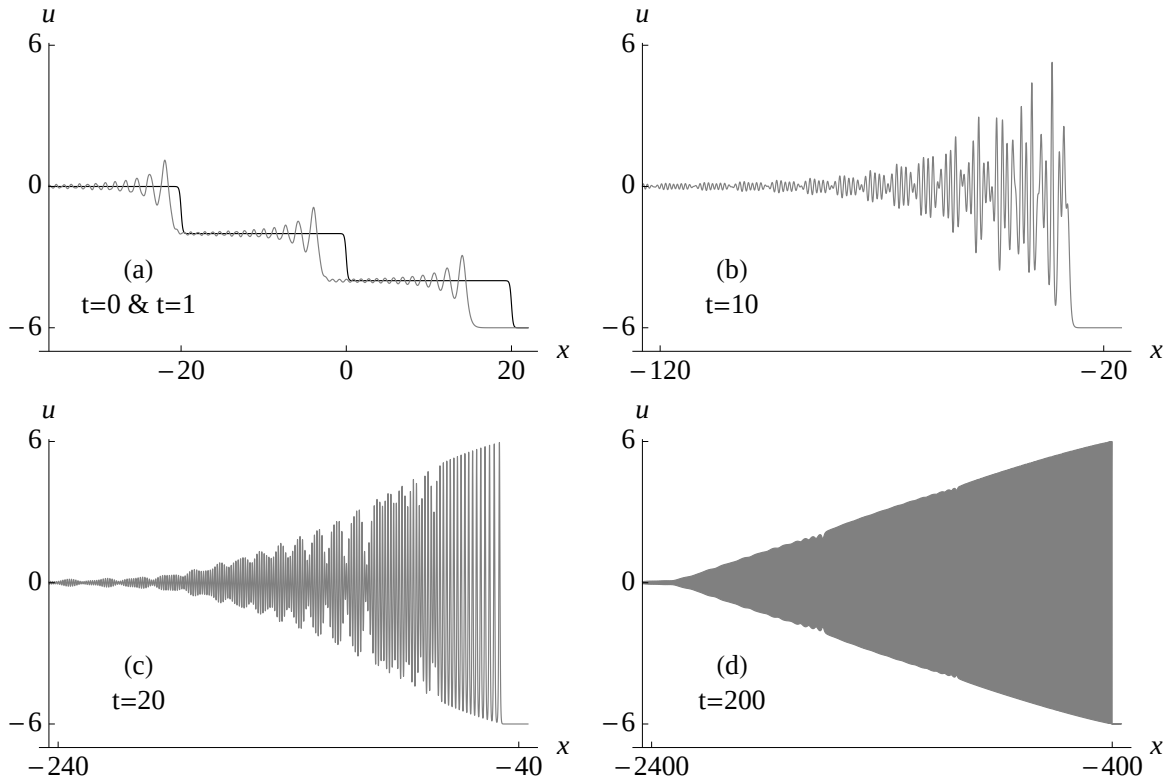

Figure 3.1: Numerical simulations (using the scheme in (Ablowitz et al., 2009)) of three well-separated steps (at $t = 0$, with $\varepsilon^2 = 0.1$ and $c = 1$). Here we see: (a) three single-phase DSWs at $t = 1$; (b) and (c) strong interaction and multiphase dynamics; and (d) eventual merging to form a single-phase DSW.

The KdV and NLS equations are universal models: they are the leading-order asymptotic equations for a wide class of physical phenomena (see Ablowitz, 2011). The KdV equation is the leading-order asymptotic equation for systems with weak dispersion and weak, quadratic nonlinearity; it has important applications in shallow water waves, plasmas, lattice dynamics, and elasticity among others. The NLS equation is the leading-order asymptotic equation for quasi-monochromatic, weakly nonlinear systems; it has important applications in nonlinear optics, deep water waves, Bose–Einstein condensates, and magnetic-spin waves among others.

Here we consider the DSWs that the KdV equation describe; the KdV equation, written in dimensionless form, is

$$u_t + uu_x + \varepsilon^2 u_{xxx} = 0, \tag{3.1}$$

where subscripts denote partial derivatives. We will consider the boundary conditions

$$\lim_{x\to-\infty} u = 0 \quad \text{and} \quad \lim_{x\to+\infty} u = -6c^2. \tag{3.2}$$

Here, ε and c are real, positive constants, and ε corresponds to the size of the regularizing dispersive effects. We require that u goes to these limits sufficiently rapidly; so we assume that

$$\int_{-\infty}^{\infty} \left| u(x,t) + 6c^2 H(x) \right| (1 + |x|^n)\, \mathrm{d}x < \infty, \tag{3.3}$$

for $n = 1, 2, \ldots$ and where $H(x > 0) = 1$ and $H(x \leq 0) = 0$ is the Heaviside function. Since the KdV equation is Galilean invariant, we can transform any constant boundary conditions where $\lim_{x\to-\infty} u > \lim_{x\to+\infty} u$ to (3.2). We use the IST method (see Ablowitz et al., 1974; Deift and Trubowitz, 1979; Ablowitz and Segur, 1981a; Ablowitz and Clarkson, 1991b) and matched-asymptotic expansions (see Ablowitz and Segur, 1977; Segur and Ablowitz, 1981) to find a long-time-asymptotic solution.

3.1.1 IST method

The IST method is the nonlinear analog of the Fourier transform method: we transform the initial data into scattering data; we evolve this scattering data in time; and we then recover the solution from the evolved scattering data. First we associate the nonlinear partial differential equation (PDE) with a (linear) Lax pair. Then we use the scattering equation of the Lax pair to transform the initial data into scattering data. Then we use the other linear equation of the Lax pair to evolve the scattering data. Finally, we use a linear integral equation, the Gel'fand–Levitan–Marchenko (GLM) integral equation, to recover the solution at any time.

Elegant and powerful asymptotic methods based on Riemann–Hilbert problems can also be used to recover the solution at any time. They have been used to find the asymptotic solution for large time with vanishing boundary conditions (see Deift and Zhou, 1993; Deift et al., 1997); see (Buckingham and Venakides, 2007) for a NLS shock example. For our purposes, the GLM integral equation and our matched-asymptotic method is sufficient.

Hruslov (1976) and then Cohen (1984) and Cohen and Kappeler (1985) studied the IST theory for step-like initial data; we state the IST results that we need to find our asymptotic solution in section 3.2. Hruslov (1976), based on (Buslaev and Fomin, 1962), presented the GLM integral equations and investigated the soliton train at the DSW's right. Cohen (1984) and Cohen and Kappeler (1985), using the methods of (Deift and Trubowitz, 1979; Buslaev and Fomin, 1962), rigorously studied some scattering-data properties, rederived the GLM integral equations, and analyzed existence for piecewise-constant initial conditions. We derive the GLM integral equations in a different way in section 3.2.3.

3.1.2 Long-time asymptotic solution

Our long-time-asymptotic-analysis results are new. We find the long-time-asymptotic solution for non-vanishing boundary conditions (where $c \neq 0$) by using and suitably modifying the methods in (Ablowitz and Segur, 1977; Segur and Ablowitz, 1981). Ablowitz and Segur (1977) and Segur and Ablowitz (1981) developed these IST and matched-asymptotic methods to find the long-time-asymptotic solution for vanishing boundary conditions (where $c = 0$). We show, for large time, that $u(x,t)$ goes to a single-phase DSW that has three basic regions (fig. 3.2):

- an exponentially small solution for $x \geq O(t)$ (region A in fig. 3.2a);
- a slowly varying cnoidal-wave solution for $|x| \leq O(t)$ (region B in fig. 3.2a), which has a soliton train on its right and an oscillatory wave on its left; and
- a slowly varying oscillatory solution for $(-x) \geq O(t)$ (region C in fig. 3.2a).

3.1.3 Comparison with vanishing boundary conditions

The long-time-asymptotic solution of the KdV equation when $c \neq 0$ is quite different from when $c = 0$ (see fig. 3.2): the strong nonlinearity when $c = 0$ is only over $|x| \leq O[t^{1/3}(\log t)^{2/3}]$, but when $c \neq 0$ it is over $|x| \leq O(t)$. Ablowitz and Segur (1977) showed that the long-time-asymptotic solution when $c = 0$ has four basic regions:

- an exponentially small solution for $x \geq O(t)$ (region I in fig. 3.2b);
- a growing similarity solution for $|x| \leq O(t^{1/3})$ (region II in fig. 3.2b), which is related to Painlevé II's solution;
- a collisionless-shock solution for $(-x) = O[t^{1/3}(\log t)^{2/3}]$ (region III in fig. 3.2b), which is a slowly varying cnoidal wave analogous to a DSW; and
- an oscillatory similarity solution for $(-x) \geq O(t)$ (region IV in fig. 3.2b), which has the same form as region C in figure 3.2a.

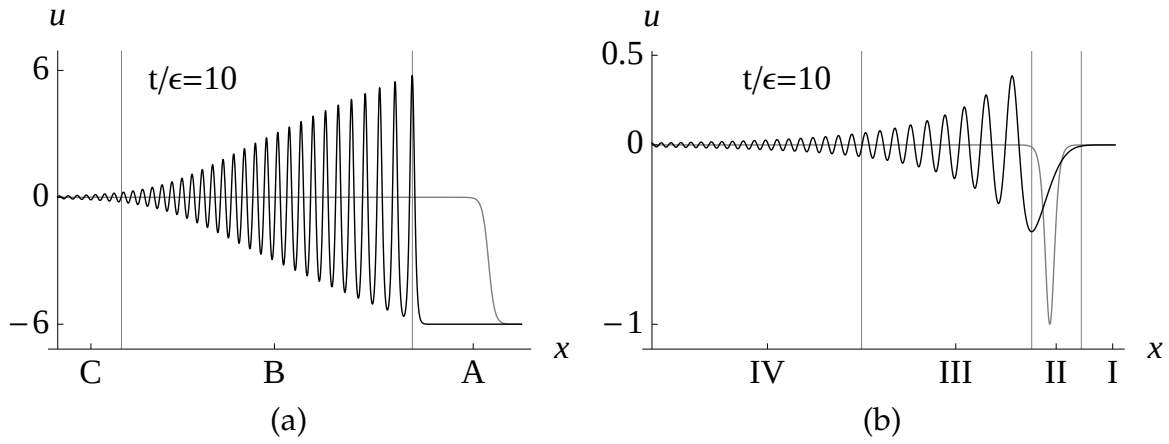

Figure 3.2: Numerically computed solutions of the KdV equation for the initial conditions shown in gray. (a) Non-vanishing boundary conditions, $c \neq 0$. This solution has three basic regions: rapid decay in region A, right of the DSW; strong nonlinearity of width $O(t)$ in region B; and an oscillating tail in region C, left of the DSW. (b) A vanishing boundary conditions, $c = 0$. Here, the solution that has four basic regions (see Ablowitz and Segur, 1977). Region III has strong nonlinearity with height $O[(\log t)^{1/2} t^{-2/3}]$ and width $O[t^{1/3}(\log t)^{2/3}]$.

The amplitude for all these regions when $c = 0$ decays in time at least as $O(t^{-1/2})$; the amplitude when $c \neq 0$ is $O(1)$.

3.1.4 Comparison with the linear problem

The long-time-asymptotic solution of the KdV equation is also quite different from the linear problem ($\tilde{u}_t + \varepsilon^2 \tilde{u}_{xxx} = 0$). Both problems have three basic regions; but the middle regions have different widths: the linear KdV equation has a middle region with strong nonlinearity over $|x| \leq O(t^{1/3})$, while the nonlinear KdV equation has a middle region (region B in fig. 3.2a) over $|x| \leq O(t)$. The linear problem's solution in the middle region is

$$\tilde{u}(x,t) \sim U_0(0) \int_{-\infty}^{\eta} \mathrm{Ai}(\eta')\, \mathrm{d}\eta', \qquad \eta = \frac{x}{(3\varepsilon^2 t)^{1/3}},$$

where $\mathrm{Ai}(x)$ is the Airy function and U_0 is the Fourier transform of $\tilde{u}_x(x,0)$.

3.1.5 Comparison with viscous shock waves

In the long-time limit, both DSWs and VSWs merge to form a single shock wave. For shock waves where dissipation dominates dispersion, Burgers' equation is the leading-order asymptotic equation. Burgers' equation, in normalized form, is

$$w_t + ww_x - \nu w_{xx} = 0, \tag{3.4}$$

where $\nu > 0$ is a measure of dissipation and is typically small. If we take initial data that go rapidly to the boundary conditions $\lim_{x\to-\infty} w(x,t) = 0$ and $\lim_{x\to+\infty} w(x,t) = -h^2$, then the long-time-asymptotic solution is

$$w(x,t) \sim -\frac{h^2}{2}\left\{1 + \tanh\left[\frac{h^2}{4\nu}\left(x - x_0 + \frac{h^2}{2}t\right)\right]\right\},$$

where x_0 is a real constant that depends on the initial data — see below for details. Thus, for both Burgers' and the KdV equation, well-separated step data go to a single shock wave in the long-time limit: the boundary conditions determine its form, and the initial data determine its location. But unlike with Burgers' equation, the solution of the KdV equation can also have a finite number of solitons, which move to the DSW's right in the long-time limit.

To see this, we can transform (3.4) into the heat equation ($\phi_t = \nu\phi_{xx}$) using the Cole–Hopf transformation,

$$w = -2\nu\frac{\phi_x}{\phi}. \tag{3.5}$$

For simplicity, we take

$$w(x,t=0) = w_0(x) = \begin{cases} 0, & x \le x_\ell \\ f(x), & x_\ell \le x \le x_r \\ -h^2, & x \ge x_r \end{cases},$$

where h is real and f is bounded. So, from (3.5),

$$\phi(x, t=0) = \phi_0(x) = \exp\left(\frac{-1}{2\nu}\int_{-\infty}^{x} w_0(x')\,\mathrm{d}x'\right)$$
$$= \begin{cases} 1, & x \le x_\ell \\ \exp\left[-1/(2\nu)\int_{x_\ell}^{x} f(x')\,\mathrm{d}x'\right], & x_\ell \le x \le x_r \\ \exp\left[h^2(x-\tilde{x}_0)/(2\nu)\right], & x \ge x_r \end{cases},$$

where $\tilde{x}_0 \equiv \int_{x_\ell}^{x_r} f(x')/h^2\,\mathrm{d}x'$. Solving the heat equation gives

$$\phi(x,t) = \frac{1}{\sqrt{4\pi\nu t}}\left(\int_{-\infty}^{x_\ell} + \int_{x_\ell}^{x_r} + \int_{x_r}^{\infty}\right)\phi_0(x')e^{-(x-x')^2/(4\nu t)}\,dx' \equiv I_1 + I_2 + I_3.$$

And, in the long-time limit,

$$I_1 \sim \frac{1}{2}, \quad I_2 \to 0, \quad \text{and} \quad I_3 \sim \exp\left[\frac{h^2}{2\nu}\left(x - \tilde{x}_0 + \frac{h^2}{2}t\right)\right].$$

Therefore, from (3.5),

$$w(x,t) \sim -\frac{h^2}{2}\left\{1 + \tanh\left[\frac{h^2}{4\nu}\left(x - x_0 + \frac{h^2}{2}t\right)\right]\right\},$$

where $x_0 \equiv \tilde{x}_0 + (2\nu/h^2)\log 2$.

3.1.6 Relation to previous work

Single-step data, such as a Heaviside function, have been studied extensively (see Gurevich and Pitaevskii, 1974; Kamchatnov, 2000; El and Grimshaw, 2002; El, 2005) using wave-averaging techniques, which are often called Whitham theory (Whitham, 1965, 1974). Whitham theory averages over suitable, slowly varying periodic waves to get reduced equations; these reduced equations are a quasi-linear, first-order, hyperbolic

system that describes how the periodic wave's parameters slowly evolve.

The evolution of multiphase DSWs to a single-phase DSW was investigated in the two-phase case by Grava and Tian (2002) using Whitham theory in the zero-dispersion limit ($\varepsilon \to 0$) for finite time and in chapter 2 using numerical and asymptotic methods in the fixed-dispersion, long-time limit. Both zero-dispersion and long-time are important, but different, limits. Here we study the long-time limit with fixed dispersion. By using the IST method, we find the asymptotic solution directly: we can investigate general, step-like initial data and DSW interactions without having to find the solution at intermediate times. On the other hand, Whitham theory in the zero-dispersion limit requires that the solution is found at intermediate times through a nonlinear hyperbolic system.

The IST method also gives the behavior to the left and right of the DSW; it's nontrivial to get such behavior from the Whitham theory results. For example, it's useful to compare (Grava and Klein, 2008) with (Ablowitz and Segur, 1977; Segur and Ablowitz, 1981) to see how each matches the solution (for vanishing boundary conditions) in region III (fig. 3.2b) to that in region IV. Also compare (Claeys and Grava, 2010) with (Ablowitz and Segur, 1977) to see how each matches the solution in region II to that in region III.

The key result for the fixed-dispersion, long-time limit is that DSWs from well-separated multi-step data merge to form a single-phase DSW.

To find the KdV equation's long-time-asymptotic solution: We give the IST results that we need in section 3.2. Then we asymptotically solve the linear GLM integral equation to find the exponentially small solution right of the DSW (sec. 3.3.1); use matched asymptotics to get the DSW (sec. 3.3.2), which is a slowly varying cnoidal wave that has a soliton train on its right and an oscillatory tail on its left; and find the small, decaying, oscillatory solution left of the DSW (sec. 3.3.3) that matches into the DSW.

Finally, we draw some conclusions (sec. 3.4).

3.2 IST and the GLM integral equations

The IST method first associates a Lax pair with the nonlinear PDE. Using the Lax pair's scattering equation, we transform the initial data into the scattering data. We then evolve the scattering data in time using the associated linear equation. The GLM integral equation, a linear integral equation, provides the inversion at any time, and so we can recover the solution at any time.

3.2.1 Direct problem

The Lax pair associated with (3.1) is

$$Lv = v_{xx} + \frac{u}{6\varepsilon^2} v = -\frac{\lambda^2}{\varepsilon^2} v, \tag{3.6a}$$

$$v_t = Mv = \left(\frac{u_x}{6} + \gamma\right) v + \left(4\lambda^2 - \frac{u}{3}\right) v_x, \tag{3.6b}$$

where λ is the spectral parameter and γ is a constant. This linear pair is compatible ($v_{xxt} = v_{txx}$) when $u = u(x,t)$ satisfies (3.1) and λ is isospectral ($\partial\lambda/\partial t = 0$). That is, requiring nontrivial eigenfunctions gives Lax's equation

$$L_t + [L, M] = L_t + LM - ML = \frac{1}{6\varepsilon^2}\left(u_t + uu_x + \varepsilon^2 u_{xxx}\right) = 0.$$

We use (3.2) to define the eigenfunctions that satisfy (3.6a) (for notational simplicity, we often suppress the time dependence):

$$\phi(x;\lambda) \sim \exp(-i\lambda x/\varepsilon), \qquad \bar{\phi}(x;\lambda) \sim \exp(i\lambda x/\varepsilon), \quad \text{as } x \to -\infty \tag{3.7a}$$

$$\psi(x;\lambda_r) \sim \exp(i\lambda_r x/\varepsilon), \qquad \bar{\psi}(x;\lambda_r) \sim \exp(-i\lambda_r x/\varepsilon), \quad \text{as } x \to +\infty, \tag{3.7b}$$

where $\lambda_r \equiv \sqrt{\lambda^2 - c^2}$. From (3.7), we also have the identities

$$\phi(x;-\lambda) = \bar{\phi}(x;\lambda) \quad \text{and} \quad \psi(x;-\lambda_r) = \bar{\psi}(x;\lambda_r).$$

We take the branch cut of λ_r to be $\lambda \in [-c, c]$, and the branch cut of λ to be $\lambda_r \in [-ic, ic]$; then $\mathrm{Im}(\lambda_r) \gtrless 0$ when $\mathrm{Im}(\lambda) \gtrless 0$. This branch cut is one of the main differences between vanishing and non-vanishing boundary conditions: vanishing boundary conditions give eigenfunctions that do not have a branch cut.

The Wronskian, $W(f,g) \equiv fg_x - f_x g$, is constant (in x) for (3.6a) by Abel's identity; so, from (3.7), $W(\phi, \bar{\phi}) = 2i\lambda/\varepsilon$ and $W(\psi, \bar{\psi}) = -2i\lambda_r/\varepsilon$. Note that when $|\lambda| < c$, $\lambda_r(\lambda)$ is pure imaginary; this implies that ψ is real valued and so $W(\psi, \bar{\psi}) = 0$. Therefore, ϕ and $\bar{\phi}$ are linearly independent solutions for $|\lambda| > 0$ and ψ and $\bar{\psi}$ are linearly independent solutions for $|\lambda| > c$.

The scattering eigenfunctions and scattering data a and b associated with (3.6a) satisfy

$$\phi(x;\lambda) = a(\lambda, \lambda_r)\bar{\psi}(x;\lambda_r) + b(\lambda, \lambda_r)\psi(x;\lambda_r) \tag{3.8}$$

for $\lambda_r \neq 0$, $\lambda_r \in \mathbb{R}$ (or, equivalently, $|\lambda| > c$, $\lambda \in \mathbb{R}$). The scattering data can be written as

$$a = \frac{\varepsilon}{2i\lambda_r} W(\phi, \psi) \quad \text{and} \quad b = \frac{\varepsilon}{2i\lambda_r} W(\bar{\psi}, \phi). \tag{3.9}$$

We can use this to extend a to $|\lambda| < c$, $\lambda \in \mathbb{R}$ (where λ_r is pure imaginary); when $|\lambda| < c$, $\lambda \in \mathbb{R}$, ψ is real and exponentially decaying. This also gives that $a = -b$ for $|\lambda| \leq c$, $\lambda \in \mathbb{R}$ and $|a|^2 - |b|^2 = \lambda/\lambda_r$ for $|\lambda| > c$, $\lambda \in \mathbb{R}$.

3.2.2 Time evolution

It's convenient to define the transmission coefficient $T \equiv 1/a$ and the reflection coefficient $R \equiv b/a$. Then (3.8) can be written as

$$T(\lambda, \lambda_r)\phi(x;\lambda) = \bar{\psi}(x;\lambda_r) + R(\lambda, \lambda_r)\psi(x;\lambda_r). \tag{3.10}$$

Recall that the time-dependent scattering equation (3.6b) is

$$v_t = \left(\frac{u_x}{6} + \gamma\right) v + \left(4\lambda^2 - \frac{u}{3}\right) v_x.$$

First consider the change of variables $v(x;\lambda;t) = M(x;\lambda;t)e^{-i\lambda x/\varepsilon}$; then

$$M_t = \left[\gamma - \frac{i\lambda}{3\varepsilon}(12\lambda^2 - u) + \frac{u_x}{6}\right] M + \frac{1}{3}(12\lambda^2 - u)M_x. \tag{3.11}$$

From (A.2) in appendix A, the asymptotic behavior of $M(x;\lambda,\lambda_r;t)$ is given by

$$\begin{aligned} &M(x;\lambda;t) \sim 1, && \text{as } x \to -\infty, \\ &M(x;\lambda;t) \sim a(\lambda,\lambda_r;t)e^{i(\lambda-\lambda_r)x/\varepsilon} + b(\lambda,\lambda_r;t)e^{i(\lambda+\lambda_r)x/\varepsilon}, && \text{as } x \to +\infty. \end{aligned}$$

Using the limits of u as $x \to \pm\infty$, (3.11) goes to

$$\begin{aligned} &M_t = \left(\gamma - 4i\lambda^3/\varepsilon\right) M + 4\lambda^2 M_x, && \text{as } x \to -\infty, \\ &M_t = \left[\gamma - i\lambda(4\lambda^2 + 2c^2)/\varepsilon\right] M + (4\lambda^2 + 2c^2)M_x, && \text{as } x \to +\infty; \end{aligned}$$

substituting in the asymptotic expressions for $M(x;\lambda;t)$ we find that

$$\begin{aligned} \gamma &= 4i\lambda^3/\varepsilon, \\ a_t &= (4i\lambda^3 - 4i\lambda^2\lambda_r - 2ic^2\lambda_r)a/\varepsilon, \end{aligned}$$

$$b_t = (4i\lambda^3 + 4i\lambda^2\lambda_r + 2ic^2\lambda_r)b/\varepsilon,$$

and so

$$T(\lambda, \lambda_r; t) = T(\lambda, \lambda_r; 0)\exp[i(4\lambda^2\lambda_r - 4\lambda^3 + 2c^2\lambda_r)t/\varepsilon]$$

and

$$R(\lambda, \lambda_r; t) = R(\lambda, \lambda_r; 0)\exp[i(8\lambda^2\lambda_r + 4c^2\lambda_r)t/\varepsilon].$$

For vanishing boundary conditions ($c = 0$), the transmission coefficient T does not depend on time. But here, where $c \neq 0$, the transmission coefficient does depends on time; this dependance when $|\lambda| < c$, $\lambda \in \mathbb{R}$ is not pure phase.

3.2.3 Derivation of GLM integral equation

The associated GLM integral equation — which is not new but is derived differently below — is

$$G(x, y; t) + \Omega(x + y; t) + \int_x^\infty \Omega(y + z; t)G(x, z; t)\,\mathrm{d}z = 0, \tag{3.12}$$

where

$$\Omega(\xi; t) = \frac{1}{2\varepsilon\pi}\int_{-\infty}^{\infty} Re^{i\lambda_r\xi/\varepsilon}\,\mathrm{d}\lambda_r + \sum_j c_j e^{-\tilde{\kappa}_j\xi/\varepsilon} + \frac{1}{2\varepsilon\pi}\int_0^c |\lambda T/\lambda_r|^2 e^{-\sqrt{c^2-\lambda^2}\xi/\varepsilon}\,\mathrm{d}\lambda,$$

the constants $\{i\kappa_j\}_{j=1}^N$ are the (simple) poles of $T(i\kappa_j, \lambda_r(i\kappa_j); t)$, $\tilde{\kappa}_j = \sqrt{\kappa_j^2 + c^2}$, $c_j = -i\mu_j/[\varepsilon\partial_{\lambda_r}a(i\kappa_j)]$, $\phi(x; i\kappa_j, t) \equiv \mu_j(t)\psi(x; i\kappa_j, t)$, and $0 < \kappa_1 < \cdots < \kappa_N$ are real. The kernel Ω has contributions from the reflection coefficient, from the poles, and from the branch cut (the $|\lambda T/\lambda_r|^2$ term) — there is no branch-cut contribution in the $c = 0$ case. We will omit any contributions from poles in our asymptotics. These poles relate to the solitons, which move to the right of the DSW, and so do not affect the DSW in the long-time limit.

From G, we recover $u(x,t)$ using

$$u(x,t) = -6c^2 + 12\varepsilon^2 \frac{\mathrm{d}}{\mathrm{d}x} G(x,x;t). \tag{3.13}$$

To find (3.12), the GLM integral equation, we need to know the eigenfunctions's and the scattering data's analyticity; see appendix A and (Cohen and Kappeler, 1985) for more details. Using Green's functions, we can write $e^{i\lambda x/\varepsilon}\phi$, $e^{i\lambda x/\varepsilon}\bar{\phi}$, $e^{i\lambda_r x/\varepsilon}\psi$, and $e^{i\lambda_r x/\varepsilon}\bar{\psi}$ as Volterra integral equations, which can be solved using Neumann series. From these Neumann series, we find that

- $e^{i\lambda x/\varepsilon}\phi$ is analytic for $\mathrm{Im}(\lambda) > 0$,
- $e^{-i\lambda x/\varepsilon}\bar{\phi}$ is analytic for $\mathrm{Im}(\lambda) < 0$,
- $e^{-i\lambda_r x/\varepsilon}\psi$ is analytic for $\mathrm{Im}(\lambda_r) > 0$, and
- $e^{i\lambda_r x/\varepsilon}\bar{\psi}$ is analytic for $\mathrm{Im}(\lambda_r) < 0$.

From (3.9), we have that a is analytic for $\mathrm{Im}(\lambda) > 0$. If $n = 1, 2, \ldots, N$ in (3.3), then: $e^{i\lambda x/\varepsilon}\phi$ and $e^{-i\lambda x/\varepsilon}\bar{\phi}$ are N-fold differentiable (with respect to λ) on $\mathrm{Im}(\lambda) = 0$, $\lambda \neq 0$ and $(N-1)$-differentiable at $\lambda = 0$; $e^{-i\lambda_r x/\varepsilon}\psi$ and $e^{i\lambda_r x/\varepsilon}\bar{\psi}$ are N-fold differentiable (with respect to λ_r) on $\mathrm{Im}(\lambda_r) = 0$, $\lambda_r \neq 0$ and $(N-1)$-differentiable at $\lambda_r = 0$. Likewise, if $u(x,t)$ satisfies

$$\int_{-\infty}^{\infty} |u(x,t) + 6c^2 H(x)| e^{d|x|}\, \mathrm{d}x < \infty, \qquad 0 < d \in \mathbb{R},$$

then $e^{i\lambda x/\varepsilon}\phi$ and $e^{-i\lambda x/\varepsilon}\bar{\phi}$ are analytic in $-d < \mathrm{Im}(\lambda) < d$, $e^{-i\lambda_r x/\varepsilon}\psi$ and $e^{i\lambda_r x/\varepsilon}\bar{\psi}$ are analytic in $-d < \mathrm{Im}(\lambda_r) < d$, and b is analytic, from (3.9), in $-d < \mathrm{Im}(\lambda)$ and $\mathrm{Im}(\lambda_r) < d$.

Using the eigenfunctions's and the scattering-data's analyticity, we find the GLM integral equation by: assuming that ψ and $\bar{\psi}$ have triangular forms; substituting these forms into (3.10); and operating on this equation with $(2\varepsilon\pi)^{-1}\int_{-\infty}^{\infty} \mathrm{d}\lambda_r$ to get (3.12). Following Ablowitz and Clarkson (1991b), we assume that ψ and $\bar{\psi}$ have the triangular

forms

$$\begin{aligned}\psi(x;\lambda_r;t) &= e^{i\lambda_r x/\varepsilon} + \int_x^\infty G(x,s;t)e^{i\lambda_r s/\varepsilon}\,\mathrm{d}s,\\ \bar{\psi}(x;\lambda_r;t) &= e^{-i\lambda_r x/\varepsilon} + \int_x^\infty G(x,s;t)e^{-i\lambda_r s/\varepsilon}\,\mathrm{d}s,\end{aligned} \tag{3.14}$$

with $G(x,s;t) \equiv 0$ when $s < x$. Substituting (3.14) into (3.10) gives

$$T\phi = e^{-i\lambda_r x/\varepsilon} + \int_x^\infty G(x,s;t)e^{-i\lambda_r s/\varepsilon}\,\mathrm{d}s + R\left\{e^{i\lambda_r x/\varepsilon} + \int_x^\infty G(x,s;t)e^{i\lambda_r s/\varepsilon}\,\mathrm{d}s\right\};$$

multiplying by $e^{i\lambda_r y/\varepsilon}$ and rearranging gives

$$\begin{aligned}\left(T\phi e^{i\lambda_r x/\varepsilon} - 1\right)e^{i\lambda_r(y-x)/\varepsilon} &= \int_x^\infty G(x,s;t)e^{i\lambda_r(y-s)/\varepsilon}\,\mathrm{d}s\\ &\quad + R\left\{e^{i\lambda_r(x+y)/\varepsilon} + \int_x^\infty G(x,s;t)e^{i\lambda_r(y+s)/\varepsilon}\,\mathrm{d}s\right\}.\end{aligned} \tag{3.15}$$

Now we operate on (3.15) with $(2\varepsilon\pi)^{-1}\int_{-\infty}^{\infty}\mathrm{d}\lambda_r$, interchange integrals, and use $\delta(x) = (2\varepsilon\pi)^{-1}\int_{-\infty}^{\infty} e^{i\lambda_r x/\varepsilon}\,\mathrm{d}\lambda_r$. So, for example,

$$\begin{aligned}&\frac{1}{2\varepsilon\pi}\int_{-\infty}^{\infty}\int_x^\infty G(x,s;t)e^{i\lambda_r(y-s)/\varepsilon}\,\mathrm{d}s\,\mathrm{d}\lambda_r\\ &\qquad = \int_x^\infty G(x,s;t)\left(\frac{1}{2\varepsilon\pi}\int_{-\infty}^{\infty} e^{i\lambda_r(y-s)/\varepsilon}\,\mathrm{d}\lambda_r\right)\mathrm{d}s\\ &\qquad = \int_x^\infty G(x,s;t)\delta(y-s)\,\mathrm{d}s = G(x,y;t)\end{aligned}$$

and

$$\begin{aligned}&\frac{1}{2\varepsilon\pi}\int_{-\infty}^{\infty} R(\lambda,t)\int_x^\infty G(x,s;t)e^{i\lambda_r(y+s)/\varepsilon}\,\mathrm{d}s\,\mathrm{d}\lambda_r\\ &\qquad = \int_x^\infty G(x,s;t)\left(\frac{1}{2\varepsilon\pi}\int_{-\infty}^{\infty} R(\lambda,t)e^{i\lambda_r(y+s)/\varepsilon}\,\mathrm{d}\lambda_r\right)\mathrm{d}s\\ &\qquad = \int_x^\infty G(x,s;t)F(y+s;t)\,\mathrm{d}s,\end{aligned}$$

where

$$F(z;t) \equiv \frac{1}{2\varepsilon\pi}\int_{-\infty}^{\infty} R(\lambda,t)e^{i\lambda_r z/\varepsilon}\,\mathrm{d}\lambda_r. \tag{3.16}$$

Thus,

$$G(x,y;t) + F(x+y;t) + \int_x^{\infty} F(y+z;t)G(x,z;t)\,\mathrm{d}z = I,$$

where

$$I \equiv \frac{1}{2\varepsilon\pi}\int_{-\infty}^{\infty}\left(T\phi e^{i\lambda_r x/\varepsilon} - 1\right)e^{i\lambda_r(y-x)/\varepsilon}\,\mathrm{d}\lambda_r.$$

We find I by closing in the upper-half λ_r-plane because $\phi e^{i\lambda_r x/\varepsilon}$ is analytic in $\mathrm{Im}(\lambda) > 0$. We find $I \equiv -I_b - I_p$, where I_b is the contribution from the branch cut and I_p is the contribution from the zeros of a.

To find I_b, we recall that the branch cut of λ is $\lambda_r \in [-ic, ic]$, and the branch cut of λ_r is $\lambda \in [-c, c]$. Therefore,

$$\begin{aligned} I_b &= \frac{1}{2\varepsilon\pi}\left(\int_{0-0^-}^{ic-0^-} - \int_{0+0^+}^{ic+0^+}\right)\left\{\frac{\phi e^{i\lambda_r x/\varepsilon}}{a} - 1\right\}e^{i\lambda_r(y-x)/\varepsilon}\,\mathrm{d}\lambda_r \\ &= \frac{1}{2\varepsilon\pi}\int_0^{ic}\left\{\left(\frac{\phi}{a}\right)_{\lambda=-|\lambda|} - \left(\frac{\phi}{a}\right)_{\lambda=|\lambda|}\right\}e^{i\lambda_r y/\varepsilon}\,\mathrm{d}\lambda_r. \end{aligned}$$

Now we define α and β — the scattering data from the left — such that

$$\psi \equiv \alpha\bar{\phi} + \beta\phi, \qquad \lambda \neq 0; \tag{3.17}$$

then

$$\alpha = \frac{\varepsilon}{2i\lambda}W(\phi,\psi) = \frac{\lambda_r a}{\lambda} \quad \text{and} \quad \beta = \frac{\varepsilon}{2i\lambda}W(\psi,\bar{\phi}).$$

For $\lambda_r \in [0, ic]$, $\phi^* = \bar{\phi}$, $\psi = \psi^* = \bar{\psi}$, and $\alpha^* = \beta$ from (3.7), where $*$ denotes the complex conjugate. So

$$I_b = \frac{1}{2\varepsilon\pi}\int_0^{ic}\left\{\left(\frac{\phi}{\lambda\alpha}\right)_{\lambda=-|\lambda|} - \left(\frac{\phi}{\lambda\alpha}\right)_{\lambda=|\lambda|}\right\}e^{i\lambda_r y/\varepsilon}\lambda_r\,\mathrm{d}\lambda_r.$$

Using $(\phi/\alpha)_{\lambda=-|\lambda|} = (\phi^*/\alpha^*)_{\lambda=|\lambda|}$, from (3.7a), and noting λ's sign change, gives

$$\begin{aligned} I_b &= -\frac{1}{2\varepsilon\pi}\int_0^{ic}\left(\frac{\phi}{\lambda\alpha}+\frac{\phi^*}{\lambda\alpha^*}\right)_{\lambda=|\lambda|} e^{i\lambda_r y/\varepsilon}\lambda_r\,\mathrm{d}\lambda_r \\ &= -\frac{1}{2\varepsilon\pi}\int_0^{ic}\left[\frac{1}{\lambda\alpha^*}\left(\phi^*+\frac{\alpha^*}{\alpha}\phi\right)\right]_{\lambda=|\lambda|} e^{i\lambda_r y/\varepsilon}\lambda_r\,\mathrm{d}\lambda_r. \end{aligned}$$

Using the identities $\psi^* = \bar{\psi}$ and $\alpha^* = \beta$ for $\lambda_r \in [0, ic]$ and then using (3.17) gives

$$\begin{aligned} I_b &= -\frac{1}{2\varepsilon\pi}\int_0^{ic}\left[\frac{1}{\lambda\alpha^*}\left(\bar{\phi}+\frac{\beta}{\alpha}\phi\right)\right]_{\lambda=|\lambda|} e^{i\lambda_r y/\varepsilon}\lambda_r\,\mathrm{d}\lambda_r \\ &= -\frac{1}{2\varepsilon\pi}\int_0^{ic}\left[\frac{1}{\lambda|\alpha|^2}\psi\right]_{\lambda=|\lambda|} e^{i\lambda_r y/\varepsilon}\lambda_r\,\mathrm{d}\lambda_r. \end{aligned}$$

Making the change of variable from λ_r to λ and using that $T \equiv 1/a$ gives

$$I_b = \frac{1}{2\varepsilon\pi}\int_0^{c} |\lambda T/\lambda_r|^2\psi e^{-y\sqrt{c^2-\lambda^2}/\varepsilon}\,\mathrm{d}\lambda.$$

To find I_p, we use the residue theorem to get

$$\begin{aligned} I_p &= -\frac{i}{\varepsilon}\sum_j \mathrm{Res}\left(\frac{\phi e^{iy\lambda_r/\varepsilon}}{a}, \lambda=\lambda_j\right) \\ &= \sum_j c_j\psi(x; i\kappa_j, t)e^{-\tilde{\kappa}_j y/\varepsilon}, \end{aligned}$$

where the constants $\{i\kappa_j\}$ are the simple zeros of $a(\lambda, t)$, $\tilde{\kappa}_j = \sqrt{\kappa_j^2 + c^2}$,

$$c_j = -\frac{i\mu_j}{\varepsilon[\partial_{\lambda_r} a]_{\lambda=i\kappa_j}}, \qquad \phi(x; i\kappa_j, t) \equiv \mu_j(t)\psi(x; i\kappa_j, t),$$

and $0 < \kappa_1 < \cdots < \kappa_N$ are real.

Using (3.14) again gives (3.12),

$$G(x, y; t) + \Omega(x + y; t) + \int_x^\infty \Omega(y + z; t)G(x, z; t)\,\mathrm{d}z = 0,$$

where

$$\Omega(\xi;t) = \frac{1}{2\varepsilon\pi}\int_{-\infty}^{\infty} Re^{i\lambda_r\xi/\varepsilon}\,\mathrm{d}\lambda_r + \sum_j c_j e^{-\tilde{\kappa}_j\xi/\varepsilon} + \frac{1}{2\varepsilon\pi}\int_0^c |\lambda T/\lambda_r|^2 e^{-\sqrt{c^2-\lambda^2}\xi/\varepsilon}\,\mathrm{d}\lambda.$$

To get u from G: we differentiate (3.14) twice with respect to x; multiply (3.14) by $\lambda_r^2/\varepsilon^2$; and substitute these into (3.6a) (using $\lambda^2 = \lambda_r^2 + c^2$) to get

$$e^{i\lambda_r x/\varepsilon}\left(\frac{u(x,t)}{6\varepsilon^2} + \frac{c^2}{\varepsilon^2} - 2\frac{\mathrm{d}}{\mathrm{d}x}G(x,x;t)\right) + \int_x^\infty \left[\frac{\partial^2}{\partial x^2}G(x,s;t) - \frac{\partial^2}{\partial s^2}G(x,s;t) + \left(\frac{u(x,t)}{6\varepsilon^2} + \frac{c^2}{\varepsilon^2}\right)G(x,s;t)\right] e^{i\lambda_r s/\varepsilon}\,\mathrm{d}s = 0.$$

Therefore,

$$u(x,t) = -6c^2 + 12\varepsilon^2\frac{\mathrm{d}}{\mathrm{d}x}G(x,x;t)$$

and

$$\frac{\partial^2}{\partial x^2}G(x,s;t) - \frac{\partial^2}{\partial s^2}G(x,s;t) + \left(\frac{u(x,t)}{6\varepsilon^2} + \frac{c^2}{\varepsilon^2}\right)G(x,s;t) = 0.$$

3.3 Long-time asymptotics

For large time, we use (3.12) to asymptotically compute the behavior right of the DSW (sec. 3.3.1). When this asymptotic solution breaks down, we use the matched-asymptotic method introduced in (Ablowitz and Segur, 1977) to find the DSW's slowly varying elliptic-function solution (sec. 3.3.2). This naturally leads to Whitham's equations, which Whitham (1965) originally found by an averaging method; Luke (1966) later developed a perturbative method (and Grimshaw (1979) used such a method on the KdV equation). Then we use the method in (Segur and Ablowitz, 1981) to determine the small-amplitude, slowly varying, oscillatory solution to the left of the DSW (sec. 3.3.3);

this matches the slowly varying elliptic-function solution in the middle region.

3.3.1 Shock front

On the immediate right of the DSW: we asymptotically compute $\Omega(\xi;t)$ for large time, use Ω to compute G using a Neumann series, and use G in (3.13) to find u. When our asymptotic expansion for Ω breaks down, the Neumann series for G becomes disordered: this gives us the boundary condition for the DSW's right edge.

Far right of the DSW, where $x \gg -2c^2t$, the reflection coefficient's contribution to Ω dominates. Using the steepest-descent method (see Ablowitz and Fokas, 2003; Bleistein and Handelsman, 1986) gives

$$\Omega(\xi;t) = -\frac{R_+(\lambda_*)e^{-2t[\xi/(6t)+2c^2]^{3/2}/\varepsilon}}{8\sqrt{\varepsilon\pi}[\xi/(6t)+2c^2]^{1/4}\sqrt{t}}\left[1+O(t^{-1/2})\right] + \text{cc},$$

where $\lambda_* = \sqrt{c^2/2 - \xi/(24t)}$ and cc is the complex conjugate. We can then find G using the Neumann series from the iterates $G^{(0)}(x,y;t) = -\Omega(x+y;t)$ and

$$G^{(n)}(x,y;t) = -\Omega(x+y;t) - \int_x^\infty \Omega(y+z;t)G^{(n-1)}(x,z;t)\,\mathrm{d}z.$$

Using (3.13) then gives the exponentially small solution

$$u(x,t) = -6c^2 + \frac{\operatorname{Re}\{R_+(\lambda_*)\}\,e^{-2t[x/(3t)+2c^2]^{3/2}/\varepsilon}}{4\sqrt{\varepsilon\pi}[x/(3t)+2c^2]^{1/4}\sqrt{t}}\left[1+O(t^{-1/2})\right],$$

for $x \gg -2c^2t$.

Near the DSW's right, the transmission coefficient's contribution to Ω dominates. The contribution from $\lambda = 0$ dominates: the contribution from $\lambda_* = \sqrt{c^2/2 - \xi/(24t)}$ is asymptotically zero in comparison and the contributions from $\lambda = c$ exactly cancels with the reflection-coefficient contribution from $\lambda = c$. The contribution from $\lambda = 0$ is

$$\Omega(\xi;t) = -\frac{e^{-ct(\xi/t+4c^2)/\varepsilon}\sqrt{\varepsilon}}{16\sqrt{\pi}\eta^{3/2}}\Bigg[H_2(0)t^{-3/2} + \frac{\varepsilon[2c^2\eta H_4(0) - 15(\eta-24c)H_2(0)]}{16c^2\eta^2}t^{-5/2} + O(t^{-7/2})\Bigg],$$

where $\eta = 6c - \xi/(2ct)$ and

$$H_j(\lambda_*) \equiv \left[\frac{\partial^j}{\partial\lambda^j}|T(\lambda,\lambda_r(\lambda);0)|^2\right]_{\lambda=\lambda_*}.$$

The first few terms in the Neumann series are

$$G^{(1)} - G^{(0)} = \frac{e^{-c[8c^2t+3x+y]/\varepsilon}\varepsilon^2 H_2^2(0)}{512c\pi\left[6c-\frac{x}{ct}\right]^{3/2}\left[6c-\frac{x+y}{2ct}\right]^{3/2}t^3}\left[1+O(t^{-1})\right]$$

and

$$G^{(2)} - G^{(1)} = \frac{e^{-c[12c^2t+5x+y]/\varepsilon}\varepsilon^{7/2}H_2^3(0)}{16384c^2\pi^{3/2}\left[6c-\frac{x}{ct}\right]^{3}\left[6c-\frac{x+y}{2ct}\right]^{3/2}t^{9/2}}\left[1+O(t^{-1})\right].$$

Thus, the terms in the Neumann series become disordered when

$$[x + 2c^2t + 3\varepsilon/(4c)\log(6c^2t - x)] = O(1).$$

This is the DSW's right edge. (See the asymptotic principles discussed in (Kruskal, 1962).) When we sum the Neumann series, we find that

$$\begin{aligned} u(x,t) &= -6c^2 + 12\varepsilon^2\tfrac{\mathrm{d}}{\mathrm{d}x}G(x,x;t), \\ &= -6c^2 + A_0e^{2c\zeta/\varepsilon} - \frac{1}{24c^2}\left(A_0e^{2c\zeta/\varepsilon}\right)^2(1+O(t^{-1})) \\ &\quad + \frac{1}{768c^4}\left(A_0e^{2c\zeta/\varepsilon}\right)^3(1+O(t^{-1})) + \cdots, \\ &\sim -6c^2 + 12c^2\,\mathrm{sech}^2\left[\frac{c}{\varepsilon}(\zeta-\zeta_0)\right], \end{aligned} \tag{3.18}$$

where

$$\zeta_0 = \frac{\varepsilon}{2c}\log\left\{\frac{32\sqrt{\pi}}{H_2(0)c^{1/2}\varepsilon^{3/2}}\right\},$$

$$\zeta = -x - 2c^2t - \frac{3\varepsilon}{4c}\log(6c^2t - x) + A_1(x/t)t^{-1} + \cdots, \tag{3.19}$$

and

$$A_1(x/t + 6c^2) = \frac{3\varepsilon^2}{8c^2x/t} + \frac{135\varepsilon^2}{16(x/t)^2} + \frac{3c^2\varepsilon^2H_4(0)}{8(x/t)^2H_2(0)}.$$

This provides the boundary condition on the DSW's right edge.

This procedure gives the DSW's phase, ζ_0. This phase only depends on $H_2(0)$ (since $H_0(0) = H_1(0) = 0$). In the vanishing case, (Ablowitz and Segur, 1977, Eq. (2.25c)) found a similar phase term: $r''(0) - [r'(0)]^2/r(0)$, where r is the corresponding reflection coefficient. Burgers' equation's long-time-asymptotic solution also has a phase term that depends on the initial data in a similar way (see sec. 3.1.5).

3.3.2 DSW

For the DSW, we find the slowly varying, cnoidal-wave solution using matched asymptotics. First we make a variable change in (3.1) based on (3.18). Then we use the multiple-scales method (see Ablowitz, 2011) to determine how its solution slowly varies: the secularity and compatibility conditions lead to three conservation laws, which we can transform into Whitham's equations (Whitham, 1965). Matching to (3.18) and assuming a similarity solution determines the DSW's long-time-asymptotic solution.

Analogous to (Ablowitz and Segur, 1977), we look for a solution of the form

$$u(x,t) = -6c^2 + g(\zeta,t),$$

based on (3.18), where ζ is defined in (3.19). We substitute this into (3.1). Then we introduce the slow-variables $Z \equiv \delta\zeta$ and $T \equiv \delta t$, where $\delta = O(t^{-1})$ is a small parameter.

Grouping terms in like powers of δ gives

$$\varepsilon^2 g_{\zeta\zeta\zeta} + g g_\zeta - 4c^2 g_\zeta - g_t = \delta \left\{ \frac{3\varepsilon(3\varepsilon^2 g_{\zeta\zeta\zeta} + g g_\zeta - 12c^2 g_\zeta)}{4c(8c^2 T + Z)} \right\} + \cdots . \tag{3.20}$$

To leading order, (3.20) is

$$\varepsilon^2 g_{\zeta\zeta\zeta} + g g_\zeta - 4c^2 g_\zeta - g_t \sim 0$$

and has the special solution

$$g(\zeta, t) \sim 4c^2 - V + 4\varepsilon^2\kappa^2(1 - 2k^2) + 12k^2\varepsilon^2\kappa^2 \,\mathrm{cn}^2\left[\kappa(\zeta - \zeta_0 - Vt), k\right], \tag{3.21}$$

where $\mathrm{cn}(z, k)$ is the Jacobian elliptic 'cosine' (see Olver et al., 2010); it can be found using the methods in (Baldwin et al., 2004). If we neglect the right-hand side of (3.20), κ, k, and V are arbitrary constants but vary slowly in general. In the special case

$$k = 1,\ \kappa = \frac{c}{\varepsilon},\ \text{and}\ V = 0, \quad \text{then} \quad g(\zeta, t) = 12c^2 \,\mathrm{sech}^2\left[\frac{c}{\varepsilon}(\zeta - \zeta_0)\right],$$

which exactly matches (3.18).

As in (Luke, 1966), we use the multiple-scales method — with a fast variable θ — to determine how κ, k, and V vary with the slow-variables Z and T. This leads to three conservation laws from a compatibility condition and two secularity conditions; we can transform these conservation laws into a convenient diagonal system of quasilinear, first-order equations, which were first found by Whitham (1965).

To get the compatibility condition, we introduce the rapid-variable $\theta(\zeta, t)$ with

$$\theta_\zeta \equiv \kappa(Z, T) \quad \text{and} \quad \theta_t \equiv -\omega(Z, T) \equiv -\kappa V. \tag{3.22}$$

This leads to the compatibility condition $(\theta_\zeta)_t = (\theta_t)_\zeta$ or

$$\kappa_T + \omega_Z = 0, \tag{3.23}$$

which is a conservation law.

To get the secularity conditions: we rewrite (3.20) in terms of θ, and then require that the leading-order solution is periodic in θ. Thus, we use

$$\frac{\partial}{\partial t} = -\omega\frac{\partial}{\partial\theta} + \delta\frac{\partial}{\partial T}, \qquad \frac{\partial}{\partial\zeta} = \kappa\frac{\partial}{\partial\theta} + \delta\frac{\partial}{\partial Z},$$

$$\frac{\partial^2}{\partial\zeta^2} = \kappa^2\frac{\partial^2}{\partial\theta^2} + \delta\left(\kappa_Z\frac{\partial}{\partial\theta} + 2\kappa\frac{\partial^2}{\partial\theta\partial Z}\right) + O(\delta^2),$$

$$\frac{\partial^3}{\partial\zeta^3} = \kappa^3\frac{\partial^3}{\partial\theta^3} + 3\delta\left(\kappa\kappa_Z\frac{\partial^2}{\partial\theta^2} + \kappa^2\frac{\partial^3}{\partial\theta^2\partial Z}\right) + O(\delta^2),$$

to transform (3.20) into

$$\begin{aligned}\varepsilon^2\kappa^3 g_{\theta\theta\theta} + \kappa g g_\theta + (\omega - 4c^2\kappa)g_\theta \\ = \delta\Bigg[\frac{3\varepsilon\kappa}{4c(8c^2T + Z)}\Big(3\varepsilon^2\kappa^2 g_{\theta\theta\theta} + g g_\theta - 12c^2 g_\theta\Big) \\ + g_T - \Big(3\varepsilon^2\kappa(\kappa g_{\theta\theta})_Z + g g_Z - 4c^2 g_Z\Big)\Bigg] + \cdots.\end{aligned} \tag{3.24}$$

Then we expand

$$g(\theta, Z, T) = g_0(\theta, Z, T) + \delta g_1(\theta, Z, T) + \delta^2 g_2(\theta, Z, T) + \cdots$$

and group the terms in like powers of δ. The $O(1)$ equation is

$$\varepsilon^2\kappa^3 g_{0,\theta\theta\theta} + \kappa g_0 g_{0,\theta} + (\omega - 4c^2\kappa)g_{0,\theta} = 0; \tag{3.25}$$

the $O(\delta)$ equation is

$$\varepsilon^2\kappa^3 g_{1,\theta\theta\theta} + \kappa(g_0 g_1)_\theta + (\omega - 4c^2\kappa)g_{1,\theta} = \frac{3\varepsilon\kappa}{4c(8c^2T+Z)}\left(3\varepsilon^2\kappa^2 g_{0,\theta\theta\theta} + g_0 g_{0,\theta} - 12c^2 g_{0,\theta}\right) + g_{0,T} - 3\varepsilon^2\kappa(\kappa g_{0,\theta\theta})_Z - g_0 g_{0,Z} + 4c^2 g_{0,Z} \equiv F. \quad (3.26)$$

To eliminate secular terms (that is, terms that grow arbitrarily large), we enforce the periodicity of $g_0(\theta, Z, T)$ in θ:

$$\int_0^1 F\,\mathrm{d}\theta = 0 \quad \text{and} \quad \int_0^1 g_0 F\,\mathrm{d}\theta = 0.$$

Using

$$\int_0^1 \frac{\partial^i g_0}{\partial\theta^i}\,\mathrm{d}\theta = 0, \qquad \int_0^1 g_0\frac{\partial^j g_0}{\partial\theta^j}\,\mathrm{d}\theta = 0,$$

for $i = 1, 2, 3, \ldots$ and $j = 1, 3, 5, \ldots$, and

$$\int_0^1 g_0 g_{0,\theta\theta}\,\mathrm{d}\theta = -\int_0^1 g_{0,\theta}^2\,\mathrm{d}\theta,$$

we get from $\int_0^1 F\,\mathrm{d}\theta = 0$ that

$$\frac{\partial}{\partial T}\int_0^1 g_0\,\mathrm{d}\theta + \frac{\partial}{\partial Z}\left(4c^2\int_0^1 g_0\,\mathrm{d}\theta - \frac{1}{2}\int_0^1 g_0^2\,\mathrm{d}\theta\right) = 0 \quad (3.27)$$

and from $\int_0^1 g_0 F\,\mathrm{d}\theta = 0$ that

$$\frac{\partial}{\partial T}\int_0^1 g_0^2\,\mathrm{d}\theta + \frac{\partial}{\partial Z}\left(4c^2\int_0^1 g_0^2\,\mathrm{d}\theta - \frac{2}{3}\int_0^1 g_0^3\,\mathrm{d}\theta + 3\varepsilon^2\kappa^2\int_0^1 g_{0,\theta}^2\,\mathrm{d}\theta\right) = 0. \quad (3.28)$$

The solution of (3.25) (using $\omega = \kappa V$) is

$$g_0(\theta, Z, T) = a(Z, T) + b(Z, T)\,\mathrm{cn}^2[2(\theta - \theta_0)K, k(Z, T)], \quad (3.29)$$

where $K \equiv K(k(Z,T))$ is the complete elliptic integral of the first kind,

$$\kappa^2 = \frac{b}{48\varepsilon^2 k^2 K^2}, \quad \text{and} \quad a = 4c^2 - V - \frac{2}{3}b + \frac{b}{3k^2}. \tag{3.30}$$

Note that $\mathrm{cn}^2(z,k)$ has period $2K(k)$ and so $g_0(\theta, Z, T)$ is periodic in θ with period 1. We can use these to rewrite the conservation law (3.23) as

$$\frac{\partial}{\partial T}\left(\frac{1}{4\sqrt{3}\varepsilon K}\sqrt{\frac{b}{k^2}}\right) + \frac{\partial}{\partial Z}\left(\frac{V}{4\sqrt{3}\varepsilon K}\sqrt{\frac{b}{k^2}}\right) = 0.$$

We can also use (3.29) to rewrite the conservation laws (3.27) and (3.28) in terms of b/k^2, V, and k. From (3.29) and the properties of elliptic functions (see Byrd and Friedman, 1971, formulas 312 and special values 122), we find that

$$\begin{aligned}
\int_0^1 g_0 \,\mathrm{d}\theta &= (4c^2 - V) + \frac{1}{3}\left(3\frac{E}{K} + k^2 - 2\right)\frac{b}{k^2}, \\
\int_0^1 g_0^2 \,\mathrm{d}\theta &= (4c^2 - V)^2 + \frac{2(4c^2 - V)}{3}\left(3\frac{E}{K} + k^2 - 2\right)\frac{b}{k^2} + \frac{1}{9}\left(1 - k^2 + k^4\right)\left(\frac{b}{k^2}\right)^2, \\
\int_0^1 g_0^3 \,\mathrm{d}\theta &= (4c^2 - V)^3 + (4c^2 - V)^2\left(3\frac{E}{K} + k^2 - 2\right)\frac{b}{k^2} \\
&\qquad + \frac{(4c^2 - V)}{3}(1 - k^2 + k^4)\left(\frac{b}{k^2}\right)^2 \\
&\qquad + \frac{1}{5}\left[\frac{E}{K}(1 - k^2 + k^4) - \frac{1}{27}(22 - 33k^2 + 21k^4 - 5k^6)\right]\left(\frac{b}{k^2}\right)^3, \\
\omega^2 \int_0^1 g_{0,\theta}^2 \,\mathrm{d}\theta &= \frac{1}{45\varepsilon^2}\left[2\left(1 - k^2 + k^4\right)\frac{E}{K} - \left(2 - 3k^2 + k^4\right)\right]\left(\frac{b}{k^2}\right)^3,
\end{aligned}$$

where $K \equiv K(k)$ and $E \equiv E(k)$ are the complete integrals of the first and second kind. Using these identities in (3.27) and (3.28) give the conservation laws

$$\begin{aligned}
&\frac{\partial}{\partial T}\left[(4c^2 - V) + \frac{1}{3}\left(3\frac{E}{K} + k^2 - 2\right)\frac{b}{k^2}\right] \\
&\quad + \frac{\partial}{\partial Z}\left[\frac{1}{2}(4c^2 - V)(4c^2 + V) + \frac{V}{3}\left(3\frac{E}{K} + k^2 - 2\right)\frac{b}{k^2} - \frac{1}{18}(1 - k^2 + k^4)\left(\frac{b}{k^2}\right)^2\right] = 0
\end{aligned}$$

and

$$\frac{\partial}{\partial T}\left[(4c^2-V)^2+\frac{2(4c^2-V)}{3}\left(3\frac{E}{K}+k^2-2\right)\frac{b}{k^2}+\frac{1}{9}\left(1-k^2+k^4\right)\left(\frac{b}{k^2}\right)^2\right]$$
$$+\frac{\partial}{\partial Z}\left[\frac{2}{3}(4c^2-V)^2(2c^2+V)+\frac{2V}{3}(4c^2-V)\left(3\frac{E}{K}+k^2-2\right)\frac{b}{k^2}\right.$$
$$\left.-\frac{2}{9}(2c^2-V)(1-k^2+k^4)\left(\frac{b}{k^2}\right)^2+\frac{1}{81}(2-k^2)(1+k^2)(2k^2-1)\left(\frac{b}{k^2}\right)^3\right]=0.$$

These three conservation laws determine b, k, and V.

We can transform these conservation laws into Whitham's equations. Make the variable changes

$$\frac{b}{k^2}=2(r_3-r_1),\quad k^2=\frac{r_2-r_1}{r_3-r_1},\quad V=4c^2-\frac{r_1+r_2+r_3}{3}.$$

Simplifying then gives the convenient diagonal system

$$\frac{\partial r_i}{\partial T}+v_i(r_1,r_2,r_3)\frac{\partial r_i}{\partial Z}=0,\qquad i=1,2,3, \tag{3.31}$$

where

$$v_1=4c^2-\frac{r_1+r_2+r_3}{3}+\frac{2}{3}(r_2-r_1)\frac{K}{K-E}=V+\frac{b}{3}\frac{K}{K-E},$$
$$v_2=4c^2-\frac{r_1+r_2+r_3}{3}+\frac{2}{3}(r_2-r_1)\frac{(1-k^2)K}{E-(1-k^2)K}=V+\frac{b}{3}\frac{(1-k^2)K}{E-(1-k^2)K},$$
$$v_3=4c^2-\frac{r_1+r_2+r_3}{3}-\frac{2}{3}(r_3-r_1)\frac{(1-k^2)K}{E}=V-\frac{b}{3k^2}\frac{(1-k^2)K}{E},$$

and

$$g_0(\theta,Z,T)=r_1-r_2+r_3+2(r_2-r_1)\,\mathrm{cn}^2\left[2(\theta-\theta_0)K,k\right].$$

Whitham first found (3.31) in (Whitham, 1965) (see also Gurevich and Pitaevskii, 1974; Ablowitz et al., 2009). Here, θ is found through integrating with (3.22).

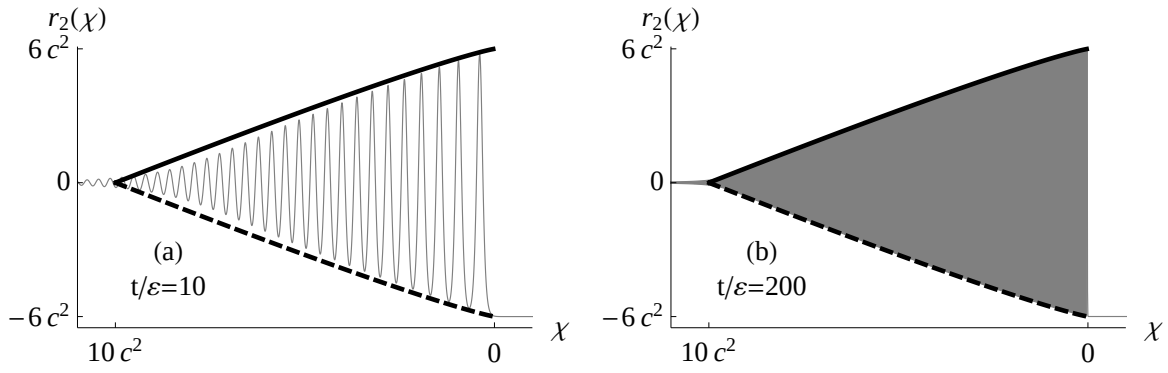

Figure 3.3: The value of $r_2(\chi)$ found numerically for $0 < \chi < 10c^2$, where $\chi \equiv \zeta/t$. For comparison, we include $-r_2(\chi)$ as a dashed line and a numerical simulation of $u(x,t)$ in gray (inside the envelope of r_2 and $-r_2$) for a single-step at (a) $t/\varepsilon = 10$ and (b) $t/\varepsilon = 200$. Note that $\chi = 0$ corresponds to $x \sim -2c^2t$ and $\chi = 10c^2$ to $x \sim -12c^2t$.

For large time, the solution tends to a self-similar solution. We assume that $r_i = r_i(\chi)$ with $\chi \equiv Z/T = \zeta/t$. Taking $r_1 = 0$ and $r_3 = 6c^2$ satisfies the boundary conditions; so (3.31) reduces to $(v_2 - \chi)r_2'(\chi) = 0$ or

$$v_2 = 2c^2 - r_2 + \frac{2}{3}\frac{r_2 E\left(\sqrt{\frac{r_2}{6c^2}}\right)}{E\left(\sqrt{\frac{r_2}{6c^2}}\right) - \left(1 - \frac{r_2}{6c^2}\right) K\left(\sqrt{\frac{r_2}{6c^2}}\right)} = \chi.$$

We can numerically solve this implicit equation for r_2 (fig. 3.3). We can also directly compute the DSW's left- and right-edge speed: At the right edge, we take the limit $r_2 \to r_3$, and get that $v_2 \to 0$ or $x \sim -2c^2t$ — the leading soliton's speed. At the left edge, we take the limit $r_2 \to r_1$, and get that $v_2 \to 10c^2$ or $x \sim -12c^2t$. Moreover, at the left edge where $0 < (10c^2 - \chi) \ll 1$, we have that $r_2 = 2(10c^2 - \chi)/3 + O[(10c^2 - \chi)^2]$; using this and taking $x \to -12c^2t$ gives $u = (2/3)(10c^2 - \chi)\cos[16c^3t/\varepsilon + O(\log t)]$.

3.3.3 Trailing edge

The solution left of the DSW has the same form for both vanishing ($c = 0$) and non-vanishing ($c \neq 0$) boundary conditions. In both cases, the GLM integral equation formulated from $-\infty$ to x has the same form.

The scaling symmetry of (3.1) — $(u, x, t) \to (\gamma^2 u, \gamma^{-1} x, \gamma^{-3} t)$ — leads to a similarity solution. Indeed, we seek a similarity solution of the form

$$u(x,t) = \frac{Z^{1/4}}{\sqrt{\tau}} f(\chi, \tau), \qquad \chi \equiv \frac{2}{3\varepsilon} \tau Z^{3/2}$$

based on the first few terms of Neumann series solution of the GLM integral equation formulated from $-\infty$ to x. Using this in (3.1) gives $\tau f_\tau + \Delta(\chi, f, f_\chi, \ldots, f_{\chi\chi\chi}) = 0$ and this suggest that

$$u(x,t) = \frac{Z^{1/4}}{\sqrt{\tau}} g\left[\frac{2}{3\varepsilon}\tau Z^{3/2} + c_{1,1}(Z)\log\tau + c_{1,0}(Z)\right].$$

When we substitute this into (3.1), we find $g'''(\theta) + g'(\theta) = 0$ at order $O(\tau^{-1/2})$ and this implies that

$$u(x,t) = \frac{Z^{1/4}}{\sqrt{\tau}}\Big\{A_0 + A_1\cos(\theta) + B_1\sin(\theta)\Big\} + O(\tau^{-1}),$$

where

$$\theta = \tau\left(\frac{2}{3\varepsilon}Z^{3/2} + c_{1,1}(Z)\frac{\log\tau}{\tau} + \frac{c_{1,0}(Z)}{\tau} + O(\tau^{-2})\right).$$

Substituting this into (3.1) gives terms with $\cos(2\theta)$ and $\sin(2\theta)$ at the next order, $O(\tau^{-1})$, and $\cos(3\theta)$ and $\sin(3\theta)$ at the following order, $O(\tau^{-3/2})$, and so we now consider

$$u(x,t) = \frac{Z^{1/4}}{\sqrt{\tau}}\left\{A_0 + A_1\cos(\theta) + B_1\sin(\theta) + \frac{A_3}{\tau Z^{3/2}}\cos(3\theta) + \frac{B_3}{\tau Z^{3/2}}\sin(3\theta)\right\}$$
$$+ \frac{1}{\tau\sqrt{Z}}\Big\{A_{00} + A_2\cos(2\theta) + B_2\sin(2\theta)\Big\} + O(t^{-2});$$

after substituting this into (3.1) and equating the coefficients of τ^{-1} and $\tau^{-3/2}$ to zero we get that the slowly varying, asymptotic similarity solution is

$$u(x,t) = 2A\frac{X^{1/4}}{\sqrt{\tau}}\cos(\theta) - \frac{A^2(1-\cos 2\theta)}{3\tau\sqrt{X}} + O(\tau^{-3/2}), \tag{3.32}$$

where $X = -x/(3t)$, $\tau = 3t$, and

$$\theta = \frac{\tau}{\varepsilon}\left[\frac{2}{3}X^{3/2} - \frac{A^2}{18}\frac{\log(\tau X^{3/2})}{\tau} + \frac{\theta_0}{\tau} + O(\tau^{-2})\right].$$

We can use several methods to find A and θ_0 in terms of the scattering data.

One method for finding A and θ_0 is to use the GLM integral equation formulated from $-\infty$ to x. Following the same procedure as section 3.3.1 requires that we sum the whole Neumann series: that is, unlike section 3.3.1, we cannot get A and θ_0 from the Neumann series's first few terms. But the first few terms are sufficient to show our main result: the long-time limit of general, step-like data is a single-phase DSW.

While we don't need expressions for A and θ_0 to show our main result, we can use the method as (Segur and Ablowitz, 1981) to find A and θ_0. We find that

$$A^2(X) \sim -\frac{9\varepsilon}{\pi}\log\left(1 - \left|R\left(\sqrt{X}/2\right)\right|^2\right), \tag{3.33}$$

where $R(\sqrt{X}/2) \equiv R(\lambda = \sqrt{X}/2, \lambda_r(\lambda), t = 0)$, and

$$\begin{aligned}\frac{\theta_0}{\varepsilon} \sim \frac{\pi}{4} - \arg\{\tilde{r}(\lambda)\} - \arg\left\{\Gamma\left(1 - \frac{iA^2(4\lambda^2)}{18\varepsilon}\right)\right\} \\ - \frac{c^2A^2(4c^2)}{9\varepsilon\lambda^2}\log\left(\frac{c-\lambda}{c+\lambda}\right) - \frac{A^2}{6\varepsilon}\log 2 \\ - \frac{1}{9\lambda^2\varepsilon}\int_c^\lambda \left(\xi^2A^2(4\xi^2)\right)_\xi \log\left(\frac{\xi-\lambda}{\xi+\lambda}\right)\mathrm{d}\xi,\end{aligned} \tag{3.34}$$

where $\lambda = \sqrt{X}/2$, $\tilde{r} \equiv \tilde{b}/\tilde{a}$, and $\phi \to \tilde{a}(\lambda)e^{-i\lambda x/\varepsilon} + \tilde{b}(\lambda)e^{i\lambda(x+8\lambda^2 t)/\varepsilon}$ as $x \to -12c^2t$. This $\tilde{r}$ can be related to a and b through the GLM integral equation formulated from $-\infty$ to x.

To determine A and θ_0, we do the following: We substitute (3.32) into (3.6a) and use the boundary values $v \to \phi$ as $x \to -\infty$ and $v \to \tilde{a}e^{-i\lambda x/\varepsilon} + \tilde{b}e^{i\lambda(x+8\lambda^2 t)/\varepsilon}$ as $x \to -12c^2t$. Here, $\tilde{a}$ and $\tilde{b}$ can be found through the GLM integral equation from the left or by relating them to a and b through the asymptotic forms of u for $-12c^2t \ll x \ll \infty$.

Then we asymptotically solve for the eigenfunction ϕ; this is a WKB-type problem that leads to a matched-asymptotic problem. From the asymptotic form of ϕ, we get A and θ_0 in terms of $\tilde{r} \equiv \tilde{b}/\tilde{a}$.

To get a WKB-type problem for the eigenfunctions: we substitute (3.32) and $v = \phi = \phi_1 e^{i\lambda x/\varepsilon} + \phi_2 e^{-i\lambda x/\varepsilon}$ into (3.6a), break it into two consistent relations, and keep only the leading-order terms. This gives

$$\begin{aligned} \frac{\partial \phi_1}{\partial x} &\sim i\frac{AX^{1/4}}{12\lambda\varepsilon\sqrt{\tau}}\left(e^{i(\theta-\eta)} + e^{-i(\theta+\eta)}\right)\phi_2, \\ \frac{\partial \phi_2}{\partial x} &\sim -i\frac{AX^{1/4}}{12\lambda\varepsilon\sqrt{\tau}}\left(e^{i(\theta+\eta)} + e^{-i(\theta-\eta)}\right)\phi_1, \end{aligned} \tag{3.35}$$

where $\eta \equiv 2\lambda x/\varepsilon$. This has *two* rapidly varying phases, $(\theta+\eta)$ and $(\theta-\eta)$. Then we expand ϕ_1 and ϕ_2 as

$$\phi_i = \phi_{i,0}(\theta,\eta,X) + \tau^{-1/2}\phi_{i,1}(\theta,\eta,X) + \tau^{-1}\phi_{i,2}(\theta,\eta,X) + \cdots,$$

substitute this into (3.35), and group terms with like powers of τ. At $O(\tau^{-1/2})$, we find a resonance or turning-point region near

$$1 \pm \frac{\eta_x}{\theta_x} = 0 \quad \text{or} \quad X \sim 4\lambda^2,$$

where secular terms appear. This gives three regions to consider: $X \gg 4\lambda^2$, $X \sim 4\lambda^2$, and $4\lambda^2 \gg X \gg 4c^2$.

In the left-most region, where $4\lambda^2 \ll X < \infty$, perturbation theory gives

$$\begin{aligned} &\phi_{1,0}(X) = 0, \\ &\phi_{2,0}(X) \sim \exp\left\{\tfrac{i}{144\lambda^2\varepsilon^2}\int_X^\infty A^2(z)\sqrt{z}\left(\tfrac{1}{\theta_x(z)+\eta_x} - \tfrac{1}{\theta_x(z)-\eta_x}\right)\,\mathrm{d}z\right\}, \end{aligned}$$

after matching to $\phi_1 \to 0$ and $\phi_2 \to 1$ as $x \to -\infty$. In the limit as $X \to 4\lambda^2$, we get that

$$\phi_{2,0}(X) \sim (X - 4\lambda^2)^{\nu}(4\lambda)^{-2\nu} e^{I(\lambda)},$$

where $\nu \equiv iA^2(4\lambda^2)/(18\varepsilon)$ and

$$I(\lambda) \equiv \frac{i}{18\lambda^2\varepsilon} \int_{\lambda}^{\infty} \left(\xi^2 A^2(4\xi^2)\right)_{\xi} \log\left(\frac{\xi - \lambda}{\xi + \lambda}\right) \mathrm{d}\xi.$$

In the middle region, where $X \sim 4\lambda^2$, we can represent the solution in terms of parabolic cylinder functions:

$$\begin{aligned} w_{1,0}(Y) &= e^{-\tilde{Y}^2/4}\left(c_1 U\left(\tfrac{1}{2} - \nu, \tilde{Y}\right) + c_2 U\left(\tfrac{1}{2} - \nu, -\tilde{Y}\right)\right), \\ w_{2,0}(Y) &= e^{\tilde{Y}^2/4}\left(c_3 U\left(-\tfrac{1}{2} - \nu, \tilde{Y}\right) + c_4 U\left(-\tfrac{1}{2} - \nu, -\tilde{Y}\right)\right), \end{aligned}$$

where U is the parabolic cylinder function (see Olver et al., 2010),

$$Y \equiv (X - 4\lambda^2)\sqrt{\tau} \equiv -\frac{x - x_0}{\sqrt{3t}}, \qquad \tilde{Y} \equiv \frac{Y e^{i\pi/4}}{\sqrt{4\lambda\varepsilon}},$$

and

$$\begin{aligned} c_1 &= c_3 \frac{A(4\lambda^2)}{3\sqrt{2\varepsilon}} \exp\left\{i\left(\frac{\pi}{4} - \frac{2\lambda x_0 + \tilde{\theta}_0}{\varepsilon}\right)\right\}, \\ c_2 &= -c_4 \frac{A(4\lambda^2)}{3\sqrt{2\varepsilon}} \exp\left\{i\left(\frac{\pi}{4} - \frac{2\lambda x_0 + \tilde{\theta}_0}{\varepsilon}\right)\right\}. \end{aligned}$$

Matching w_i as $Y \to +\infty$ to ϕ_i as $X \to 4\lambda^2$ gives

$$c_3 = e^{-i\pi\nu/4}\left(\frac{\varepsilon}{(4\lambda)^3\tau}\right)^{\nu/2} e^{I(\lambda)} \quad \text{and} \quad c_4 = 0.$$

Taking the limit in the other direction, $Y \to -\infty$, then gives

$$\begin{aligned}\phi_{1,0}(Y) &= \frac{\sqrt{2\pi\nu}}{\Gamma(1-\nu)}(4\lambda^2 - X)^{-\nu} e^{-i\pi\nu/2}(4\lambda\tau)^{-\nu}\varepsilon^{\nu} \\ &\qquad \times \exp\left\{ -i\frac{2\lambda x_0 + \tilde{\theta}_0}{\varepsilon} + I(\lambda)\right\} + O(|Y|^{-1}), \\ \phi_{2,0}(Y) &= (4\lambda^2 - X)^{\nu} e^{-i\pi\nu}(4\lambda)^{-2\nu} e^{I(\lambda)} + O(|Y|^{-1}).\end{aligned}$$

For $4\lambda^2 \gg X \gg 4c^2$, perturbation theory and matching to $\phi_1 \to \tilde{b}(\lambda)e^{8i\lambda^3 t/\varepsilon}$ and $\phi_2 \to \tilde{a}(\lambda)$ as $x \to -12c^2 t$ gives

$$\phi_{1,0}(X) \sim \tilde{b}(\lambda)e^{i8\lambda^3 t/\varepsilon + J(X;\lambda)} \quad \text{and} \quad \phi_{2,0}(X) \sim \tilde{a}(\lambda)e^{-J(X;\lambda)},$$

where

$$J(X;\lambda) \equiv \frac{i}{144\lambda^2\varepsilon^2}\int_{4c^2}^{X} A^2(z)\sqrt{z}\left(\tfrac{1}{\theta_x(z)+\eta_x} - \tfrac{1}{\theta_x(z)-\eta_x}\right)\,\mathrm{d}z.$$

Matching the limits of ϕ_2 as $X \to 4\lambda^2$ and as $Y \to -\infty$ gives

$$\tilde{a}(\lambda) \sim \exp\left\{ \frac{c^2}{\lambda^2}\frac{iA^2(4c^2)}{18\varepsilon}\log\left(\frac{c-\lambda}{c+\lambda}\right) + \frac{i}{18\lambda^2\varepsilon}\int_c^{\infty}\left(\xi^2 A^2(4\xi^2)\right)_{\xi}\log\left|\frac{\xi-\lambda}{\xi+\lambda}\right|\,\mathrm{d}\xi\right\}.$$

So, after contour integration,

$$A^2(X) \sim \frac{9\varepsilon}{\pi}\log\left|\tilde{a}(\sqrt{X}/2)\right|^2 = -\frac{9\varepsilon}{\pi}\log\left(1 - \left|R\left(\sqrt{X}/2\right)\right|^2\right),$$

since $X = 4\lambda^2$, $\tilde{r}(\lambda,t) \equiv \tilde{b}(\lambda,t)/\tilde{a}(\lambda)$ and $|\tilde{r}(\lambda,t)| = |R(\lambda,t)|$. Likewise, matching the limits of ϕ_1 as $X \to 4\lambda^2$ and as $Y \to -\infty$ gives

$$\begin{aligned}\tilde{b}(\lambda) \sim \frac{\sqrt{2\pi\nu}}{\Gamma(1-\nu)}e^{i\pi\nu/2}\varepsilon^{\nu}\exp\Bigg\{ &-i\frac{\theta_0}{\varepsilon} - 3\nu\log 2 - \frac{c^2}{\lambda^2}\frac{iA^2(4c^2)}{18\varepsilon}\log\left(\frac{c-\lambda}{c+\lambda}\right) \\ &+ \frac{i}{18\lambda^2\varepsilon}\left(-\int_c^{\lambda} + \int_{\lambda}^{\infty}\right)\left(\xi^2 A^2(4\xi^2)\right)_{\xi}\log\left(\frac{\xi-\lambda}{\xi+\lambda}\right)\,\mathrm{d}\xi\Bigg\}.\end{aligned}$$

Using $\tilde{r} \equiv \tilde{b}/\tilde{a}$ gives (3.34).

This matches the DSW's left boundary since taking the limits $x \to -12c^2t$ and $r_2 \sim 2(10c^2 - \chi)/3 \sim 2AX^{1/4}\tau^{-1/2}$ gives $u \sim 2\sqrt{2c/(3t)}\cos[16c^3t/\varepsilon + O(\log t)]$.

3.4 Conclusion

DSWs appear when weak dispersion and weak nonlinearity dominate the physics; they arise in many physical systems, including fluid dynamics, plasmas, superfluids, and nonlinear optics. For systems with weak dispersion and weak, quadratic nonlinearity, the KdV equation is the leading-order asymptotic equation. Here we showed that the long-time-asymptotic solution of the KdV equation for general, step-like initial data tend to a single-phase DSW; we found this long-time-asymptotic solution using the IST method and matched-asymptotic expansions. Therefore, a single-phase DSW eventually forms from well-separated, multi-step initial data, despite having more complex multiphase dynamics at intermediate times. We anticipate that our IST and matched-asymptotic procedure for general, step-like data will be applied to other important nonlinear integrable systems.

The long-time-asymptotic solution of the KdV equation for general, step-like initial data has three basic regions: an exponentially small region right of the DSW; the main DSW region, which is a slowly varying cnoidal wave with a soliton-train on its right and oscillatory behavior on its left; and a small, decaying, oscillatory region left of the DSW. The DSW region is over $|x| \leq O(t)$ and has height $O(1)$. Compare this with the linear KdV equation with step-like data and the nonlinear KdV equation with vanishing data: the linear KdV equation with step-like data has a middle region with strong nonlinearity over $|x| \leq O(t^{1/3})$ and has height $O(1)$; the nonlinear KdV equation with vanishing data has a collisionless-shock region over $(-x) = O[t^{1/3}(\log t)^{2/3}]$ and has height $O[(\log t)^{1/2}t^{-2/3}]$. The merging of shocks from multistep data is similar for both

the KdV and Burgers' equations: in both, the boundary conditions determine its form and the initial data determine its position — but the KdV equation can also have a finite number of solitons.

Chapter 4

Dispersive shock wave interactions and asymptotics — the modified Korteweg–de Vries equation

In this chapter, we look for a large-time asymptotic approximation of the mKdV equation's solution for non-vanishing boundary data. To find this solution, we use IST theory and matched-asymptotic expansions—as we did in chapter 3.

Unlike chapter 3, we needed to develop the IST theory for the mKdV equation,

$$q_t + 6q^2 q_x + q_{xxx} = 0,$$

with non-vanishing boundary data since it was not available in the literature. We will assume that the initial data go rapidly to

$$\lim_{x\to-\infty} q(x,t) \equiv q_\ell \quad \text{and} \quad \lim_{x\to\infty} q(x,t) \equiv q_r.$$

As with the KdV equation, we use this boundary data and the scattering equation of the mKdV equation's Lax pair to define eigenfunctions as $x \to \pm\infty$. From these

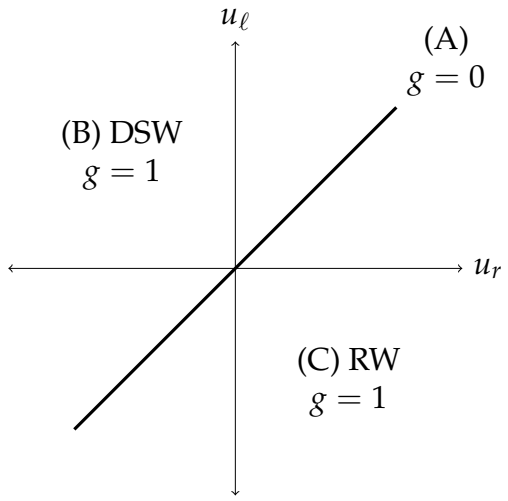

Figure 4.1: The three canonical cases for the KdV equations with constant boundary data $\lim_{x\to\infty} u(x,t) = u_r$ and $\lim_{x\to-\infty} u(x,t) = u_\ell$. Here, g is the genus of the scattering data; that is, the number of branch cuts. Case A was first solved in Ablowitz and Segur (1977). Case B is solved in chapter 3 and was also published in (Ablowitz and Baldwin, 2013b,a). We expect to solve case C using IST in a future paper.

eigenfunctions, we define a transmission and a reflection coefficient—the scattering data. Where the KdV equation has three canonical solution based on the boundary data (fig. 4.1), the mKdV equation has seventeen (fig. 4.2) because it's not Galilean invariant. These canonical solutions and the scattering data's analytic structure are inextricably linked: in chapter 3 for $u_\ell > u_r$, the scattering data's branch cut led to a contribution from the transmission coefficient in the GLM integral equation formulated from x to $+\infty$ and led to a DSW; likewise, when $u_r > u_\ell$, the scattering data's branch cut leads to a contribution from the transmission coefficient in the GLM integral equation formulated from $-\infty$ to x and this leads to a RW. In this chapter, we get a DSW when $q_\ell^2 > q_r^2$ and a RW when $q_r^2 > q_\ell^2$ because the scattering data's analytic structure lead to a contribution from the transmission coefficient in the GLM integral equation when formulated from x to $+\infty$ and $-\infty$ to x, respectively. Since the mKdV equation is invariant under $q \to -q$, we can reduce these seventeen cases down to nine cases and take $q_\ell \geq q_r$ (we can recover the other cases by taking $q \to -q$).

For the DSW-forming cases 2–4 (and 10–12 by symmetry) in figure 4.2, we will

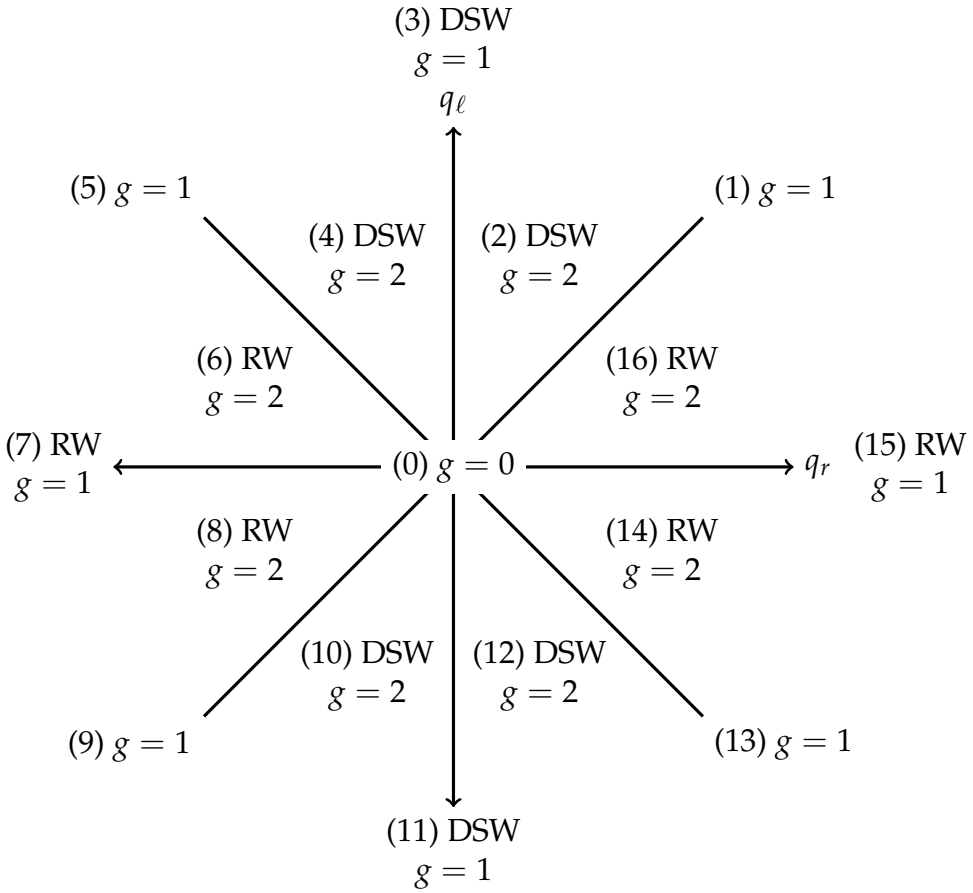

Figure 4.2: The seventeen canonical cases for the mKdV equations with constant boundary data. Here, g is the genus of the scattering data; that is, the number of branch cuts. Since the mKdV equation is invariant under $q \to -q$, cases 9–16 can be mapped to cases 1–8 by taking $q \to -q$. Cases 2–3 (and 10–12 by symmetry) are investigated in this chapter. See Ablowitz and Segur (1981a, sec. 1.7.b) for case 0. We leave the other cases to a future paper.

look for the solution's large-time asymptotic approximation. As for the KdV equation, we approximate the GLM integral equation's kernel to the DSW's right in the large-time limit; then we use a Neumann series to solve this asymptotic approximation of the GLM integral equation. When this asymptotic approximation of the solution breaks down, it gives us a boundary condition for the DSW. Using multiple-scales perturbation theory, we find a slowly varying similarity solution that matches this boundary condition. This slowly varying elliptic-function solution has three integration constants—since the mKdV equation is third order—and multiple-scales perturbation theory gives three conservation laws for determining these integration constants. With a variable change, we can diagonalize these conservation laws and get a system for the solution's Riemann invariants; matching to the boundary condition on the DSW's right implies that two of these Riemann invariants are constant and gives an implicit algebraic equation for the last. This completely determines the behavior in the DSW region.

4.1 IST theory

4.1.1 Direct problem

The mKdV equation, in dimensionless form, is

$$q_t + 6q^2 q_x + q_{xxx} = 0, \tag{4.1}$$

where subscripts denote partial derivatives. We will consider the boundary conditions

$$\lim_{x\to-\infty} q(x,t) = q_\ell \quad \text{and} \quad \lim_{x\to+\infty} q(x,t) = q_r. \tag{4.2}$$

Here, q_ℓ and q_r are real constants such that $q_\ell > q_r$; the solution for $q_\ell < q_r$ can be found using the symmetry $q \to -q$; the solution when $q_\ell = q_r$ will not be considered. We

require that q goes to these boundary conditions sufficiently rapidly; so we assume that

$$\int_{-\infty}^{\infty} |q(x,t) - q_\ell H(-x) - q_r H(x)|(1+|x|^n)\,\mathrm{d}x < \infty, \qquad n = 1, 2, \ldots N, \tag{4.3}$$

where $H(x > 0) = 1$ and $H(x \leq 0) = 0$ is the Heaviside function.

The mKdV equation (4.1) has a (linear) Lax pair (see Ablowitz et al., 1974); the Lax pair's scattering equation is

$$\begin{aligned} (v_1)_x &= -i\zeta v_1 + q v_2, \\ (v_2)_x &= -q v_1 + i\zeta v_2. \end{aligned} \tag{4.4}$$

From this scattering equation and q's boundary conditions (4.2), we define the eigenfunctions ϕ, $\bar{\phi}$, ψ, and $\bar{\psi}$:

$$\phi \sim \begin{pmatrix} 1 \\ i\frac{\zeta-\zeta_\ell}{q_\ell} \end{pmatrix} e^{-ix\zeta_\ell} \quad \text{and} \quad \bar{\phi} \sim \begin{pmatrix} i\frac{\zeta-\zeta_\ell}{q_\ell} \\ 1 \end{pmatrix} e^{ix\zeta_\ell} \quad \text{as } x \to -\infty, \tag{4.5a}$$

$$\psi \sim \begin{pmatrix} i\frac{\zeta-\zeta_r}{q_r} \\ 1 \end{pmatrix} e^{ix\zeta_r} \quad \text{and} \quad \bar{\psi} \sim \begin{pmatrix} 1 \\ i\frac{\zeta-\zeta_r}{q_r} \end{pmatrix} e^{-ix\zeta_r} \quad \text{as } x \to +\infty, \tag{4.5b}$$

where $\zeta_\ell \equiv \sqrt{\zeta^2 + q_\ell^2}$ and $\zeta_r \equiv \sqrt{\zeta^2 + q_r^2}$. If $q_\ell \neq 0$, then ζ_ℓ has branch points at $\zeta = \pm iq_\ell$; likewise, if $q_r \neq 0$, then ζ_r has branch points at $\zeta = \pm iq_r$. Since $q_\ell > q_r$, we choose the following branch cuts for ζ_ℓ and ζ_r to make the eigenfunctions single-valued with respect to ζ:

- $q_\ell > q_r > 0$ (case 2) has the branch cuts $\zeta \in [-iq_\ell, -iq_r]$ and $\zeta \in [iq_r, iq_\ell]$,
- $q_\ell > q_r = 0$ (case 3) has the branch cut $\zeta \in [-iq_\ell, +iq_\ell]$,
- $q_\ell > -q_r > 0$ (case 4) has the branch cuts $\zeta \in [-iq_\ell, -iq_r]$ and $\zeta \in [iq_r, iq_\ell]$,
- $q_\ell = -q_r$ (case 5) has the branch cut $\zeta \in [-iq_\ell, +iq_\ell]$,

- $-q_r > q_\ell > 0$ (case 6) has the brach cuts $\zeta \in [-iq_r, -iq_\ell]$ and $\zeta \in [iq_\ell, iq_r]$,
- $q_r < q_\ell = 0$ (case 7) has the branch cut $\zeta \in [-iq_r, +iq_r]$, and
- $q_r < q_\ell < 0$ (case 8) has the brach cuts $\zeta \in [-iq_r, -iq_\ell]$ and $\zeta \in [iq_\ell, iq_r]$.

With these branch cut choices, $\mathrm{Im}(\zeta_\ell) \gtrless 0$ and $\mathrm{Im}(\zeta_r) \gtrless 0$ when $\mathrm{Im}(\zeta) \gtrless 0$.

If q goes rapidly enough to (4.2) that $N \geq 1$ in (4.3), then (except for branch cuts)

- $e^{ix\zeta_\ell}\phi$ is analytic for $\mathrm{Im}(\zeta_\ell) > 0$ and continuous on $\mathrm{Im}(\zeta_\ell) = 0$,
- $e^{-ix\zeta_r}\psi$ is analytic for $\mathrm{Im}(\zeta_r) > 0$ and continuous on $\mathrm{Im}(\zeta_r) = 0$,
- $e^{-ix\zeta_\ell}\bar{\phi}$ is analytic for $\mathrm{Im}(\zeta_\ell) < 0$ and continuous on $\mathrm{Im}(\zeta_\ell) = 0$, and
- $e^{ix\zeta_r}\bar{\psi}$ is analytic for $\mathrm{Im}(\zeta_r) < 0$ and continuous on $\mathrm{Im}(\zeta_r) = 0$;

see section 4.1.2 for details.

Using the Wronskian, $W(u, v) = u_1 v_2 - u_2 v_1$, we find

$$W(\bar{\psi}, \psi) = 1 + \frac{(\zeta - \zeta_r)^2}{q_r^2} = \frac{2\zeta_r}{\zeta + \zeta_r} \quad \text{and} \quad W(\phi, \bar{\phi}) = 1 + \frac{(\zeta - \zeta_\ell)^2}{q_\ell^2} = \frac{2\zeta_\ell}{\zeta + \zeta_\ell}. \tag{4.6}$$

So ψ and $\bar{\psi}$ are linearly independent except at $\zeta_r = 0$ (or $\zeta = \pm iq_r$). Likewise, ϕ and $\bar{\phi}$ are linearly independent except at $\zeta_\ell = 0$ (or $\zeta = \pm iq_\ell$).

Since these eigenfunctions are linearly independent, we define the scattering eigenfunctions and scattering data a, b, α, and β associated with (4.1) by

$$\phi(\zeta, x) \equiv a(\zeta)\bar{\psi}(\zeta, x) + b(\zeta)\psi(\zeta, x) \quad \text{for } \zeta_r \neq 0, \tag{4.7a}$$

$$\psi(\zeta, x) \equiv \alpha(\zeta)\bar{\phi}(\zeta, x) + \beta(\zeta)\phi(\zeta; x) \quad \text{for } \zeta_\ell \neq 0. \tag{4.7b}$$

From the properties of the Wronskian, we have that

$$a = \frac{W(\phi, \psi)}{W(\bar{\psi}, \psi)}, \qquad b = \frac{W(\phi, \bar{\psi})}{W(\psi, \bar{\psi})}, \qquad \alpha = \frac{W(\psi, \phi)}{W(\bar{\phi}, \phi)}, \qquad \beta = \frac{W(\psi, \bar{\phi})}{W(\phi, \bar{\phi})}; \tag{4.8}$$

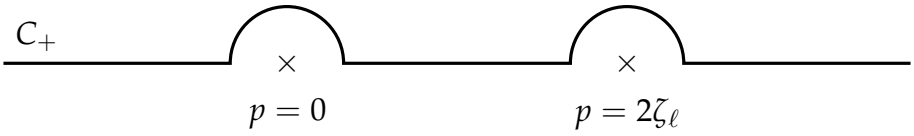

Figure 4.3: The contour C_+.

it's convenient to define

$$\begin{aligned} T_- &\equiv \frac{1}{a} = \frac{W(\bar{\psi}, \psi)}{W(\phi, \psi)}, \quad R_+ \equiv \frac{b}{a} = -\frac{W(\phi, \bar{\psi})}{W(\phi, \psi)}, \\ T_+ &\equiv \frac{1}{\alpha} = \frac{W(\bar{\phi}, \phi)}{W(\psi, \phi)}, \quad R_- \equiv \frac{\beta}{\alpha} = -\frac{W(\psi, \bar{\phi})}{W(\psi, \phi)}; \end{aligned} \tag{4.9}$$

we refer to $T_\pm$ as the transmission coefficients and $R_\pm$ as the reflection coefficients. From the analyticity of ϕ and ψ (see sec. 4.1.2), a and α are analytic in $\mathrm{Im}(\zeta) > 0$, except for the branch cuts; b and β are not necessarily analytic in either the upper- or the lower-half ζ-plane.

4.1.2 Scattering data analyticity

Theorem 4.1.

- *$e^{ix\zeta_\ell}\phi$ can be analytically extended to the upper half ζ_ℓ-plane and tends to* $\begin{pmatrix} 1 \\ 0 \end{pmatrix}$ *as $|\lambda| \to \infty$ (for $\mathrm{Im}(\zeta_\ell) > 0$);*
- *$e^{ix\zeta_r}\bar{\psi}$ can be analytically extended to the lower half ζ_r-plane and tends to* $\begin{pmatrix} 1 \\ 0 \end{pmatrix}$ *as $|\lambda| \to \infty$ (for $\mathrm{Im}(\zeta_r) < 0$).*

Proof. To do this, we use an integral formulation of (4.4).

Let's first consider the analyticity of $e^{ix\zeta_\ell}\phi$: In (4.4), make the change of variables

$$v(x;\zeta) = m(x;\zeta)e^{-ix\zeta_\ell}$$

to get

$$(m_1)_x + i(\zeta - \zeta_\ell)m_1 = q_0(x)m_2,$$
$$(m_2)_x - i(\zeta + \zeta_\ell)m_2 = -q_0(x)m_1,$$

where $q_0(x) \equiv q(x,0)$. In matrix form, this is

$$\begin{pmatrix}(m_1)_x\\(m_2)_x\end{pmatrix} + \begin{pmatrix}i(\zeta-\zeta_\ell) & -q_\ell\\ q_\ell & -i(\zeta+\zeta_\ell)\end{pmatrix}\begin{pmatrix}m_1\\m_2\end{pmatrix} = \begin{pmatrix}(q_0(x)-q_\ell)m_2\\(q_\ell - q_0(x))m_1\end{pmatrix}.$$

So we consider the Green's functions defined by

$$\begin{pmatrix}(G_1)_x\\(G_2)_x\end{pmatrix} + \begin{pmatrix}i(\zeta-\zeta_\ell) & -q_\ell\\ q_\ell & -i(\zeta+\zeta_\ell)\end{pmatrix}\begin{pmatrix}G_1\\G_2\end{pmatrix} = \begin{pmatrix}\delta(x)\\\delta(x)\end{pmatrix}.$$

Taking the Fourier transform gives

$$\begin{pmatrix}i(p+\zeta-\zeta_\ell) & -q_\ell\\ q_\ell & i(p-\zeta-\zeta_\ell)\end{pmatrix}\begin{pmatrix}\hat{G}_1\\\hat{G}_2\end{pmatrix} = \begin{pmatrix}1\\1\end{pmatrix};$$

solving for G and taking the inverse Fourier transform gives

$$\begin{pmatrix}G_1(x;\zeta)\\G_2(x;\zeta)\end{pmatrix} = \frac{1}{2\pi i}\int_C \begin{pmatrix}p-\zeta-\zeta_\ell - iq_\ell\\ p+\zeta-\zeta_\ell+iq_\ell\end{pmatrix}\frac{e^{ipx}\,\mathrm{d}p}{p(p-2\zeta_\ell)},$$

where C_+ is given in figure 4.3. We close C_+ in the lower-half p-plane for G (since we're interested in $x \to -\infty$ for $e^{ix\zeta_\ell}\phi$), and so

$$\begin{pmatrix}G_1(x;\zeta)\\G_2(x;\zeta)\end{pmatrix} = \frac{H(x)}{2\zeta_\ell}\begin{pmatrix}1 & e^{2ix\zeta_\ell}\\ e^{2ix\zeta_\ell} & 1\end{pmatrix}\begin{pmatrix}\zeta+\zeta_\ell+iq_\ell\\-\zeta+\zeta_\ell-iq_\ell\end{pmatrix} \equiv G_\zeta(x),$$

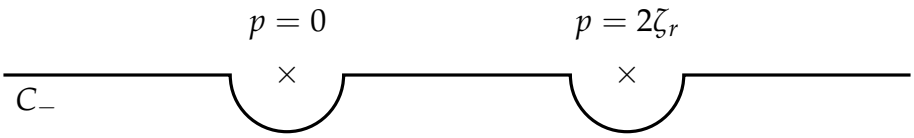

Figure 4.4: The contour C_-.

where $H(x)$ is the Heaviside function. Thus,

$$e^{ix\zeta_\ell}\phi(x;\zeta) = \begin{pmatrix} 1 \\ i\frac{\zeta-\zeta_\ell}{q_\ell} \end{pmatrix} + \int_{-\infty}^{\infty} \begin{pmatrix} G_1(x-y;\zeta)(q_0(y)-q_\ell)\phi_2(y;\zeta) \\ G_2(x-y;\zeta)(q_\ell - q_0(y))\phi_1(y;\zeta) \end{pmatrix} e^{i\zeta_\ell y}\,\mathrm{d}y$$

or

$$\begin{aligned} e^{ix\zeta_\ell}\phi_1(x;\zeta) &= 1 + \frac{1}{2\zeta_\ell}\int_{-\infty}^{x}(q_0(y)-q_\ell)\Big[(\zeta+\zeta_\ell+iq_\ell) \\ &\qquad + e^{2i\zeta_\ell(x-y)}(-\zeta+\zeta_\ell-iq_\ell)\Big]e^{i\zeta_\ell y}\phi_2(y;\zeta)\,\mathrm{d}y, \\ e^{ix\zeta_\ell}\phi_2(x;\zeta) &= \frac{i(\zeta-\zeta_\ell)}{q_\ell} + \frac{1}{2\zeta_\ell}\int_{-\infty}^{x}(q_\ell - q_0(y))\Big[(-\zeta+\zeta_\ell-iq_\ell) \\ &\qquad + e^{2i\zeta_\ell(x-y)}(\zeta+\zeta_\ell+iq_\ell)\Big]e^{i\zeta_\ell y}\phi_1(y;\zeta)\,\mathrm{d}y. \end{aligned}$$

Likewise,

$$e^{ix\zeta_r}\bar{\psi}(x;\zeta) = \begin{pmatrix} 1 \\ i\frac{\zeta-\zeta_r}{q_r} \end{pmatrix} + \int_{-\infty}^{\infty} \begin{pmatrix} H_1(x-y;\zeta)(q_0(y)-q_r)\bar{\psi}_2(y;\zeta) \\ H_2(x-y;\zeta)(q_r - q_0(y))\bar{\psi}_1(y;\zeta) \end{pmatrix} e^{i\zeta_r y}\,\mathrm{d}y,$$

where

$$\begin{pmatrix} H_1(x;\zeta) \\ H_2(x;\zeta) \end{pmatrix} = \frac{H(-x)}{2\zeta_r}\begin{pmatrix} 1 & e^{2ix\zeta_r} \\ e^{2ix\zeta_r} & 1 \end{pmatrix}\begin{pmatrix} -\zeta-\zeta_r-iq_r \\ \zeta-\zeta_r+iq_r \end{pmatrix} \equiv H_\zeta(x),$$

since here we closed C_- (given in fig. 4.4) in the upper-half p-plane. Thus,

$$\begin{aligned} e^{ix\zeta_r}\bar{\psi}_1(x;\zeta) &= 1 + \frac{1}{2\zeta_r}\int_{x}^{\infty}(q_0(y)-q_r)\Big[(-\zeta-\zeta_r-iq_r) \\ &\qquad + e^{-2i\zeta_r(y-x)}(\zeta-\zeta_r+iq_r)\Big]e^{i\zeta_r y}\bar{\psi}_2(y;\zeta)\,\mathrm{d}y, \end{aligned}$$

$$e^{ix\zeta_r}\bar{\psi}_2(x;\zeta) = \frac{i(\zeta-\zeta_r)}{q_r} + \frac{1}{2\zeta_r}\int_x^\infty (q_r - q_0(y))\Big[(\zeta-\zeta_r+iq_r) + e^{-2i\zeta_r(y-x)}(-\zeta-\zeta_r-iq_r)\Big]e^{i\zeta_r y}\bar{\psi}_1(y;\zeta)\,\mathrm{d}y.$$

These are Volterra integral equations, and they can be solved using the Neumann series

$$e^{ix\zeta_\ell}\phi(x;\zeta) = \begin{pmatrix} 1 \\ i\frac{\zeta-\zeta_\ell}{q_\ell} \end{pmatrix} + \sum_{n=1}^{\infty} g_n(x;\zeta), \tag{4.10a}$$

$$e^{ix\zeta_r}\bar{\psi}(x;\zeta) = \begin{pmatrix} 1 \\ i\frac{\zeta-\zeta_r}{q_r} \end{pmatrix} + \sum_{n=1}^{\infty} h_n(x;\zeta), \tag{4.10b}$$

where

$$g_n(x;\zeta) \equiv \int_{-\infty}^{y_n\le\cdots\le y_1\le x} G_\zeta(x-y_1)\cdots G_\zeta(y_{n-1}-y_n) \times (q_0(y_1)-q_\ell)\cdots(q_0(y_n)-q_\ell)\,\mathrm{d}y_n\cdots\mathrm{d}y_1,$$

$$h_n(x;\zeta) \equiv \int_{x\le y_1\le\cdots\le y_n}^{\infty} H_\zeta(x-y_1)\cdots H_\zeta(y_{n-1}-y_n) \times (q_0(y_1)-q_r)\cdots(q_0(y_n)-q_r)\,\mathrm{d}y_n\cdots\mathrm{d}y_1.$$

For $\mathrm{Im}(\zeta_\ell)\ge 0$, $y\ge 0$ implies that $|e^{2i\zeta_\ell y}|\le 1$; so $|G_j(y;\zeta)|\le(1+2|q_\ell|/|\zeta_\ell|)$, for $j=1,2$. Using this bound for $G_\zeta(x)$ gives, for example,

$$\left|e^{ix\zeta_\ell}\phi_1(x;\zeta)\right| \le 1 + \frac{|\zeta-\zeta_\ell|}{|q_\ell|}\left(1+2\frac{|q_\ell|}{|\zeta_\ell|}\right)\int_{-\infty}^{x}|q_0(y)-q_\ell|\,\mathrm{d}y + \left(1+2\frac{|q_\ell|}{|\zeta_\ell|}\right)^2\int_{-\infty}^{x}\int_{-\infty}^{y}|q_0(y)-q_\ell||q_0(z)-q_\ell|\left|e^{iz\zeta_\ell}\phi_1(z;\zeta)\right|\,\mathrm{d}z\,\mathrm{d}y.$$

So using $|\zeta - \zeta_\ell|/|q_\ell| \leq 1$ gives

$$|g_n(x;\zeta)| \leq \left(1 + 2\frac{|q_\ell|}{|\zeta_\ell|}\right)^n \frac{\left(\int_{-\infty}^x |q_0(y) - q_\ell| \, \mathrm{d}y\right)^n}{n!}$$

and

$$\left|e^{ix\zeta_\ell}\phi(x;\zeta)\right| \leq \exp\left\{\left(1 + 2\frac{|q_\ell|}{|\zeta_\ell|}\right)\int_{-\infty}^x |q_0(y) - q_\ell| \, \mathrm{d}y\right\} < \infty \tag{4.11}$$

for finite x.

This estimate (4.11) blows up for small ζ_ℓ. So, for small ζ_ℓ, we use $|G_j(y;\zeta)| \leq 1 + 2|q_\ell|y$, for $j = 1, 2$. Using this gives, for example,

$$\begin{aligned}\left|e^{ix\zeta_\ell}\phi_1(x;\zeta)\right| \leq 1 + \frac{|\zeta - \zeta_\ell|}{|q_\ell|}\int_{-\infty}^x \{1 + 2|q_\ell|(x-y)\}|q_0(y) - q_\ell| \, \mathrm{d}y \\ + \int_{-\infty}^x \int_{-\infty}^y \{1 + 2|q_\ell|(x-y)\}\{1 + 2|q_\ell|(y-z)\} \\ \times |q_0(y) - q_\ell||q_0(z) - q_\ell| \left|e^{iz\zeta_\ell}\phi_1(z;\zeta)\right| \, \mathrm{d}z \, \mathrm{d}y;\end{aligned}$$

using $|\zeta - \zeta_\ell|/|q_\ell| \leq 1$ again gives

$$|g_n(x;\zeta)| \leq \frac{\left(\int_{-\infty}^x \{1 + 2|q_\ell|(x-y)\}|q_0(y) - q_\ell| \, \mathrm{d}y\right)^n}{n!},$$

and summing gives

$$\left|e^{ix\zeta_\ell}\phi(x;\zeta)\right| \leq \exp\left\{\int_{-\infty}^x \{1 + 2|q_\ell|(x-y)\}|q_0(y) - q_\ell| \, \mathrm{d}y\right\} < \infty$$

for finite x. Therefore, we find that $e^{ix\zeta_\ell}\phi$ is analytic in $\mathrm{Im}(\zeta_\ell) > 0$ and continuous in $\mathrm{Im}(\zeta_\ell) \geq 0$ if $N \geq 1$ in (4.3).

Like the non-decaying KdV, it can be shown using the same techniques that $e^{ix\zeta_\ell}\phi(x;\zeta)$ is N-fold differentiable (with respect to ζ_ℓ, for finite x) on $\mathrm{Im}(\zeta_\ell) = 0$ and $\zeta_\ell \neq 0$ and is $(N-1)$-fold differentiable at $\zeta_\ell = 0$, where N is given in (4.3).

Likewise, $e^{ix\zeta_r}\bar{\psi}(x;\zeta)$ is analytic in $\mathrm{Im}(\zeta_r) < 0$ and continuous in $\mathrm{Im}(\zeta_r) \leq 0$, $\zeta_r \neq 0$ when $N = 1$ in (4.3); for $N > 1$, then $e^{ix\zeta_r}\bar{\psi}(x;\zeta)$ is also continuous at $\zeta_r = 0$. Moreover, $e^{ix\zeta_r}\bar{\psi}(x;\zeta)$ is N-fold differentiable (with respect to ζ_r, for finite x) on $\mathrm{Im}(\zeta_r) = 0$ and $\zeta_r \neq 0$ and is $(N-1)$-fold differentiable at $\zeta_r = 0$.

Following the same techniques, if

$$\int_{-\infty}^{\infty} |q(x,t) - q_\ell H(-x) - q_r H(x)| e^{d|x|}\,\mathrm{d}x < \infty,$$

then $e^{ix\zeta_\ell}\phi(x;\zeta)$ is analytic for $\mathrm{Im}(\zeta_\ell) > -d$ and $e^{ix\zeta_r}\bar{\psi}(x;\zeta)$ is analytic for $\mathrm{Im}(\zeta_r) < d$.

□

4.1.3 Time evolution

The eigenfunctions evolve (see Ablowitz et al., 1974) as

$$v_t = \begin{pmatrix} A & B \\ C & -A \end{pmatrix} v, \tag{4.12}$$

where $A = -4i\zeta^3 + 2i\zeta q^2$, $B = 4\zeta^2 q + 2i\zeta q_x - 2q^3 - q_{xx}$, and $C = -4\zeta^2 q + 2i\zeta q_x + 2q^3 + q_{xx}$. If we take the limit $x \to -\infty$, so $q \to q_\ell$, then

$$v_t = \begin{pmatrix} -4i\zeta^3 + 2i\zeta q_\ell^2 & 4\zeta^2 q_\ell - 2q_\ell^3 \\ -4\zeta^2 q_\ell + 2q_\ell^3 & 4i\zeta^3 - 2i\zeta q_\ell^2 \end{pmatrix} v;$$

this is satisfied by $\phi e^{A_- t}$ and $\bar{\phi} e^{-A_- t}$, where

$$A_- \equiv 2i(q_\ell^2 - 2\zeta^2)\zeta_\ell.$$

So we have that

$$\phi_t = \begin{pmatrix} A - A_- & B \\ C & -A - A_- \end{pmatrix} \phi \quad \text{and} \quad \bar{\phi}_t = \begin{pmatrix} A + A_- & B \\ C & -A + A_- \end{pmatrix} \bar{\phi}.$$

Likewise, if we take the limit $x \to +\infty$ in (4.12), so $q \to q_r$, then it's satisfied by $\psi e^{-A_+ t}$ and $\bar{\psi} e^{A_+ t}$, where

$$A_+ \equiv 2i(q_r^2 - 2\zeta^2)\zeta_r.$$

From this time evolution of the eigenfunctions, we find how the scattering data evolves from (4.7): we find

$$a(\zeta, t) = a(\zeta, 0)e^{(A_+ - A_-)t} = a(\zeta, 0)e^{i\left[4(\zeta_\ell - \zeta_r)\zeta^2 - 2(q_\ell^2 \zeta_\ell - q_r^2 \zeta_r)\right]t}, \tag{4.13a}$$

$$b(\zeta, t) = b(\zeta, 0)e^{-(A_+ + A_-)t} = b(\zeta, 0)e^{i\left[4(\zeta_\ell + \zeta_r)\zeta^2 - 2(q_\ell^2 \zeta_\ell + q_r^2 \zeta_r)\right]t}, \tag{4.13b}$$

$$\alpha(\zeta, t) = \alpha(\zeta, 0)e^{(A_+ - A_-)t} = \alpha(\zeta, 0)e^{i\left[4(\zeta_\ell - \zeta_r)\zeta^2 - 2(q_\ell^2 \zeta_\ell - q_r^2 \zeta_r)\right]t}, \tag{4.13c}$$

$$\beta(\zeta, t) = \beta(\zeta, 0)e^{(A_+ + A_-)t} = \beta(\zeta, 0)e^{-i\left[4(\zeta_\ell + \zeta_r)\zeta^2 - 2(q_\ell^2 \zeta_\ell + q_r^2 \zeta_r)\right]t}. \tag{4.13d}$$

From the reflection coefficient definitions (4.9),

$$R_+(\zeta, t) = R_+(\zeta, 0)e^{4i(2\zeta^2 \zeta_r - q_r^2 \zeta_r)t} \quad \text{and} \quad R_-(\zeta, t) = R_-(\zeta, 0)e^{-4i(2\zeta^2 \zeta_\ell - q_\ell^2 \zeta_\ell)t}. \tag{4.13e}$$

4.1.4 Derivation of GLM integral equation

From the scattering data — which we have for all time t — we derive the GLM integral equations, which can then be used to compute $q(x, t)$. To derive the GLM integral equations, we first derive some properties about the scattering data and eigenfunctions (such as symmetries and connection formulas). Then we find a triangular representation of the eigenfunctions and show that its kernel can be used to find $q(x, t)$. We substitute these triangular representations into (4.4), integrate over an appropriate contour, and,

after simplification, get the GLM integral equations.

Scattering data symmetries

From (4.6) and (4.8), we have that

$$a = \frac{\zeta_\ell(\zeta + \zeta_r)}{\zeta_r(\zeta + \zeta_\ell)}\alpha, \qquad \zeta_r \neq 0, \zeta_\ell \neq 0. \tag{4.14}$$

From (4.4) and (4.5), we have that

$$\bar{\psi}(x,\zeta,\zeta_r) = \begin{pmatrix} \psi_2(x,\zeta^*,\zeta_r^*) \\ -\psi_1(x,\zeta^*,\zeta_r^*) \end{pmatrix}^* \quad \text{and} \quad \phi(x,\zeta,\zeta_\ell) = \begin{pmatrix} \bar{\phi}_2(x,\zeta^*,\zeta_\ell^*) \\ -\bar{\phi}_1(x,\zeta^*,\zeta_\ell^*) \end{pmatrix}^*, \tag{4.15}$$

where $*$ denotes complex conjugate. We also have that

$$\bar{\psi}(x,\zeta,\zeta_r) = \begin{pmatrix} \psi_2(x,-\zeta,-\zeta_r) \\ -\psi_1(x,-\zeta,-\zeta_r) \end{pmatrix} \quad \text{and} \quad \phi(x,\zeta,\zeta_\ell) = \begin{pmatrix} \bar{\phi}_2(x,-\zeta,-\zeta_\ell) \\ -\bar{\phi}_1(x,-\zeta,-\zeta_\ell) \end{pmatrix} \tag{4.16}$$

and

$$[\psi(x,\zeta^*,-\zeta_r^*)]^* = i\frac{\zeta+\zeta_r}{q_r}\begin{pmatrix} -\psi_2(x,\zeta,\zeta_r) \\ \psi_1(x,\zeta,\zeta_r) \end{pmatrix}, \tag{4.17}$$

$$[\phi(x,\zeta^*,-\zeta_\ell^*)]^* = i\frac{\zeta+\zeta_\ell}{q_\ell}\begin{pmatrix} \phi_2(x,\zeta,\zeta_\ell) \\ -\phi_1(x,\zeta,\zeta_\ell) \end{pmatrix}.$$

A triangular representations

We'll assume that ψ, $\bar{\psi}$, ϕ, and $\bar{\phi}$ have the following triangular representations:

$$\psi(\zeta,x;t) = \begin{pmatrix} i\frac{\zeta-\zeta_r}{q_r} \\ 1 \end{pmatrix} e^{ix\zeta_r} + \int_x^\infty \mathbf{K}_+(x,s;t)\begin{pmatrix} i\frac{\zeta-\zeta_r}{q_r} \\ 1 \end{pmatrix} e^{is\zeta_r}\,\mathrm{d}s, \tag{4.18a}$$

$$\bar{\psi}(\zeta,x;t)=\begin{pmatrix}1\\ i\frac{\zeta-\zeta_r}{q_r}\end{pmatrix}e^{-ix\zeta_r}+\int_x^\infty \bar{\mathbf{K}}_+(x,s;t)\begin{pmatrix}1\\ i\frac{\zeta-\zeta_r}{q_r}\end{pmatrix}e^{-is\zeta_r}\,\mathrm{d}s, \tag{4.18b}$$

$$\phi(\zeta,x;t)=\begin{pmatrix}1\\ i\frac{\zeta-\zeta_\ell}{q_\ell}\end{pmatrix}e^{-ix\zeta_\ell}+\int_{-\infty}^x \mathbf{K}_-(x,s;t)\begin{pmatrix}1\\ i\frac{\zeta-\zeta_\ell}{q_\ell}\end{pmatrix}e^{-is\zeta_\ell}\,\mathrm{d}s, \tag{4.18c}$$

$$\bar{\phi}(\zeta,x;t)=\begin{pmatrix}i\frac{\zeta-\zeta_\ell}{q_\ell}\\ 1\end{pmatrix}e^{ix\zeta_\ell}+\int_{-\infty}^x \bar{\mathbf{K}}_-(x,s;t)\begin{pmatrix}i\frac{\zeta-\zeta_\ell}{q_\ell}\\ 1\end{pmatrix}e^{is\zeta_\ell}\,\mathrm{d}s, \tag{4.18d}$$

where $\mathbf{K}_\pm$ and $\bar{\mathbf{K}}_\pm$ are 2×2 matrices.

To find $q(x)$ from $\mathbf{K}_\pm$ or $\bar{\mathbf{K}}_\pm$, we substitute (4.18) into (4.4), use integration-by-parts, and group like terms. For example, let's consider

$$\psi(\zeta,x;t)=v_+(\zeta)e^{ix\zeta_r}+\int_x^\infty \mathbf{K}_+(x,s;t)e^{is\zeta_r}v_+(\zeta)\,\mathrm{d}s,$$

where

$$\mathbf{K}_+\equiv\begin{pmatrix}K_{11}^+ & K_{12}^+\\ K_{21}^+ & K_{22}^+\end{pmatrix}\quad\text{and}\quad v_+(\zeta)\equiv\begin{pmatrix}v_1^+\\ v_2^+\end{pmatrix}=\begin{pmatrix}i\frac{\zeta-\zeta_r}{q_r}\\ 1\end{pmatrix};$$

differentiating with respect to x gives

$$\frac{\partial\psi}{\partial x}=i\zeta_r v_+(\zeta)e^{ix\zeta_r}-\mathbf{K}_+(x,x;t)e^{ix\zeta_r}v_+(\zeta)+\int_x^\infty\left(\frac{\partial}{\partial x}\mathbf{K}_+(x,s;t)\right)e^{is\zeta_r}v_+(\zeta)\,\mathrm{d}s.$$

Substituting these into

$$(v_1)_x=-i\zeta v_1+q(x)v_2$$

gives

$$\begin{aligned}\left[i\zeta_r v_1^+-(K_{11}^+v_1^++K_{12}^+v_2^+)\right]e^{ix\zeta_r}+\int_x^\infty(\partial_xK_{11}^+v_1^++\partial_xK_{12}^+v_2^+)e^{is\zeta_r}\,\mathrm{d}s=\\ -i\zeta\left(v_1^+e^{ix\zeta_r}+\int_x^\infty(K_{11}^+v_1^++K_{12}^+v_2^+)e^{is\zeta_r}\,\mathrm{d}s\right)\end{aligned}$$

$$+ q(x)\left(v_2^+ e^{ix\zeta_r} + \int_x^\infty (K_{21}^+ v_1^+ + K_{22}^+ v_2^+) e^{is\zeta_r}\,\mathrm{d}s\right)$$

or

$$\begin{aligned}\left[i(\zeta+\zeta_r)v_1^+ - K_{11}^+ v_1^+ - K_{12}^+ v_2^+ - q(x)v_2^+\right] e^{ix\zeta_r} \\ = \int_x^\infty \Big(- \partial_x K_{11}^+ v_1^+ - i\zeta K_{12}^+ v_2^+ + q(x) K_{21}^+ v_1^+ \\ - \partial_x K_{12}^+ v_2^+ - i\zeta K_{11}^+ v_1^+ + q(x) K_{22}^+ v_2^+ \Big) e^{is\zeta_r}\,\mathrm{d}s.\end{aligned}$$

From integration-by-parts, we have that

$$K_{ij}^+(x,x;t) v_j^+ e^{ix\zeta_r} = -i\zeta_r \int_x^\infty K_{ij}^+(x,s;t) e^{is\zeta_r} v_j^+\,\mathrm{d}s - \int_x^\infty \left(\frac{\partial}{\partial s} K_{ij}^+(x,s;t)\right) e^{is\zeta_r} v_j^+\,\mathrm{d}s.$$

So adding $(K_{11}^+ v_1^+ - K_{12}^+ v_2^+) e^{ix\zeta_r}$ to both sides and using this identity gives

$$\begin{aligned}\left[i(\zeta_r+\zeta)v_1^+ - 2K_{12}^+ v_2^+ - q(x)v_2^+\right] e^{ix\zeta_r} \\ = \int_x^\infty \Big[- (\partial_x + \partial_s) K_{11}^+ v_1^+ + i(\zeta_r - \zeta) K_{12}^+ v_2^+ + q(x) K_{21}^+ v_1^+ \\ - (\partial_x - \partial_s) K_{12}^+ v_2^+ - i(\zeta_r + \zeta) K_{11}^+ v_1^+ + q(x) K_{22}^+ v_2^+ \Big] e^{is\zeta_r}\,\mathrm{d}s.\end{aligned}$$

Using $v_1^+ / v_2^+ = i(\zeta - \zeta_r)/q_r$ and $\zeta_r^2 - \zeta^2 = q_r^2$, gives

$$\begin{aligned}\left[q_r - 2K_{12}^+ - q(x)\right] v_2^+ e^{ix\zeta_r} = \int_x^\infty \Big\{ \left[-(\partial_x + \partial_s) K_{11}^+ - q_r K_{12}^+ + q(x) K_{21}^+\right] v_1^+ \\ + \left[-(\partial_x - \partial_s) K_{12}^+ - q_r K_{11}^+ + q(x) K_{22}^+\right] v_2^+ \Big\} e^{is\zeta_r}\,\mathrm{d}s.\end{aligned}$$

Therefore, we have that

$$\begin{aligned} q(x) &= q_r - 2K_{12}^+, \\ (\partial_x + \partial_s) K_{11}^+ &= -q_r K_{12}^+ + q(x) K_{21}^+, \end{aligned}$$

$$(\partial_x - \partial_s)K_{12}^+ = -q_r K_{11}^+ + q(x)K_{22}^+.$$

Likewise, for $(v_2)_x = -q(x)v_1 + i\zeta v_2$, we get

$$\begin{aligned}\left[i(\zeta_r - \zeta)v_2^+ - 2K_{21}^+ v_1^+ + q(x)v_1^+\right] e^{ix\zeta_r} \\ = \int_x^\infty \Big[&- (\partial_x - \partial_s)K_{21}^+ v_1^+ + i(\zeta - \zeta_r)K_{22}^+ v_2^+ - q(x)K_{11}^+ v_1^+ \\ &- (\partial_x + \partial_s)K_{22}^+ v_2^+ + i(\zeta + \zeta_r)K_{21}^+ v_1^+ - q(x)K_{12}^+ v_2^+ \Big] e^{is\zeta_r}\,\mathrm{d}s.\end{aligned}$$

Again, using $v_1^+ / v_2^+ = i(\zeta - \zeta_r)/q_r$ and $\zeta_r^2 - \zeta^2 = q_r^2$ gives

$$\begin{aligned}\left[-q_r - 2K_{21}^+ + q(x)\right] v_1^+ e^{ix\zeta_r} \\ = \int_x^\infty \Big\{ &\left[-(\partial_x - \partial_s)K_{21}^+ - q(x)K_{11}^+ + q_r K_{22}^+\right] v_1^+ \\ &+ \left[-(\partial_x + \partial_s)K_{22}^+ - q(x)K_{12}^+ + q_r K_{21}^+\right] v_2^+ \Big\} e^{is\zeta_r}\,\mathrm{d}s.\end{aligned}$$

Combining this with what we had before, we get the Goursat problem

$$\begin{aligned}(\partial_x + \partial_s)\begin{pmatrix} K_{11}^+ \\ K_{22}^+ \end{pmatrix} &= \begin{pmatrix} -q_r & q(x) \\ -q(x) & q_r \end{pmatrix}\begin{pmatrix} K_{12}^+ \\ K_{21}^+ \end{pmatrix}, \\ (\partial_x - \partial_s)\begin{pmatrix} K_{12}^+ \\ K_{21}^+ \end{pmatrix} &= \begin{pmatrix} -q_r & q(x) \\ -q(x) & q_r \end{pmatrix}\begin{pmatrix} K_{11}^+ \\ K_{22}^+ \end{pmatrix},\end{aligned}$$

with the boundary conditions

$$\begin{aligned}q(x) = q_r - 2K_{12}^+(x,x) = q_r + 2K_{21}^+(x,x), \qquad (4.19) \\ \lim_{s\to\infty} K_{ij}(x,s) = 0.\end{aligned}$$

This implies that $K_{12}^+(x,x) = -K_{21}^+(x,x)$ and $K_{11}^+(x,x) = K_{22}^+(x,x)$. We can use (4.17) to

show that $\mathbf{K}_+$ is real. Using (4.15) and (4.16) gives that $\mathbf{K}_+ = \bar{\mathbf{K}}_+$.

Inverse problem from the right

For $q_\ell^2 > q_r^2$, ζ is pure imaginary and ζ_ℓ is real when $\zeta_r \in \left[0, i\sqrt{q_\ell^2 - q_r^2}\right]$. So, from (4.4) and (4.5),

$$\phi^* = i\frac{\zeta + \zeta_\ell}{q_\ell}\bar{\phi} \quad \text{and} \quad \psi = \psi^* \quad \text{for } \zeta_r \in \left[0, i\sqrt{q_\ell^2 - q_r^2}\right]; \tag{4.20}$$

using these and (4.9) gives

$$R_- = i\frac{\zeta + \zeta_\ell}{q_\ell}\frac{\alpha^*}{\alpha} \quad \text{for } \zeta_r \in \left[0, i\sqrt{q_\ell^2 - q_r^2}\right]. \tag{4.21}$$

Across the cut, we have — from (4.5), (4.8), and (4.20) — that

$$\left(\frac{\phi}{\alpha}\right)_{\zeta_\ell = -|\zeta_\ell|} = \left(\frac{\phi^*}{\alpha^*}\right)_{\zeta_\ell = |\zeta_\ell|} \quad \text{for } \zeta_r \in \left[0, i\sqrt{q_\ell^2 - q_r^2}\right]. \tag{4.22}$$

Using (4.9) to rewrite (4.7) gives

$$T_-(\zeta, t)\phi(\zeta, x; t) = \bar{\psi}(\zeta, x; t) + R_+(\zeta, t)\psi(\zeta, x; t).$$

Substituting (4.18) into this gives

$$\begin{aligned} T_-(\zeta, t)\phi(\zeta, x; t) = &\begin{pmatrix} 1 \\ i\frac{\zeta - \zeta_r}{q_r} \end{pmatrix} e^{-ix\zeta_r} + \int_x^\infty \mathbf{K}_+(x, s; t) \begin{pmatrix} 1 \\ i\frac{\zeta - \zeta_r}{q_r} \end{pmatrix} e^{-is\zeta_r}\, \mathrm{d}s \\ &+ R_+(\zeta, t)\left\{ \begin{pmatrix} i\frac{\zeta - \zeta_r}{q_r} \\ 1 \end{pmatrix} e^{ix\zeta_r} + \int_x^\infty \mathbf{K}_+(x, s; t) \begin{pmatrix} i\frac{\zeta - \zeta_r}{q_r} \\ 1 \end{pmatrix} e^{is\zeta_r}\, \mathrm{d}s \right\}. \end{aligned}$$

Multiply this by $e^{iy\zeta_r}$ and consider

$$\left(T_- \phi e^{ix\zeta_r} - \begin{pmatrix} 1 \\ i\frac{\zeta-\zeta_r}{q_r} \end{pmatrix} \right) e^{i(y-x)\zeta_r} = \int_x^\infty \mathbf{K}_+(x,s;t) \begin{pmatrix} 1 \\ i\frac{\zeta-\zeta_r}{q_r} \end{pmatrix} e^{i(y-s)\zeta_r}\,\mathrm{d}s$$
$$+ R_+(\zeta,t) \left\{ \begin{pmatrix} i\frac{\zeta-\zeta_r}{q_r} \\ 1 \end{pmatrix} e^{i(x+y)\zeta_r} + \int_x^\infty \mathbf{K}_+(x,s;t) \begin{pmatrix} i\frac{\zeta-\zeta_r}{q_r} \\ 1 \end{pmatrix} e^{i(y+s)\zeta_r}\,\mathrm{d}s \right\}. \quad (4.23)$$

Operating on (4.23) with $(2\pi)^{-1}\int_{-\infty}^{\infty}\mathrm{d}\zeta_r$, interchanging integrals, and using $\delta(x) = (2\pi)^{-1}\int_{-\infty}^{\infty} e^{i\zeta_r x}\,\mathrm{d}\zeta_r$ gives

$$\frac{1}{2\pi}\int_{-\infty}^{\infty}\int_x^\infty \mathbf{K}_+(x,s;t) \begin{pmatrix} 1 \\ i\frac{\zeta-\zeta_r}{q_r} \end{pmatrix} e^{i(y-s)\zeta_r}\,\mathrm{d}s\,\mathrm{d}\zeta_r$$
$$= \frac{1}{2\pi}\int_x^\infty \mathbf{K}_+(x,s;t)\int_{-\infty}^{\infty} \begin{pmatrix} 1 \\ \frac{-iq_r}{\zeta+\zeta_r} \end{pmatrix} e^{i(y-s)\zeta_r}\,\mathrm{d}\zeta_r\,\mathrm{d}s$$
$$= \int_x^\infty \mathbf{K}_+(x,s;t) \begin{pmatrix} \delta(y-s) \\ 0 \end{pmatrix} \mathrm{d}s = \begin{pmatrix} K_{11}^+(x,y;t) \\ K_{21}^+(x,y;t) \end{pmatrix},$$

where we've used that $(\zeta-\zeta_r)/q_r = -q_r/(\zeta+\zeta_r)$, and

$$\frac{1}{2\pi}\int_{-\infty}^{\infty} R_+(\zeta,t)\int_x^\infty \mathbf{K}_+(x,s;t) \begin{pmatrix} i\frac{\zeta-\zeta_r}{q_r} \\ 1 \end{pmatrix} e^{i(y+s)\zeta_r}\,\mathrm{d}s\,\mathrm{d}\zeta_r$$
$$= \frac{1}{2\pi}\int_x^\infty \mathbf{K}_+(x,s;t)\int_{-\infty}^{\infty} R_+(\zeta,t) \begin{pmatrix} i\frac{\zeta-\zeta_r}{q_r} \\ 1 \end{pmatrix} e^{i(y+s)\zeta_r}\,\mathrm{d}\zeta_r\,\mathrm{d}s$$
$$= \int_x^\infty \mathbf{K}_+(x,s;t)F(y+s)\,\mathrm{d}s,$$

where

$$F(z;t) \equiv \frac{1}{2\pi}\int_{-\infty}^{\infty} R_+(\zeta,t) \begin{pmatrix} i\frac{\zeta-\zeta_r}{q_r} \\ 1 \end{pmatrix} e^{iz\zeta_r}\,\mathrm{d}\zeta_r. \quad (4.24)$$

Therefore,

$$\begin{pmatrix} K_{11}^{+}(x,y;t) \\ K_{21}^{+}(x,y;t) \end{pmatrix} + F(x+y;t) + \int_x^\infty \mathbf{K}_+(x,s;t)F(y+s)\,\mathrm{d}s = I,$$

with

$$I \equiv \frac{1}{2\pi}\int_{-\infty}^{\infty}\left\{ T_-\phi e^{ix\zeta_r} - \begin{pmatrix} 1 \\ i\frac{\zeta-\zeta_r}{q_r} \end{pmatrix} \right\} e^{i(y-x)\zeta_r}\,\mathrm{d}\zeta_r \equiv I_b + I_p.$$

Since $e^{ix\zeta_\ell}\phi(\zeta,x;t)$ is analytic in the upper-half ζ_r-plane and $y > x$, we can close I in the upper-half ζ_r-plane. Here, I_b is the contribution from the branch cut (when $q_\ell^2 > q_r^2$) and I_p is the contribution from the zeros of $a(\zeta,t)$.

The branch points of $e^{ix\zeta_r}\phi$ in the ζ_r-plane are the branch points of ζ and ζ_ℓ. The branch points of ζ are $\zeta_r = \pm q_r$; the branch points of ζ_ℓ are $\zeta_r = \pm q_+$, where

$$q_+ \equiv i\sqrt{q_\ell^2 - q_r^2},$$

which is pure-imaginary when $q_\ell^2 > q_r^2$. Thus, we must integrate around $\zeta_r \in [0, q_+]$ in the upper-half ζ_r-plane.

The contribution from the branch-cut is

$$\begin{aligned} I_b &= \lim_{\varepsilon\to 0}\frac{1}{2\pi}\left(\int_{0-\varepsilon}^{q_+-\varepsilon} - \int_{0+\varepsilon}^{q_++\varepsilon}\right)\left\{ \frac{e^{ix\zeta_r}\phi}{a} - \begin{pmatrix} 1 \\ i\frac{\zeta-\zeta_r}{q_r} \end{pmatrix} \right\} e^{i\zeta_r(y-x)}\,\mathrm{d}\zeta_r \\ &= \frac{1}{2\pi}\int_0^{q_+}\left\{ \left(\frac{\phi}{a}\right)_{\zeta_\ell=-|\zeta_\ell|} - \left(\frac{\phi}{a}\right)_{\zeta_\ell=|\zeta_\ell|} \right\} e^{iy\zeta_r}\,\mathrm{d}\zeta_r. \end{aligned}$$

Using (4.14) gives

$$I_b = \frac{1}{2\pi}\int_0^{q_+}\left\{ \left(\frac{\zeta+\zeta_\ell}{\zeta_\ell}\frac{\phi}{\alpha}\right)_{\zeta_\ell=-|\zeta_\ell|} - \left(\frac{\zeta+\zeta_\ell}{\zeta_\ell}\frac{\phi}{\alpha}\right)_{\zeta_\ell=|\zeta_\ell|} \right\} e^{iy\zeta_r}\frac{\zeta_r\,\mathrm{d}\zeta_r}{\zeta+\zeta_r}.$$

Using (4.22) gives

$$I_b = \frac{1}{2\pi}\int_0^{q_+}\left(\frac{\zeta_\ell-\zeta}{\zeta_\ell}\frac{\phi^*}{\alpha^*}-\frac{\zeta+\zeta_\ell}{\zeta_\ell}\frac{\phi}{\alpha}\right)_{\zeta_\ell=|\zeta_\ell|} e^{iy\zeta_r}\frac{\zeta_r\,\mathrm{d}\zeta_r}{\zeta+\zeta_r}$$
$$= \frac{1}{2\pi}\int_0^{q_+}\left[\frac{1}{\zeta_\ell\alpha^*}\left((\zeta_\ell-\zeta)\phi^*-(\zeta+\zeta_\ell)\frac{\alpha^*}{\alpha}\phi\right)\right]_{\zeta_\ell=|\zeta_\ell|} e^{iy\zeta_r}\frac{\zeta_r\,\mathrm{d}\zeta_r}{\zeta+\zeta_r}.$$

Using (4.20) and (4.21) gives

$$I_b = \frac{1}{2\pi}\int_0^{q_+}\left[\frac{iq_\ell}{\zeta_\ell\alpha^*}\left(\bar{\phi}+R_-\phi\right)\right]_{\zeta_\ell=|\zeta_\ell|} e^{iy\zeta_r}\frac{\zeta_r\,\mathrm{d}\zeta_r}{\zeta+\zeta_r}.$$

Using (4.7) gives

$$I_b = \frac{1}{2\pi}\int_0^{q_+}\left(\frac{iq_\ell}{\zeta_\ell|\alpha|^2}\psi\right)_{\zeta_\ell=|\zeta_\ell|} e^{iy\zeta_r}\frac{\zeta_r\,\mathrm{d}\zeta_r}{\zeta+\zeta_r}.$$

Making the variable change from ζ_r to ζ_ℓ gives

$$I_b = -\frac{1}{2\pi}\int_0^{\sqrt{q_\ell^2-q_r^2}}\frac{iq_\ell}{\zeta+\zeta_r}|T_+|^2\psi e^{-y\sqrt{q_\ell^2-q_r^2-\zeta_\ell^2}}\,\mathrm{d}\zeta_\ell.$$

Note that both ζ and ζ_r are pure-imaginary when $\zeta_\ell\in\left(0,\sqrt{q_\ell^2-q_r^2}\right)$.

The contributions from the zeros of $a(\zeta,t)$ are

$$I_p = -i\sum_j \mathrm{Res}\left(\frac{\phi e^{iy\zeta_r}}{a},\zeta=\zeta_j\right) = -\sum_j C_j(t)\psi(\zeta_j,x;t)e^{iy\zeta_r(\zeta_j)},$$

where the constants $\{\zeta_j\}_{j=1}^M$ are the simple zeros of $a(\zeta,t)$ (multiple roots are obtained as a limiting case of coalescing simple zeros) and

$$C_j(t) = i\frac{b(\zeta_j,t)}{[\partial_{\zeta_r}a(\zeta,t)]_{\zeta=\zeta_j}}.$$

Using (4.18a) then gives

$$\begin{pmatrix} K_{11}^{+}(x,y;t) \\ K_{21}^{+}(x,y;t) \end{pmatrix} + \mathbf{\Omega}(x+y;t) + \int_x^\infty \mathbf{K}_+(x,s;t)\mathbf{\Omega}(y+s)\,\mathrm{d}s = 0, \tag{4.25a}$$

with

$$\begin{aligned} \mathbf{\Omega}(z;t) &\equiv F(z;t) + G(z;t) + H(z;t) \\ &\equiv \frac{1}{2\pi}\int_{-\infty}^{\infty} R_+(\zeta,t) \begin{pmatrix} i\frac{\zeta-\zeta_r}{q_r} \\ 1 \end{pmatrix} e^{iz\zeta_r}\,\mathrm{d}\zeta_r + \sum_j \left[C_j(t) \begin{pmatrix} i\frac{\zeta-\zeta_r}{q_r} \\ 1 \end{pmatrix} e^{iz\zeta_r} \right]_{\zeta=\zeta_j} \\ &\quad + \frac{1}{2\pi}\int_0^{\sqrt{q_\ell^2-q_r^2}} \frac{iq_\ell}{\zeta+\zeta_r} \left|T_+(\zeta,t)\right|^2 \begin{pmatrix} i\frac{\zeta-\zeta_r}{q_r} \\ 1 \end{pmatrix} e^{-z\sqrt{q_\ell^2-q_r^2-\zeta_\ell^2}}\,\mathrm{d}\zeta_\ell \end{aligned} \tag{4.25b}$$

and

$$\mathbf{K}_+ = \begin{pmatrix} K_{11}^{+} & -K_{21}^{+} \\ K_{21}^{+} & K_{11}^{+} \end{pmatrix},$$

since $K_{12}^{+} = -K_{21}^{+}$ and $K_{22}^{+} = K_{11}^{+}$.

4.2 Long time asymptotic approximation

In this section, we use (4.25) to asymptotically compute the behavior at the front of the DSW for case 3 in figure 4.2, where $q_\ell > 0$ and $q_r = 0$; the other cases will be considered in subsequent publications. We omit any contributions from the poles, since these move to the right of the DSW in the long-time limit, and so they do not affect the DSW in this limit. When this asymptotic solution breaks down, we use matched asymptotics to find the DSW's slowly varying elliptic-function solution; this method naturally leads to Whitham-like equations. Finally, we show that the solution to the DSW's left decays.

4.2.1 Shock front

Approximation to the far right of the shock front

For large $x/t \gg 1$, we can use a linear approximation of (4.1):

$$q_t + q_{3x} + O(q^3) = 0.$$

The ansatz $q = \exp\{i(\lambda x - \omega t)\}$ gives the dispersion relationship $q(\lambda) = -\lambda^3$. So

$$q(x,t) \sim \frac{1}{2\pi} \int_{-\infty}^{\infty} \hat{w}_0(\lambda) e^{i\lambda(x/t+\lambda^2)t} \, \mathrm{d}\lambda,$$

where $\hat{w}_0(\lambda) = \hat{q}_0(\lambda) + 2\pi q_\ell \delta(\lambda)$. For large t and $x \gg 4q_\ell^2 t$, we can use the steepest-descent method to find

$$q(x,t) = \frac{\hat{q}_0\left(i\sqrt{x/(3t)}\right) e^{-2t[x/(3t)]^{3/2}}}{4\sqrt{3\pi}[x/(3t)]^{1/4}\sqrt{t}} \left(1 + O(t^{-1/2})\right), \tag{4.26}$$

where we have assumed that q decays rapidly enough that $\hat{q}_0(i\kappa)$ is defined. Higher-order contributions from the nonlinear terms are exponentially small compared with (4.26). Thus, the solution is asymptotically zero for $x/t \gg 1$ (except, perhaps, for solitons).

The GLM integral equation

To find the behavior near the shock front, we use the GLM integral equation from the right (4.25); using that $q_\ell > 0$ and $q_r = 0$ gives

$$\begin{pmatrix} K_{11}^+(x,y;t) \\ K_{21}^+(x,y;t) \end{pmatrix} + \begin{pmatrix} 0 \\ 1 \end{pmatrix} \Omega(x+y;t) + \int_x^\infty \begin{pmatrix} -K_{21}^+(x,s;t) \\ K_{11}^+(x,s;t) \end{pmatrix} \Omega(y+s) \, \mathrm{d}s = 0,$$

with

$$\begin{aligned}\Omega(z;t) &\equiv F(z;t) + G(z;t) + H(z;t) \\ &\equiv \frac{1}{2\pi}\int_{-\infty}^{\infty} R_+(\zeta,0)e^{i\zeta[z/t+8\zeta^2]t}\,\mathrm{d}\zeta + \sum_j \left[C_j(t)e^{iz\zeta}\right]_{\zeta=\zeta_j} \\ &\qquad + \frac{1}{2\pi}\int_0^{q_\ell} \frac{iq_\ell}{2\zeta}\,|T_+(\zeta,0)|^2\,e^{-[z/t+8\zeta^2]t\sqrt{q_\ell^2-\zeta_\ell^2}}\,\mathrm{d}\zeta_\ell, \quad (4.27)\end{aligned}$$

where we've used the time dependence in (4.13). The contribution from the poles, $G(z,t)$, correspond to solitons in the solution; since these move to the DSW's right in the long-time limit, we omit their contributions in our asymptotics.

Contribution from $F(z,t)$

From (4.16) we have that

$$R_+(-\zeta,0) = \left(R_+(\zeta,0)\right)^*,$$

so

$$F(z,t) = \frac{1}{2\pi}\int_0^{\infty} R_+(\zeta,0)e^{i\zeta[z/t+8\zeta^2]t}\,\mathrm{d}\zeta + \text{cc}.$$

This is a Fourier-type integral that we can approximate in the long-time limit. This integral has both a stationary-phase and an end-point contribution.

For the stationary-phase contribution, we define $\chi(\zeta) \equiv \zeta(z/t + 8\zeta^2)$. The stationary-phase points are where $\chi'(\zeta) = 0$; so here, $\zeta = \pm i\sqrt{z/(24t)}$ since we assume that $z/t \gg 1$. Using the stationary-phase method, we find that this contribution is

$$F_1 = -R_+(i\sqrt{z/(24t)},0)\frac{\exp\left\{-2t[z/(6t)]^{3/2}\right\}}{8\sqrt{3\pi}[z/(6t)]^{1/4}\sqrt{t}}\left(1+O(t^{-1/2})\right).$$

If $K_{21}^+ \sim -F_1$ in this region, and since $q(x) = 2K_{21}^+(x,x)$, then

$$u(x,t) = R_+\left(i\sqrt{x/(12t)},0\right)\frac{e^{-2t[x/(3t)]^{3/2}}}{4\sqrt{3\pi}[x/(3t)]^{1/4}\sqrt{t}}\left(1+O(t^{-1/2})\right);$$

this matches (4.26) if $\hat{q}_0\left(i\sqrt{x/(3t)}\right) = R_+\left(i\sqrt{x/(12t)}, 0\right)$.

We also have an end-point contribution at $\zeta = 0$, but it is exactly canceled by one of the end-point contributions from $H(z,t)$.

Contribution from $H(z,t)$

Using $\zeta^2 = \zeta_\ell^2 - q_\ell^2$, we have that

$$H(z,t) = \frac{1}{2\pi}\int_0^{q_\ell} \frac{q_\ell}{2\sqrt{q_\ell^2 - \zeta_\ell^2}} \left|T_+(\zeta,0)\right|^2 e^{\chi(\zeta_\ell)t}\, \mathrm{d}\zeta_\ell,$$

where $\chi(\zeta_\ell) \equiv -[z/t + 8\zeta_\ell^2 - 8q_\ell^2]\sqrt{q_\ell^2 - \zeta_\ell^2}$ in this subsection. This is a Laplace-type integral in the long-time that has three critical points: the end point $\zeta_\ell = 0$, the stationary-phase point where $\chi'(\zeta_\ell) = 0$, and the end point $\zeta_\ell = q_\ell$.

For the contribution from the end point $\zeta_\ell = 0$, we find that

$$H_0(z,t) = -\frac{q_\ell^{3/2} T_2(0)}{32\sqrt{\pi}} \frac{\exp\left\{-2q_\ell t[z/(2t) - 4q_\ell^2]\right\}}{\left[12q_\ell^2 - z/(2t)\right]^{3/2} t^{3/2}} \left[1 + O(t^{-1})\right], \tag{4.28}$$

where we define

$$T_j(\zeta_*) \equiv \left[\frac{\partial}{\partial \zeta_\ell^j}|T_+(\zeta,0)|^2\right]_{\zeta_\ell = \zeta_*}.$$

We used $T_0(0) = 0$ from (4.6) and that $T_j(0) = 0$ for j odd.

The stationary-phase point is $\zeta_* = \pm\sqrt{q_\ell^2 - z/(24t)}$ since then $\chi'(\zeta_\ell = \zeta_*) = 0$. The contribution from this stationary-phase point is

$$H_1(z,t) \sim i\frac{e^{-tz^{3/2}/(3\sqrt{6})}}{8\sqrt{6\pi}\sqrt{t}} \frac{(q_\ell^2 - \zeta_*)^{1/4}}{\zeta_*} T_0(\zeta_*) + \text{cc},$$

which is asymptotically zero compared with H_0. So we'll neglect this contribution.

The contribution from the end point at $\zeta_\ell = q_\ell$ exactly cancels the contribution from $F(z,t)$ at $\zeta = 0$. Intuitively, these contributions cancel because they both correspond

to the point $\zeta = 0$ and both integrals come from (4.23).

Using the GLM integral equation to find K_{21}^+

Recall that (4.25) is

$$\begin{pmatrix} K_{11}^+(x,y;t) \\ K_{21}^+(x,y;t) \end{pmatrix} + \begin{pmatrix} 0 \\ 1 \end{pmatrix} \Omega(x+y;t) + \int_x^\infty \begin{pmatrix} -K_{21}^+(x,s;t) \\ K_{11}^+(x,s;t) \end{pmatrix} \Omega(y+s)\,\mathrm{d}s = 0.$$

We can solve this with a Neumann series,

$$\begin{pmatrix} v_1^{(0)}(x,y;t) \\ v_2^{(0)}(x,y;t) \end{pmatrix} = - \begin{pmatrix} 0 \\ 1 \end{pmatrix} \Omega(x+y;t),$$

$$\begin{pmatrix} v_1^{(n+1)}(x,y;t) \\ v_2^{(n+1)}(x,y;t) \end{pmatrix} = - \begin{pmatrix} 0 \\ 1 \end{pmatrix} \Omega(x+y;t) - \int_x^\infty \begin{pmatrix} -v_2^{(n)}(x,s;t) \\ v_1^{(n)}(x,s;t) \end{pmatrix} \Omega(y+s)\,\mathrm{d}s.$$

Then, $v_2^{(n)}(x,y;t) \to K_{21}^+$ as $n \to \infty$, and we can use $q(x) = 2K_{21}^+(x,x;t)$.

Previously, we found asymptotic approximations for $\Omega(z,t)$. Near the shock front, we found that the asymptotic approximation of $\Omega(z,t)$ is dominated by (4.28), the end-point contribution from $H(z,t)$ near $\zeta_\ell = 0$. Using this, the first term in the Neumann series solution of (4.25) is

$$\mathbf{v}^{(0)} \equiv \begin{pmatrix} v_1^{(0)}(x,y;t) \\ v_2^{(0)}(x,y;t) \end{pmatrix} = - \begin{pmatrix} 0 \\ 1 \end{pmatrix} \Omega(x+y;t) = A_0 e^{q_\ell \xi(x+y)} \begin{pmatrix} 0 \\ 1 \end{pmatrix},$$

where

$$A_0 \equiv \frac{q_\ell^{3/2}}{32\sqrt{\pi}} T_2(0)$$

and

$$\xi(z) \equiv -z + 8q_\ell^2 t - \frac{3}{2q_\ell} \log\left(12q_\ell^2 t - z/2\right) + O(t^{-1}). \tag{4.29}$$

Now we asymptotically approximate

$$\begin{aligned}\mathbf{v}^{(1)} - \mathbf{v}^{(0)} &= -\int_x^\infty \begin{pmatrix} -v_2^{(0)}(x,s;t) \\ v_1^{(0)}(x,s;t) \end{pmatrix} \Omega(y+s)\,\mathrm{d}s \\ &= A_0^2 \begin{pmatrix} -1 \\ 0 \end{pmatrix} \int_x^\infty e^{q_\ell[\xi(x+s)+\xi(y+s)]}\,\mathrm{d}s\end{aligned}$$

in the long-time limit; here, the end point contribution from $s = x$ dominates and

$$\begin{aligned}\mathbf{v}^{(1)} - \mathbf{v}^{(0)} &\sim \frac{A_0^2 e^{q_\ell[\xi(2x)+\xi(x+y)]}}{-q_\ell[\xi'(2x)+\xi'(x+y)]} \begin{pmatrix} -1 \\ 0 \end{pmatrix} \\ &\sim \frac{A_0^2 e^{q_\ell[\xi(2x)+\xi(x+y)]}}{2q_\ell} \begin{pmatrix} -1 \\ 0 \end{pmatrix},\end{aligned}$$

since $\xi'(z) = -1 + O(t^{-1})$.

Now we repeat this procedure two more times, so we have an asymptotic approximation for the first four terms in the Neumann series. The next two terms in the Neumann series are

$$\mathbf{v}^{(2)} - \mathbf{v}^{(1)} = \frac{A_0^3}{2q_\ell} \begin{pmatrix} 0 \\ -1 \end{pmatrix} \int_x^\infty e^{q_\ell[\xi(2x)+\xi(x+s)+\xi(y+s)]}\,\mathrm{d}s,$$

which is

$$\mathbf{v}^{(2)} - \mathbf{v}^{(1)} \sim \frac{A_0^3 e^{q_\ell[2\xi(2x)+\xi(x+y)]}}{4q_\ell^2} \begin{pmatrix} 0 \\ -1 \end{pmatrix}$$

in the long-time limit. Likewise,

$$\mathbf{v}^{(3)} - \mathbf{v}^{(2)} = \frac{A_0^4}{4q_\ell^2} \begin{pmatrix} 1 \\ 0 \end{pmatrix} \int_x^\infty e^{q_\ell[2\xi(2x)+\xi(x+s)+\xi(y+s)]}\,\mathrm{d}s \sim \frac{A_0^4 e^{q_\ell[3\xi(2x)+\xi(x+y)]}}{8q_\ell^3} \begin{pmatrix} 1 \\ 0 \end{pmatrix}$$

and

$$\mathbf{v}^{(4)} - \mathbf{v}^{(3)} = \frac{A_0^5}{8q_\ell^3} \begin{pmatrix} 0 \\ 1 \end{pmatrix} \int_x^\infty e^{q_\ell[3\xi(2x)+\xi(x+s)+\xi(y+s)]}\, \mathrm{d}s \sim \frac{A_0^5 e^{q_\ell[4\xi(2x)+\xi(x+y)]}}{16q_\ell^4} \begin{pmatrix} 0 \\ 1 \end{pmatrix}.$$

Since $q(x) = 2K_{21}^+(x,x)$, this asymptotic Neumann-series solution approximation gives

$$\begin{aligned} q(x,t) &= 2A_0 e^{q_\ell \xi(2x)} - \frac{1}{2q_\ell^2}\left(A_0 e^{q_\ell \xi(2x)}\right)^3 (1 + O(t^{-1})) \\ &\quad + \frac{1}{8q_\ell^4}\left(A_0 e^{q_\ell \xi(2x)}\right)^5 (1 + O(t^{-1})) + \cdots \\ &\sim 2q_\ell \operatorname{sech}\left[q_\ell(\xi - \xi_0)\right], \end{aligned} \tag{4.30}$$

where ξ, from (4.29), is

$$\xi = -2x + 8q_\ell^2 t - \frac{3}{2q_\ell}\log\left(12q_\ell^2 t - x\right) + O(t^{-1}). \tag{4.31}$$

and

$$\xi_0 = \frac{1}{q_\ell}\log\left(\frac{32\sqrt{\pi}}{T_2(0)q_\ell^{3/2}}\right);$$

note how, like the KdV equation, the phase only depends on $T_2(0)$. This gives the boundary condition on the DSW's right.

Traveling wave solution

Let's suppose that the DSW's front has a traveling wave solution locally. Then we can make the variable change $q(x,t) \to q(\theta)$, with $\theta = x - Vt$; then (4.1) becomes

$$-Vq' + 6q^2q' + q''' = 0.$$

If we integrate, then multiply by q', and then integrate again, we get

$$(q')^2 = -q^4 + Vq^2 + Bq + A = (a-q)(q-b)(q-c)(q-d), \tag{4.32}$$

where A, B, a, b, c, and d are constants with $a+b+c+d=0$. Thus, we get the elliptic integral

$$\int \frac{\mathrm{d}q}{\sqrt{(a-q)(q-b)(q-c)(q-d)}} = \theta - \theta_0;$$

from Byrd and Friedman (1971, eq. 257), we can evaluate this integral when $a > q \geq b > c > d$ and get

$$\frac{2F(\phi,k)}{\sqrt{(a-c)(b-d)}} = \theta - \theta_0,$$

where

$$\phi = \arcsin\sqrt{\frac{(b-d)(a-q)}{(a-b)(q-d)}}, \qquad k^2 = \frac{(a-b)(c-d)}{(a-c)(b-d)} = \frac{(a-b)(a+b+2c)}{(a-c)(a+2b+c)},$$

and $F(\phi,k)$ is Legendre's incomplete integral of the first kind (see also Olver et al., 2010, Chap. 19). Solving for q gives

$$q(x,t) = -(a+b+c) + \frac{(2a+b+c)(a+2b+c)}{(a+2b+c)+(a-b)\,\mathrm{sn}^2\left[\frac{\sqrt{(a-c)(a+2b+c)}}{2}(\theta-\theta_0),k\right]},$$

where $\mathrm{sn}(z,k)$ is the Jacobian elliptic 'sine' function (see Olver et al., 2010, Chap. 22). It's convenient to define

$$r_3 = \frac{a+b}{2}, \quad r_2 = \frac{a+c}{2}, \quad r_1 = \frac{b+c}{2},$$

so $r_3 > r_2 > r_1$ and

$$q(x,t) = r_3 - r_2 + r_1 + \frac{2(r_2-r_1)(r_3+r_1)\left\{1-\mathrm{sn}^2\left[\sqrt{r_3^2-r_1^2}(\theta-\theta_0),k\right]\right\}}{r_3+r_1+(r_2-r_1)\,\mathrm{sn}^2\left[\sqrt{r_3^2-r_1^2}(\theta-\theta_0),k\right]}, \tag{4.33}$$

where

$$k^2 = \frac{r_2^2 - r_1^2}{r_3^2 - r_1^2}.$$

Taking the limit $r_2 \to r_3$ so $k \to 1$ gives

$$q(x,t) = r_1 + \frac{2(r_3^2 - r_1^2)\left\{1 - \tanh^2\left[\sqrt{r_3^2 - r_1^2}(\theta - \theta_0)\right]\right\}}{r_3 + r_1 + (r_3 - r_1)\tanh^2\left[\sqrt{r_3^2 - r_1^2}(\theta - \theta_0)\right]}; \tag{4.34}$$

here $q \to r_1$ as $x \to \infty$ and $q(\theta_0) = 2r_3 - r_1$, which gives a solitary-wave height of $2(r_3 - r_1)$.

To match (4.34) with (4.30), we take

$$r_3 = q_\ell, \qquad r_2 = q_\ell, \quad \text{and} \quad r_1 = q_r = 0,$$

and note that $V = 4q_\ell^2 + O(t^{-1}\log t)$.

4.2.2 The DSW

First we change variables based on (4.30) and (4.31). Then we use multiple-scales perturbation theory to find three conservation laws. After some algebra, these conservation laws can be written as a diagonal system. This diagonal system describes how the slowly varying parameters change in the DSW region.

Variable changes

Equation (4.30) suggests the variable change

$$q(x,t) = g(\xi, t),$$

where ξ is space-like and defined in (4.31) and t is time-like. It's convenient to introduce the slow-variables $X = \delta\xi$ and $T = \delta t$, where $\delta = O(t^{-1})$. Substituting this into (4.1)

gives

$$g_{\xi\xi\xi\xi} + 6g^2 g_\xi - 4q_\ell^2 g_\xi - g_t = \delta \left\{ \frac{9\left[g_{\xi\xi\xi\xi} + 2g^2 g_\xi - 4q_\ell^2 g_\xi\right]}{4q_\ell(8q_\ell^2 T + X)} \right\} + \cdots .$$

Now we introduce the rapid-variable $\theta(\xi, t)$, such that

$$\theta_\xi \equiv \kappa(X,T) \quad \text{and} \quad \theta_t \equiv -\omega(X,T) \equiv -\kappa(X,T)V(X,T);$$

this gives the compatibility condition $(\theta_\xi)_t = (\theta_t)_\xi$ or

$$\kappa_T + \omega_X = 0, \tag{4.35}$$

often called the conservation of waves. Using

$$\frac{\partial}{\partial t} = -\omega\frac{\partial}{\partial\theta} + \delta\frac{\partial}{\partial T} \quad \text{and} \quad \frac{\partial}{\partial\xi} = \kappa\frac{\partial}{\partial\theta} + \delta\frac{\partial}{\partial X}$$

gives

$$\kappa^3 g_{\theta\theta\theta} + \kappa(6g^2 + V - 4q_\ell^2)g_\theta = \mathcal{O}(\delta).$$

Expanding

$$g(\theta, X, T) = g_0(\theta, X, T) + \delta g_1(\theta, X, T) + \delta^2 g_2(\theta, X, T) + \ldots$$

and grouping terms with like powers of δ gives

$$\kappa^3 g_{0,\theta\theta\theta} + \kappa\left(6g_0^2 + V - 4q_\ell^2\right) g_{0,\theta} = 0 \tag{4.36}$$

and

$$\kappa^3 g_{1,\theta\theta\theta} + 6\kappa(g_0^2 g_1)_\theta + \kappa\left(V - 4q_\ell^2\right) g_{1,\theta}$$

$$= \frac{9\kappa\left[\kappa^2 g_{0,\theta\theta\theta} + (2g_0^2 - 4q_\ell^2)g_{0,\theta}\right]}{4q_\ell(8q_\ell^2 T + X)} + g_{0,T} - (6g_0^2 - 4q_\ell^2)g_{0,X} - 3\kappa(\kappa g_{0,\theta\theta})_X \equiv \Theta \quad (4.37)$$

Solving for g_0

We need to solve (4.36)

$$\kappa^3 g_{0,\theta\theta\theta} + \kappa\left(6g_0^2 + V - 4q_\ell^2\right) g_{0,\theta} = 0$$

for g_0. There are several methods that we can use. As before, we can integrate with respect to θ, multiply by $g_{0,\theta}$, and then integrate again to get

$$\kappa^2 g_{0,\theta}^2 = -g_0^4 + \left(4q_\ell^2 - V\right) g_0^2 + Bg_0 + A = (a - g_0)(g_0 - b)(g_0 - c)(g_0 - d),$$

where $a + b + c + d = 0$. Following the procedure we used to get (4.33), we find

$$g_0(\theta, X, T) = r_3 - r_2 + r_1 + \frac{2(r_2 - r_1)(r_3 + r_1)\left\{1 - \mathrm{sn}^2\left[2(\theta - \theta_0)K, k\right]\right\}}{r_3 + r_1 + (r_2 - r_1)\,\mathrm{sn}^2\left[2(\theta - \theta_0)K, k\right]}, \quad (4.38)$$

where

$$r_3 \equiv r_3(X, T) = \frac{a + b}{2}, \quad r_2 \equiv r_2(X, T) = \frac{a + c}{2}, \quad r_1 \equiv r_1(X, T) = \frac{b + c}{2},$$

$r_3 > r_2 > r_1$, $K \equiv K(k(X, T))$ is the complete elliptic of the first kind,

$$k^2 = \frac{r_2^2 - r_1^2}{r_3^2 - r_1^2}, \quad \kappa^2 = \frac{r_3^2 - r_1^2}{4K^2}, \quad V = 4q_\ell^2 - 2(r_3^2 + r_2^2 + r_1^2).$$

Since $\mathrm{sn}^2(z, k)$ has period $2K(k)$, g_0 is periodic in θ with period 1.

Enforcing periodicity

To eliminate secular terms, we require that $g_0(\theta, X, T)$ is periodic in θ with period 1 so that

$$\int_0^1 \Theta \, \mathrm{d}\theta = 0 \quad \text{and} \quad \int_0^1 g_0 \Theta \, \mathrm{d}\theta = 0.$$

Using

$$\int_0^1 \frac{\partial^i g_0}{\partial \theta^i} \, \mathrm{d}\theta = 0 \quad \text{for } i = 1, 2, 3, \ldots,$$
$$\int_0^1 g_0^i \frac{\partial^j g_0}{\partial \theta^j} \, \mathrm{d}\theta = 0 \quad \text{for } i = 1, 2, 3, \ldots, \text{ and } j = 1, 3, 5, \ldots,$$
$$\int_0^1 g_0 g_{0,\theta\theta} \, \mathrm{d}\theta = -\int_0^1 g_{0,\theta}^2 \, \mathrm{d}\theta,$$

we get from $\int_0^1 \Theta \, \mathrm{d}\theta = 0$ that

$$\frac{\partial}{\partial T} \int_0^1 g_0 \, \mathrm{d}\theta + \frac{\partial}{\partial X} \left(4q_\ell^2 \int_0^1 g_0 \, \mathrm{d}\theta - 2 \int_0^1 g_0^3 \, \mathrm{d}\theta \right) = 0 \tag{4.39}$$

and from $\int_0^1 g_0 \Theta \, \mathrm{d}\theta = 0$ that

$$\frac{\partial}{\partial T} \int_0^1 g_0^2 \, \mathrm{d}\theta + \frac{\partial}{\partial X} \left(4q_\ell^2 \int_0^1 g_0^2 \, \mathrm{d}\theta - 3 \int_0^1 g_0^4 \, \mathrm{d}\theta + 3\kappa^2 \int_0^1 g_{0,\theta}^2 \, \mathrm{d}\theta \right) = 0. \tag{4.40}$$

Notice that both (4.39) and (4.40) are conservation laws.

Using (4.38) and the properties of elliptic functions (see Byrd and Friedman, 1971), we can evaluate these integrals in terms of complete elliptic integrals. After significant algebraic manipulation, the conservation laws (4.35), (4.39), and (4.40) simplify to

$$\frac{\partial r_i}{\partial T} + v_i(r_1, r_2, r_3) \frac{\partial r_i}{\partial Z} = 0, \qquad i = 1, 2, 3, \tag{4.41}$$

where

$$v_1 = 4q_\ell^2 - 2(r_1^2 + r_2^2 + r_3^2) + 4(r_2^2 - r_1^2)\frac{K}{K-E}, \tag{4.42a}$$

$$v_2 = 4q_\ell^2 - 2(r_1^2 + r_2^2 + r_3^2) + \frac{4(r_3^2 - r_2^2)(r_2^2 - r_1^2)K}{(r_3^2 - r_1^2)E - (r_3^2 - r_2^2)K}, \tag{4.42b}$$

$$v_3 = 4q_\ell^2 - 2(r_1^2 + r_2^2 + r_3^2) - 4(r_3^2 - r_2^2)\frac{K}{E}. \tag{4.42c}$$

After some algebraic manipulation, the Whitham-averaging equations reported in (Driscoll and O'Neil, 1976) can be put in Riemann-invariant form and shown to be equal to (4.41) with (4.42).

For large time, the solution tends to a self-similar solution. To match (4.30) — the DSW's right boundary condition — we take $r_1 = 0$ and $r_3 = q_\ell$. Since the solution is self-similar, we take $r_2 = r_2(\chi)$ with $\chi \equiv X/T = \xi/t$. This simplifies (4.41) to $(v_2 - \chi)r_2'(\chi) = 0$ and gives us the implicit equation

$$\chi = 2(q_\ell^2 - 3r_2^2) + \frac{4q_\ell^2 r_2^2 E(r_2/q_\ell)}{q_\ell^2 E(r_2/q_\ell) - (q_\ell^2 - r_2^2)K(r_2/q_\ell)}.$$

Taking the limit $r_2 \to r_3$ gives $\chi \to 0$ or $x \sim 4q_\ell^2 t$, which is the speed at the front of the DSW. Taking the limit $r_2 \to r_1$ gives $\chi \to 10q_\ell^2$ or $x \sim -6q_\ell^2 t$, which is speed at the back of the DSW. These front and back speeds agree well with direct numerics.

4.2.3 Trailing edge

When $q_\ell^2 > q_r^2$, the GLM integral equation formulated from $-\infty$ to x only has contributions from the reflection coefficient and the discrete spectra (the solitons). The first few terms are sufficient to show our main result: the long-time limit of general, step-like data is a single-phase DSW. Details will be given in a subsequent paper.

4.3 Conclusion

DSWs appear when weak dispersion and weak nonlinearity dominate the physics; they arise in many physical systems, including fluid dynamics, plasmas, superfluids, and nonlinear optics. For systems with weak dispersion and weak, cubic nonlinearity, the mKdV equation is the leading-order asymptotic equation. Unlike the IST theory for the KdV equation in chapter 3, the IST theory for the mKdV equation with non-vanishing boundary conditions was not known in the literature. Therefore, we first needed to derive the GLM integral equations for non-vanishing boundary conditions. We found that the GLM integral equation formulated from x to ∞ has a contribution for the transmission coefficient when $q_\ell^2 > q_r^2$ and conjectured that, like the KdV equation, this implies that the solution tends to a single-phase DSW in these cases. We showed that the long-time-asymptotic solution of the mKdV equation for general step-like initial data where $\lim_{x\to-\infty} q(x,t) = q_\ell > 0$ and $\lim_{x\to\infty} q(x,t) = 0$ tend to a single-phase DSW; we found this long-time-asymptotic solution using the IST method and matched-asymptotic expansions. Therefore, a single-phase DSW eventually forms from well-separated, multi-step initial data, despite having more complex multiphase dynamics at intermediate times for this boundary data.

Part II

Two-dimensional ocean-wave soliton interactions

Chapter 5

Nonlinear shallow ocean-wave soliton interactions on flat beaches

The study of water waves has a long and storied history, with many important applications including naval architecture, oil exploration, and tsunami propagation. The mathematics of these waves is difficult because the underlying equations are strongly nonlinear and have a free boundary where water meets air; there is no comprehensive theory. This chapter reports that X, Y, H, and more complex nonlinear interactions frequently occur on two widely separated flat beaches and are not rare events, as was previously thought. In fact, these X-, H-, and Y-type interactions can be seen daily, shortly before and after low tide. These phenomena are closely related to the analytical solution of a multi-dimensional nonlinear wave equation that has been studied extensively since 1970 (Kadomtsev and Petviashvili, 1970; Ablowitz and Clarkson, 1991a) and is a generalization of an equation studied by Korteweg and de Vries in 1895 (Korteweg and de Vries, 1895), which gave rise to the concept of solitons (Zabusky and Kruskal, 1965). From the universality of the underlying equation (Ablowitz, 2011) and the fundamental nature of these waves, it is expected that similar X-, H-, and Y-type structures will be seen in many different physical problems, including fluid dynamics,

nonlinear optics, and plasma physics.

A version of this chapter was published with Mark J. Ablowitz in *Physical Review E* (Ablowitz and Baldwin, 2012).

5.1 Background and introduction

Water waves have been studied by mathematicians, physicists, and engineers for hundreds of years. While there are many types of water waves, here we will discuss solitary waves in shallow water; they are often called solitons and they have unique properties. Solitary waves in fluids (Grimshaw, 2007) and oceans (Osborne, 2010) are a major and active research area.

J. S. Russell, a naval architect, made the first recorded observation of a solitary wave in the Union Canal, Edinburgh in 1834: a stopping barge set off a solitary wave that went along the canal for one or two miles without changing its speed or its shape (Russell, 1844). He did experiments and found, among other things, that the wave's speed depends on its height; he then concluded that it must be a nonlinear effect. Boussinesq (1877) and Korteweg and de Vries (1895) derived approximate nonlinear equations for shallow water waves. They found both solitary and periodic nonlinear wave solutions to these equations; they also found that the speed is proportional to its amplitude — bigger waves move faster. So Russell's observations were quantitatively confirmed.

Between 1895 and 1960, solitary waves were mostly studied by water wave scientists, mathematicians, and coastal engineers. In the 1960s, applied mathematicians developed robust approximation techniques and found that the Korteweg–de Vries (KdV) equation appears universally when there is weak quadratic nonlinearity and weak dispersion (Ablowitz, 2011). In 1965, Zabusky and Kruskal (1965) found that the solitary waves of the KdV equation have remarkable elastic interaction properties and

termed them solitons. Gardner, Greene, Kruskal, and Miura (Gardner et al., 1967) then developed a method for solving the KdV equation with rapidly decaying initial data; this method has been extended to many other nonlinear equations and is called the inverse scattering transform (IST) (Ablowitz and Segur, 1981b; Novikov et al., 1984) — such equations are called integrable.

In 1970, Kadomtsev and Petviashvili (1970) (KP) extended the KdV equation to include transverse effects; this multi-dimensional equation, like the KdV equation, is integrable (Ablowitz and Clarkson, 1991a). Our observations in this chapter are related to soliton solutions of the KP equation that do not decay at large distances; these interacting, multi-dimensional line-soliton solutions can be found analytically (Ablowitz and Segur, 1981b). Before our observations, there was only one well-known photograph of an interacting line-soliton in the ocean and it was thought that such interactions are rare events; it was taken in the 1970s in Oregon (fig. 4.7b in Ablowitz and Segur (1981b)) and is similar to figure 5.3. Since the KP equation has other X, Y, H, and more complex line-soliton solutions, we sought and found ocean waves with similar behavior (figs. 5.1–5.6). Surprisingly, these X, Y, H, and more complex types of line-solitons appear frequently in shallow water on two relatively flat beaches, some 2,000 km apart! These freely propagating, interacting line-solitons are remarkably robust. While these interactions are not stationary, and so only last a few seconds, a casual observer will be able to see them with the insights provided in this chapter. Interestingly, in laboratory experiments involving internal waves emanating from the interaction of cylindrical wave fronts, Maxworthy (1980, fig. 11) reported an X-type internal wave interaction; Weidman et al. (1992) later showed that the length of the stem in (Maxworthy, 1980, fig. 11) follows a Hopf bifurcation when plotted against the intersection angle.

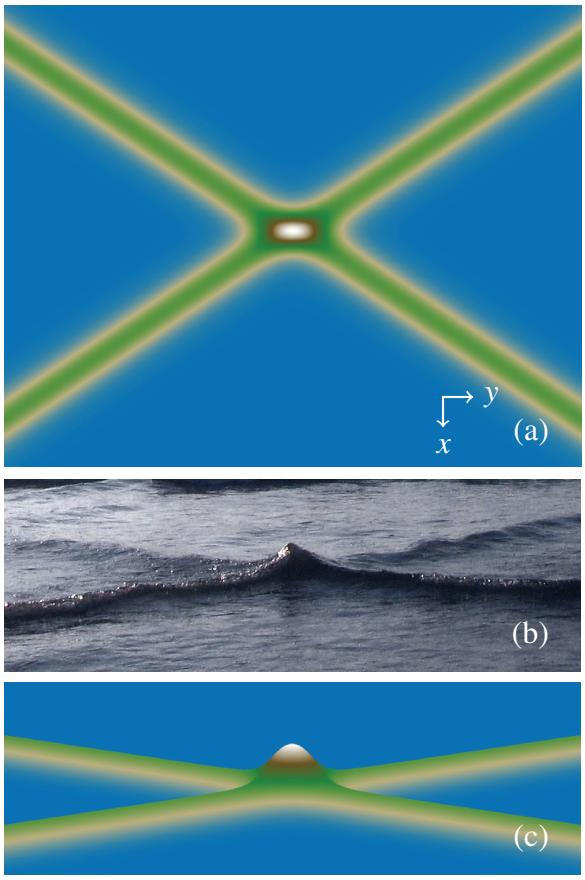

Figure 5.1: A plot and a photograph of an X-type interaction. (a) A plot of an analytical line-soliton interaction solution of the KP equation at $t = 0$ using (5.3) and (5.4). In this and the following plots, we picked the k_i and P_j to be qualitatively similar to the photograph in part (b). Here, $k_1 = k_2 = 1/2$, $P_1 = -P_2 = 2/3$ so $e^{A_{12}} \approx 2.3$. (b) Taken in Mexico on 31 December 2011; notice the large amplitude of the short stem. (c) A 3d-plot of the solution in (a), which qualitatively agrees with (b); we only include one 3d-plot because the density plots show the interaction behavior clearly.

5.2 Observations

Single line, solitary water waves are familiar to every beach goer: they are localized in the direction of propagation and have a distinctive, hump-like wave profile. These waves break when they are sufficiently large compared to the depth and they often curve from transverse beach and bottom effects. We will focus on interacting line solitary waves that form X, Y, H, and more complex interactions.

It was thought that X-type ocean wave interactions happen infrequently. This is

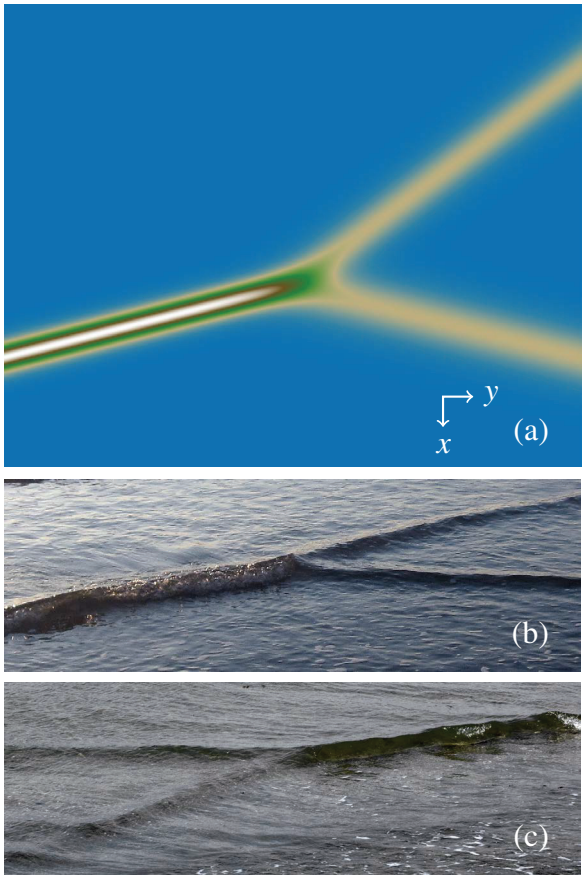

Figure 5.2: A plot and photographs of a Y-type interaction. (a) $k_1 = 1/2$, $k_2 = 1$, $P_1 = 3/4$, $P_2 = 1/4$ so $e^{A_{12}} = 0$. (b) Taken in Mexico on 6 January 2010. (c) Taken in California on 3 May 2012.

not the case: X-, H-, and Y-type ocean wave interactions occur daily, shortly before and after low tide on relatively flat beaches. M.J.A. observed these interactions near 20°41′22″ N, 105°17′44″ W in Nuevo Vallarta, Mexico from 2009 to 2013 between December and April. D.B. observed these interactions near 33°57′52″ N, 118°27′35″ W on Venice Beach, California in May 2012 — about 2,000 km away — and in Nuevo Vallarta, Mexico in February and March 2013. Figures 5.1–5.6 shows a few of the thousands of photographs that we took. The water depth where we saw these interactions was shallow, usually between 5 and 20 cm; the beaches are long and relatively flat; the interactions usually happen within 2 hours before and after low tide; the cross-waves produced near a jetty appear to help induce these interactions. We found that these X-,

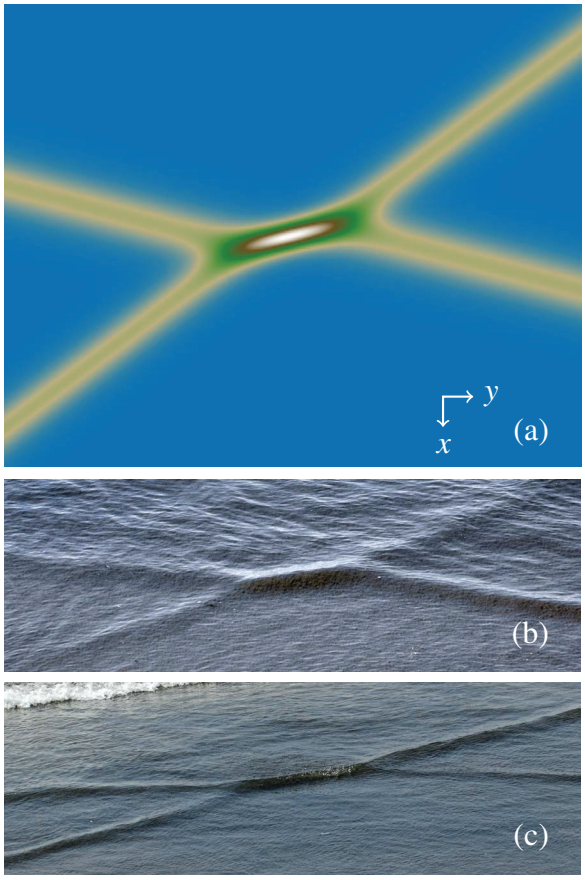

Figure 5.3: A plot and photographs of an X-type interaction with a longer stem. (a) $k_1 = k_2 = 1/2$, $P_1 = -1/4 - 10^{-2}$, $P_2 = 3/4$ so $e^{A_{12}} \approx 51$. (b) Taken in California on 2 May 2012 in shallower water than figure 5.1b. (c) Taken in California on 4 May 2012.

H-, and Y-type interactions usually come in groups, which last a few minutes. We saw many X-, H-, and Y-type interactions each day that we made observations; both M.J.A. and D.B. saw X-type interactions most frequently and H- and Y-type interactions less frequently. We also saw more complex interactions, such as three line-solitons on one side of the interaction region and two line-solitons to the other side, which we will call a 3-in-2-out interaction; these more complex interactions are much less frequent than X-, H-, or Y-type interactions. Our observations indicate that X-, H-, and Y-type interactions are remarkably robust: they typically persist through bottom-depth changes, perturbations from wind and spray, and sometimes even breaking!

We observed two types of X interactions: an interaction with a short stem (fig. 5.1)

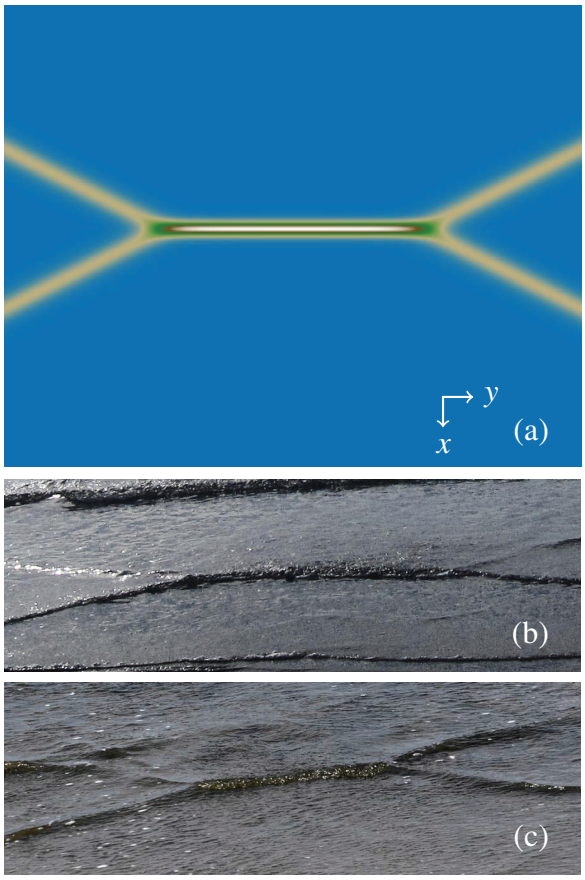

Figure 5.4: A plot and photographs of an X-type interaction with a very long stem. (a) $k_1 = k_2 = 1/2$, $P_2 = -P_1 + 10^{-10} = 1/2$ so $e^{A_{12}} \approx 5 \times 10^9$. (b) Taken in Mexico on 28 December 2011 in shallower water than figure 5.3b. (c) Taken in California on 3 May 2012.

and an interaction with a long stem where the stem height is higher than the incoming line-solitons (figs. 5.3 and 5.4). The amplitude of the short-stem X-type interaction can be quite large in deeper water. Interestingly, the length of the stem often increases as the depth decreases. We also observed H-type interactions with a long stem where the stem height is lower than the tallest incoming line-soliton (fig. 5.5). Figure 5.2 shows a typical Y-type interaction. A more complex interaction, with three 'incoming' and two 'outgoing' segments, is shown in figure 5.6.

When one knows what to look for and when and where to look for them, X-, H-, and Y-type interactions are fairly easy to observe. In addition to happening less frequently, more complex interactions are harder to see because they are highly

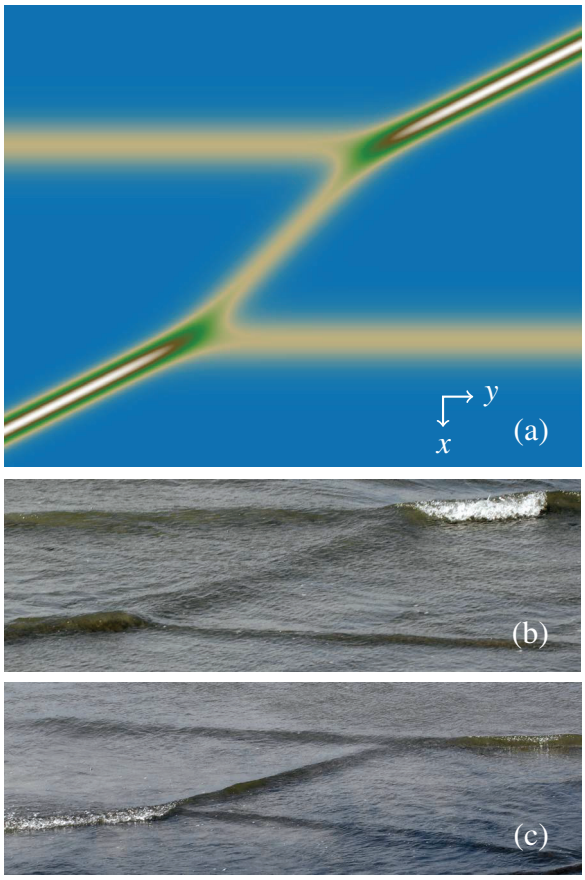

Figure 5.5: A plot and photographs of an H-type interaction, where the stem has a lower rather than a higher amplitude. (a) $k_1 = 1$, $k_2 = 1/2$, $P_1 = 1/2 - 10^{-7}$, $P_2 = 0$ so $e^{A_{12}} \approx 5 \times 10^{-8}$. (b) and (c) Taken in California on 3 May 2012.

non-stationary and have shorter interaction times than X-, H-, and Y-type interactions. Another difficulty is that most water waves break before X-, H-, or Y-type interactions form; so sustained observation may be needed. Along with the photographs here, we have also taken many videos that show the development and general dynamics of these waves; the readers can watch some of these videos and see many more photographs at our websites `http://www.markablowitz.com/line-solitons` and `http://www.douglasbaldwin.com/nl-waves.html`.

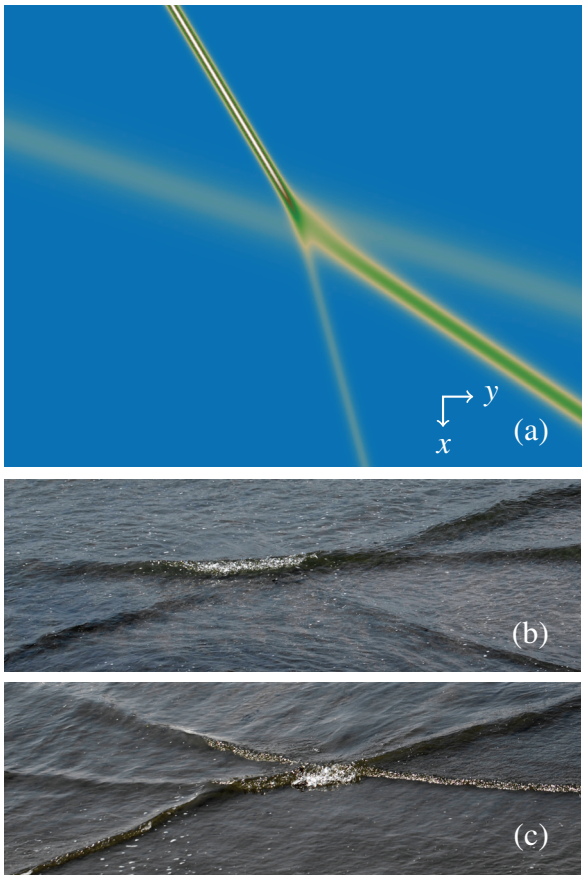

Figure 5.6: A plot and photographs of a 3-in-2-out interaction, where there are three line-solitons on one side of the interaction region and two line-solitons on the other side. (a) $k_1 = 1$, $k_2 = 2$, $k_3 = 3$, $P_1 = -1/3$, $P_2 = -2/3$, $P_3 = -5/3$. (b) and (c) Taken in California on 4 May 2012.

5.3 Mathematical description

The KP equation (Kadomtsev and Petviashvili, 1970),

$$\frac{\partial}{\partial x}\left(\frac{1}{\sqrt{gh}}\eta_t + \eta_x + \frac{3}{2h}\eta\eta_x + \frac{h^2\gamma}{2}\eta_{xxx}\right) + \frac{1}{2}\eta_{yy} = 0, \tag{5.1}$$

is the two-space and one-time dimensional equation that governs unidirectional, maximally-balanced, weakly-nonlinear shallow water waves with weak transverse variation. Here, sub-scripts denote partial derivatives, $\eta = \eta(x, y, t)$ is the wave height above the constant mean height h, g is gravity, $\gamma = 1 - \tau/3$, $\tau = T/(\rho g h^2)$ is a

dimensionless surface tension coefficient, and ρ is density. When there is no y-dependence, the equation reduces to the KdV equation (Korteweg and de Vries, 1895). The KP equation was first derived in the context of plasma physics (Kadomtsev and Petviashvili, 1970) and was later derived in water waves (Ablowitz and Segur, 1979). The sign of γ is important: there is 'large' surface tension when $\gamma < 0$, and this equation is called KPI; there is 'small' surface tension when $\gamma > 0$, and this equation is called KPII. We can rescale (5.1) into the non-dimensional form (Ablowitz, 2011)

$$(u_t + 6uu_x + u_{xxx})_x + 3\sigma u_{yy} = 0, \tag{5.2}$$

where u relates to the wave height η and $\sigma = \pm 1$ corresponds to the sign of γ.

For large surface tension, KPI has a lump-type solution that decays in both x and y but has not yet been observed. Only recently has a large-surface-tension one-dimensional soliton been observed (Falcon et al., 2002); it satisfies the KdV equation and is a depression from the mean height.

We will only discuss KPII here because surface tension is small for ocean waves. The KPII equation has solutions with a single-phase, which we will call line-solitons. We are interested in the interactions of line-solitons. These solutions can be found by so-called direct methods (Ablowitz and Segur, 1981b): special N-soliton solutions of the KP equation can be written in the form (Satsuma, 1976)

$$u = u_N = 2\frac{\partial^2 \ln F_N}{\partial x^2}, \tag{5.3}$$

where F_N is a polynomial in terms of suitable exponentials. This solution is convenient for finding the simplest such solution: the first three are

$$\begin{gathered} F_1 = 1 + e^{\eta_1}, \qquad F_2 = 1 + e^{\eta_1} + e^{\eta_2} + e^{\eta_1+\eta_2+A_{12}}, \\ F_3 = 1 + \sum_{1\le i\le 3} e^{\eta_i} + \sum_{1\le i<j\le 3} e^{\eta_i+\eta_j+A_{ij}} + e^{\eta_1+\eta_2+\eta_3+A_{12}+A_{13}+A_{23}}, \end{gathered} \tag{5.4a}$$

where $\eta_j = k_j[x + P_j y - (k_j^2 + 3\sigma P_j^2)t] + \eta_j^{(0)}$, k_j, P_j, $\eta_j^{(0)}$ are constants, and

$$e^{A_{ij}} = \frac{(k_i - k_j)^2 - \sigma(P_i - P_j)^2}{(k_i + k_j)^2 - \sigma(P_i - P_j)^2}, \qquad i < j. \tag{5.4b}$$

For KPII (where $\sigma = 1$), u_1, F_1 correspond to the simplest one line-soliton, which is essentially one-dimensional. The more interesting case of u_2, F_2 correspond to the interaction of two line-soliton waves. These interactions have distinct patterns: when $e^{A_{12}} = O(1)$, we get an X-type interaction with a short stem (fig. 5.1); when $e^{A_{12}} \gg 1$, we get an X-type interaction with a long stem where the stem height is higher than the incoming line-solitons (figs. 5.3 and 5.4); when $e^{A_{12}} \ll 1$, we get an H-type interaction with a long stem where the stem height is less than the height of the tallest incoming line-soliton (fig. 5.5); and when $e^{A_{12}} = 0$, we get a Y-type interaction (fig. 5.2). As mentioned earlier, the length of the stem appears to be correlated to the depth of the water. Short stems where $e^{A_{12}} = O(1)$ are usually found in much deeper water than long stem X-type wave interactions where $e^{A_{12}} \gg 1$.

Recently, novel and exotic web-like structures for the KP equation (N-in-M-out) have been found using Wronskian methods (Biondini and Kodama, 2003; Chakravarty and Kodama, 2008) that go beyond the simplest 'building block' solutions of X-, H-, and Y-type line-soliton solutions. We observed significantly more X-, H-, and Y-type interactions than we observed web-like interactions. Note also that an N-in-M-out solution (where $M < N$) can be found by starting with F_N and taking k_i and P_j such that $e^{A_{M,N}} = \cdots = e^{A_{N-1,N}} = 0$; figure 5.6 shows such a 3-in-2-out interaction. It was recently shown that these line interactions persist under the next order perturbations in the equations for water waves (Ablowitz and Curtis, 2011); while the stem can be four times the height of the incoming line-solitons in the KP equation, it is less than four times the height when higher-order terms are included.

5.4 X-, H-, and Y-type structures and tsunami propagation

Miles (1977a,b) first discovered that Y-type solutions could be associated with the KP equation; he also related it to "Mach-stem reflection," the phenomenon that occurs in gas dynamics. Interestingly, Wiegel (1964) reported that the 1946 Aleutian earthquake induced tsunami caused a Mach-stem reflection along the cliffs of the western edge of Hilo Bay in Hawaii. Yeh et al. (2010) revisited Mach-stem reflection in water waves with an inclined bottom, both analytically in the context of the KP equation and in a laboratory water wave tank.

Recent observations of the 2011 Japanese Tohoku–Oki earthquake induced tsunami indicate that there was a 'merging' phenomenon from a cylindrical-wave-type interaction (Song et al., 2012) that significantly amplified the tsunami and its destructive power. This effect is remarkably similar to the initial formation of an X-type wave: while it is initially a linear super-position effect, the interaction can be significantly modified or enhanced by nonlinearity after propagating to shore. Moreover, for large distances (in the open ocean direction) an earthquake induced tsunami will propagate approximately like the KP equation. So strong nonlinear effects from X-, H-, or Y-type interactions can have serious effects for land much further away; the destruction in Sri Lanka from the 2004 Sumatra–Andaman earthquake induced tsunami is an example of such a long-distance effect.

5.5 Conclusion

We reported that X-, H-, and Y-type shallow water wave interactions on a flat beach are frequent, not rare, events. Casual observers can see these fundamental wave structures once they know what to look for. Extensive ocean observations reported here enhance and complement laboratory and analytical findings. We expect that similar interactions will be observed in many other fields — including fluid dynamics, nonlinear optics, and

plasma physics — because the leading-order equation here is also the leading-order equation for many other physical phenomena.

Chapter 6

Conclusion

This dissertation first looked at DSWs: We investigated the KdV equation's six canonical two-step cases. Then the KdV equation's large-time-asymptotic solution for general step-like initial data. Then the mKdV equation's large-time-asymptotics solution for the general step-like initial data where $\lim_{x\to-\infty} q = q_\ell > 0$ and $\lim_{x\to\infty} q = 0$. This dissertation also looked at nonlinear shallow ocean-wave soliton interactions.

In chapter 2, we investigated the KdV equation's large-time solution for the initial data

$$u(x, t = 0) = \begin{cases} h_0, & x < 0 \\ h_1, & 0 < x < L \\ h_2, & x > L \end{cases}.$$

Because of Galilean-invariance, this gave six canonical cases,

$$\begin{aligned} &\text{I } (\urcorner\!\llcorner): \ h_0 > h_1 > h_2, \qquad &&\text{II } (\urcorner\!\lrcorner): \ h_0 > h_2 > h_1, \\ &\text{III } (\llcorner\!\urcorner\!\llcorner): \ h_1 > h_0 > h_2, \qquad &&\text{IV } (\llcorner\!\lrcorner\!\urcorner): \ h_2 > h_0 > h_1, \\ &\text{V } (\lrcorner\!\urcorner\!\llcorner): \ h_1 > h_2 > h_0, \qquad &&\text{VI } (\lrcorner\!\lrcorner\!\urcorner): \ h_2 > h_1 > h_0. \end{aligned}$$

Cases I ($\urcorner\!\llcorner$), II ($\urcorner\!\lrcorner$), and III ($\llcorner\!\urcorner\!\llcorner$) go to a single-phase DSW in the large-time limit.

Case I (⌐¬_) exhibited two-phase dynamics that direct numerical simulation, using ETDRK4, and Whitham-averaging theory indicated was transitory. Case II (⌐_⌐) went to a DSW with an oscillatory tail that decayed in amplitude like $O(t^{-1/2})$, as shown by both numerical simulation and Whitham theory. Case III (¬⌐_) goes to a DSW with a finite number of solitons; the exact number, speed, and height of solitons is given by IST theory and agreed with our numerical simulations.

While cases I–III went to a single-phase DSW in the large-time limit, cases IV (¬_⌐), V (_⌐¬), and VI (_¬⌐) go to a RW in the large-time limit. Case IV (¬_⌐) goes to a RW with an oscillatory tail that decays like $O(t^{-1/2})$ based on both Whitham theory and direct numerical simulation. Case V (_⌐¬) goes to a RW and a finite number of solitons, whose number, speed, and height are exactly determined from IST theory and were confirmed with numerical simulation. Case VI (_¬⌐) goes to a RW that has neither a long oscillatory tail nor any solitons.

Direct numerical simulation, Whitham theory, and IST theory each proved to be powerful tools for investigating this problem. The ETDRK4 scheme that we used to do our numerical simulations is spectrally accurate in space and fourth-order in time; our simulations took only minutes to hours to run on a desktop computer when we conservatively took five-times the Nyquist rate of the linear-wave tail, four-times the width of our DSW region, and a time-step of 10^{-3} to 10^{-4}. After the DSW forms and we have rapid oscillations amenable to averaging, Whitham theory becomes a powerful tool for investigating the asymptotic behavior of the solution. Cases II (⌐_⌐), III (¬⌐_), IV (¬_⌐), and V (_⌐¬) could be modeled with one-phase Whitham theory, while case I (⌐¬_) needed two-phase Whitham theory; all cases compared well with direct numerical simulation away from the linear-wave tail. The amplitude of the linear-wave tail—as we showed in the chapter 3—comes from the reflection coefficient's magnitude; so Whitham theory gives *reflectionless DSWs*[1] that come from initial data where the reflection

[1] I'm naming it here based on Mark Hoefer's suggestion for the name.

coefficient $R(\lambda) = 0$ for $\lambda > c$ (see equations 3.32 and 3.33), which isn't the case for piecewise-constant initial data.

In chapter 3, we generalized the results from chapter 2 for shock-forming initial data. Shock-forming initial data has $\lim_{x\to-\infty} u > \lim_{x\to+\infty} u$; because the KdV equation is Galilean invariant, we can transform this initial data to initial data where

$$\lim_{x\to-\infty} u(x,t) = 0 \quad \text{and} \quad \lim_{x\to+\infty} = -6c^2.$$

For this boundary data, we found a large-time asymptotic approximation of the solution. This solution has three basic regions: $[u + 6c^2]$ exponentially small for $x > O(t)$ except, perhaps, for a finite number of solitons; a slowly varying cnoidal wave—the DSW—for $x \leq O(t)$; and a decaying oscillatory wave for $-x < O(t)$.

In the large-time limit, the region right of the DSW is exponentially small except, perhaps, for a finite number of solitons. If the initial data admit solitons, they will come from the discrete spectra; that is, they correspond to the transmission coefficient's simple poles. Except for any solitons, $[u + 6c^2]$ will be exponentially small right of the DSW. In this region we can asymptotically solve the GLM integral equation by summing its Neumann series. To the far right, the contribution from the reflection coefficient dominates. Near the DSW's right, the contribution from the transmission coefficient dominates. Summing the Neumann series at the DSW's right edge gives

$$u(x,t) \sim -6c^2 + 12c^2 \operatorname{sech}^2\left[\frac{c}{\varepsilon}(\zeta - \zeta_0)\right],$$

where

$$\zeta_0 = \frac{\varepsilon}{2c}\log\left\{\frac{32\sqrt{\pi}}{H_2(0)c^{1/2}\varepsilon^{3/2}}\right\}$$

and

$$\zeta = -x - 2c^2t - \frac{3\varepsilon}{4c}\log(6c^2t - x) + \cdots.$$

This provides the boundary condition on the DSW's right edge. Note how the DSW is twice the height of the step, $12c^2$ compared with $6c^2$, and how its position, ζ_0, is determined by the initial data through the scattering data.

Using this as the DSW's right boundary condition, we make the variable change $u(x,t) = -6c^2 + g(\zeta, t)$ in KdV equation. Following standard perturbation theory, we introduce the slow variables $X = \delta x$ and $T = \delta t$ ($\delta = O(t^{-1})$) and the fast variable θ such that $\theta_\zeta = \kappa(Z,T)$ and $\theta_t = -\omega(Z,T)$. The compatibility condition $\theta_{\zeta t} = \theta_{t\zeta}$ leads to $\kappa_T + \omega_Z = 0$, which is usually called the conservation of waves law. After expanding $g = g_0 + \delta g_1 + \cdots$ and grouping in like powers of δ, we eliminate secularity by requiring the periodicity of g in θ to obtain two additional conservation laws. Since the KdV equation is third-order, we now have as many conservation laws as constants of integration. We transform these conservation laws with a variable change into a diagonal system that was originally found in Whitham (1965); we then find a similarity solution to this diagonal system that matches the DSW's right boundary condition. This similarity solution is the single-phase DSW that Gurevich and Pitaevskii (1974) found. Therefore, general step-like initial data go to a single-phase DSW in the large-time limit even when multiphase dynamics exist at intermediate times.

The linear-wave tail at the DSW's left can be written as a similarity solution that decays like $O(t^{-1/2})$; this similarity solution has two slowly varying parameters, A and θ_0. While we could determine A and θ_0 by summing the Neumann series that solves the GLM integral equation formulated from $-\infty$ to x, we used a WKB-type method to find A and θ_0. We find that the similarity solution's amplitude depends on the reflection coefficient's magnitude.

While the KdV equation has only three canonical cases—a DSW, a RW, and vanishing boundary conditions—the mKdV equation has seventeen canonical cases. This is because the KdV equation is Galilean invariant and the mKdV equation is not. If we only consider cases where $\lim_{x\to-\infty} q > \lim_{x\to+\infty} q$, we are left with seven cases. Of

these seven cases, we used IST and matched-asymptotic expansions to find the mKdV equation's long-time asymptotic solution when $\lim_{x\to-\infty} q = q_\ell > 0$ and $\lim_{x\to+\infty} q = 0$.

To find the large-time asymptotic solution for the DSW cases, we first needed to develop the IST theory for the mKdV equation with the non-vanishing boundary data

$$\lim_{x\to-\infty} q(x,t) = q_\ell \quad \text{and} \quad \lim_{x\to+\infty} q(x,t) = q_r$$

with $q_\ell > q_r$. From the mKdV equation's known Lax pair, we used our boundary conditions to define eigenfunction as $x \to \pm\infty$ and then define the scattering data using these eigenfunctions. Where the KdV equation's scattering data have one branch cut, the mKdV equation's scattering data have one or two branch cuts depending on q_ℓ and q_r. To find the GLM integral equations associated with mKdV for step-like data, we need to find the scattering data's analytic properties and symmetries. Once we know the scattering data's analytic properties and symmetries, we can determine the GLM integral equations. The GLM integral equation from x to ∞ has a contributuion from the transmission coefficient when $q_\ell^2 > q_r^2$; and, like the KdV equation, these cases go to a DSW in the large-time limit. In this dissertation, we only looked for the solution's long-time asymptotic approximation when $q_\ell > 0$ and $q_r = 0$.

As with the KdV equation, we find the solution's large-time asymptotic approximation by doing the following: solving the GLM integral equation with a Neumann series right of the DSW; using matched-asymptotic expansions and multiple-scales perturbation theory in the DSW region; and then showing that the solution decays to the DSW's left. To the DSW's right, we can asymptotically approximate the GLM integral equation's kernel and the resulting Neumann series; like the KdV equation, the dominant contribution is from the reflection-coefficient term away from the shock front and from the transmission-coefficient term near the shock front. Summing the Neumann series gives the DSW's right boundary condition. Matching to

this boundary condition and using multiple-scales perturbation theory gives three conservation laws that determine the slowly varying wave parameters in the DSW region; a variable change diagonalizes these conservations laws to give Riemann invariants; assuming that the solution goes to a similarity solution and matching to the boundary condition gives the DSW's large-time asymptotic approximation. Therefore, we find that general step-like initial data go to a single-phase DSW for the mKdV equation when $q_\ell > 0$ and $q_r = 0$.

A two-dimensional generalization of the KdV equation is the KP equation. The KP equation has line-soliton solutions that can be computed exactly using Hirota's bilinear method. The interaction of two KP line-solitons produces four basic solutions; these solutions have $e^{A_{12}} = 0$, $e^{A_{12}} \ll 1$, $e^{A_{12}} = O(1)$, or $e^{A_{12}} \gg 1$ and look like a Y, an H, an X, and an X with a long stem, respectively. We observed shallow ocean-wave interactions that qualitatively agreed with these solutions at two flat beaches about 2,000 km apart. We also saw more complex line-soliton interactions that qualitatively agreed with the KP equation's exact N-soliton interactions. Before our observations, there was only one X-type interaction photograph known in the literature; thus, it was thought that nonlinear shallow ocean-wave interactions where rare. They are not: they happen every day near low tide on flat beaches. The frequency of X-, H-, and Y-type interactions is much more frequent than that of more complex interactions like 3in-2out interactions; 3in-2out interactions have three line solitons on one side of the interaction region and two on the other.

Bibliography

Ablowitz, M. J. (2011). *Nonlinear Dispersive Waves, Asymptotic Analysis and Solitons*. Cambridge University Press.

Ablowitz, M. J. and D. E. Baldwin (2012). Nonlinear shallow ocean-wave soliton interactions on flat beaches. *Physical Review E 86*(3), 036305.

Ablowitz, M. J. and D. E. Baldwin (2013a). Dispersive shock wave interactions and asymptotics. *Physical Review E 87*(2), 022906.

Ablowitz, M. J. and D. E. Baldwin (2013b). Interactions and asymptotics of dispersive shock waves — Korteweg–de Vries equation. *Physics Letters A 377*, 555–559.

Ablowitz, M. J., D. E. Baldwin, and M. A. Hoefer (2009). Soliton generation and multiple phases in dispersive shock and rarefaction wave interaction. *Physical Review E 80*(1), 016603.

Ablowitz, M. J. and D. J. Benny (1970). The evolution of multi-phase modes for nonlinear dispersion waves. *Studies in Applied Mathematics 49*, 225–238.

Ablowitz, M. J. and P. A. Clarkson (1991a). *Nonlinear Evolution Equations and Inverse Scattering*. Cambridge University Press.

Ablowitz, M. J. and P. A. Clarkson (1991b). *Solitons, Nonlinear Evolution Equations and Inverse Scattering*. Cambridge University Press.

Ablowitz, M. J. and W. C. Curtis (2011). On the evolution of perturbations to solutions of the Kadomtsev-Petviashvili equation using the Benney-Luke equation. *Journal of Physics A: Mathematical and Theoretical 44*, 195202.

Ablowitz, M. J. and A. S. Fokas (2003). *Complex Variables: Introduction and Applications* (2 ed.). Cambridge Texts in Applied Mathematics. Cambridge University Press.

Ablowitz, M. J., D. J. Kaup, A. C. Newell, and H. Segur (1974). The inverse scattering transform—Fourier analysis for nonlinear problems. *Studies in Applied Mathematics 53*(4), 249–315.

Ablowitz, M. J. and H. Segur (1977). Asymptotic solutions of the Korteweg–deVries equation. *Studies in Applied Mathematics 57*, 13–44.

Ablowitz, M. J. and H. Segur (1979). Evolution of packets of water-waves. *Journal of Fluid Mechanics 92*, 691–715.

Ablowitz, M. J. and H. Segur (1981a). *Solitons and the Inverse Scattering Transform*. SIAM.

Ablowitz, M. J. and H. Segur (1981b). *Solitons and the Inverse Scattering Transform*. SIAM Publications, Philadelphia.

Baldwin, D. E., Ü. Göktaş, W. Hereman, L. Hong, R. S. Martino, and J. Miller (2004). Symbolic computation of exact solutions expressible in hyperbolic and elliptic functions for nonlinear PDEs. *Journal of Symbolic Computation 37*, 669–705.

Biondini, G. and Y. Kodama (2003). On a family of solutions of the Kadomtsev-Petviashvili equation which also satisfy the Toda lattice hierarchy. *Journal of Physics A: Mathematical and General 36*, 10519–10536.

Biondini, G. and Y. Kodama (2006). On the Whitham equations for the defocusing nonlinear Schrödinger equation with step initial data. *Journal of Nonlinear Science 16*(5), 435–481.

Bleistein, N. and R. A. Handelsman (1986). *Asymptotic Expansions of Integrals*. Dover.

Boussinesq, J. (1877). Essai sur la théorie des eaux courantes. *Mémoires Présentés par Divers Savants à l'Académie des Sciences 1*(23), 1–680.

Buckingham, R. and S. Venakides (2007). Long-time asymptotics of the nonlinear Schrödinger equation shock problem. *Communications on Pure and Applied Analysis 60*(9), 1349–1414.

Buslaev, V. S. and V. N. Fomin (1962). An inverse scattering problem for the one-dimensional Schrödinger equation on the entire axis. *Vestnik Leningradskogo Universiteta Seriya Matematika Mekhanika Astronomiya 17*(1), 56–64.

Byrd, P. F. and M. D. Friedman (1971). *Handbook of Elliptic Integrals for Engineers and Scientists* (2 ed.). Springer–Verlag.

Chakravarty, S. and Y. Kodama (2008). Classification of the line-soliton solutions of KPII. *Journal of Physics A: Mathematical and General 41*, 275209.

Chang, J. J., P. Engels, and M. A. Hoefer (2008). Formation of dispersive shock waves by merging and splitting Bose-Einstein condensates. *Physical Review Letters 101*, 170404.

Claeys, T. and T. Grava (2010). Solitonic asymptotics for the Korteweg–de Vries equation in the small dispersion limit. *SIAM Journal on Mathematical Analysis 42*(5), 2132–54.

Cohen, A. (1984). Solutions of the Korteweg–de Vries equation with steplike initial profile. *Communications in Partial Differential Equations 9*(8), 751–806.

Cohen, A. and T. Kappeler (1985). Scattering and inverse scattering for steplike potentials in the Schrödinger equation. *Indiana University Mathematics Journal 34*(1), 127–180.

Conti, C., A. Fratalocchi, M. Peccianti, G. Ruocco, and S. Trillo (2009). Observation of a gradient catastrophe generating solitons. *Physical Review Letters 102*, 083902.

Courant, R. and K. O. Friedrichs (1948). *Supersonic Flow and Shock Waves*. New York: Interscience Publishers, Inc.

Cox, S. M. and P. C. Matthews (2002). Exponential time differencing for stiff systems. *Journal of Computational Physics 176*, 430–455.

Deift, P. and E. Trubowitz (1979). Inverse scattering on the line. *Communications on Pure and Applied Mathematics 32*, 121–251.

Deift, P., S. Venakides, and X. Zhou (1997). New results in small dispersion KdV by an extension of the steepest descent method for Riemann–Hilbert problems. *International Mathematics Research Notices 6*, 285–299.

Deift, P. and X. Zhou (1993). A steepest descent method for oscillatory Riemann–Hilbert problems. Asmptotics for the MKdV equation. *Annals of Mathematics 137*, 295–368.

Driscoll, C. and T. O'Neil (1976). Modulational instability of cnoidal wave solutions of the modified Korteweg–de Vries equation. *Journal of Mathematical Physics 17*(7), 1196–1200.

Dutton, Z., M. Budde, C. Slowe, and L. V. Hau (2001). Observation of quatum shock waves created with ultra-compressed slow light pulses in a Bose–Einstein condensate. *Science 293*, 663–68.

El, G. A. (2005). Resolution of a shock in hyperbolic systems modified by weak dispersion. *Chaos 15*(037103), 1–21.

El, G. A. and R. H. J. Grimshaw (2002). Generation of undular bores in the shelves of slowly-varying solitary waves. *Chaos 12*(4), 1015–1026.

Falcon, E., C. Laroche, and S. Fauve (2002). Observation of depression solitary surface waves on a thin fluid layer. *Physical Review Letters 89*(20), 204501.

Flaschka, H., M. G. Forest, and D. W. McLaughlin (1980). Multiphase averaging and the inverse spectral solution of the korteweg-de Vries equation. *Communications on Pure and Applied Analysis 33*, 739–784.

Gardner, C. S., J. M. Greene, M. D. Kruskal, and R. M. Miura (1967). Method for solving the Korteweg-de Vries equation. *Physical Review Letters 19*, 1095–1097.

Ghofraniha, N., C. Conti, G. Ruocco, and S. Trillo (2007). Shocks in nonlocal media. *Physical Review Letters 99*(043903), 1–4.

Grava, T. and C. Klein (2008). Numerical study of a multiscale expansion of the Korteweg–de Vries equation and Painlevé-II equation. *Proceedings of the Royal Society A: Mathematical Physical and Engineering Sciences 464*, 733–57.

Grava, T. and F.-R. Tian (2002). The generation, propagation, and extinction of multiphases in the KdV zero-dispersion limit. *Communications on Pure and Applied Analysis 55*(12), 1569–1639.

Grimshaw, R. H. J. (1979). Slowly varying soliatry waves. I. Korteweg–de Vries equation. *Proceedings of the Royal Society A: Mathematical Physical and Engineering Sciences 368*, 359–75.

Grimshaw, R. H. J. (Ed.) (2007). *Solitary Waves in Fluids*. Advances in Fluid Mechanics. WIT Press.

Gurevich, A. V. and L. P. Pitaevskii (1974). Nonstationary structure of a collisionless shock wave. *Soviet Physics JETP-USSR 38*(2), 291–297.

Hoefer, M. A. and M. J. Ablowitz (2007). Interactions of dispersive shock waves. *Physica D 236*, 44–64.

Hoefer, M. A., M. J. Ablowitz, I. Coddington, E. A. Cornell, P. Engels, and

V. Schweikhard (2006). Dispersive and classical shock waves in Bose-Einstein condesates and gas dynamics. *Physical Review A 74*(023623), 1–24.

Hruslov, E. J. (1976). Asymptotics of the solution of the Cauchy problem for the Korteweg–de Vries equation with initial data of step type. *Mathematics of the USSR-Sbornik 28*, 229–248.

Jia, S., W. Wan, and J. W. Fleischer (2007). Dispersive shock waves in nonlinear arrays. *Physical Review Letters 99*(22), 223901.

Kadomtsev, B. B. and V. I. Petviashvili (1970). On the stability of solitary waves in weakly dispersive media. *Soviet Physics Doklady 15*, 539–541.

Kamchatnov, A. M. (2000). *Nonlinear Periodic Waves and Their Modulations*. River Edge, NJ: World Scientific.

Kassam, A.-K. and L. N. Trefethen (2005). Fourth-order time-stepping for stiff PDEs. *SIAM Journal on Scientific Computing 26*(4), 1214–1233.

Kodama, Y. (1999). The Whitham equations for optical communications: Mathematical theory of NRZ. *SIAM Journal on Applied Mathematics 59*(6), 2162–2192.

Korteweg, D. and G. de Vries (1895). On the change of form of long waves advancing in a rectangular canal, and on a new type of long stationary waves. *Philosophical Magazine 39*, 422–443.

Kruskal, M. D. (1962). Asymptotology. In S. Drobot and P. A. Viebrock (Eds.), *Mathematical Models in Physical Sciences*, Englewood Cliffs, NJ, pp. 17–48. University of Notre Dame: Prentice–Hall, Inc.

Lax, P. D. (1973). *Hyperbolic Systems of Conservation Laws and the Mathematical Theory of Shock Waves*. Philadelphia: SIAM.

Levermore, C. D. (1988). The hyperbolic nature of the zero dispersion KdV limit. *Communications in Partial Differential Equations 13*(4), 495–514.

Lighthill, J. (1978). *Waves in Fluids*. Cambridge University Press.

Luke, J. C. (1966). A perturbation method for nonlinear dispersive wave problems. *Proceedings of the Royal Society A: Mathematical Physical and Engineering Sciences 292*, 403–12.

Maxworthy, T. (1980). On the formation of nonlinear internal waves from the gravitational collapse of mixed regions in two and three dimensions. *Journal of Fluid Mechanics 96*(1), 47–64.

Miles, J. (1977a). Obliquely interacting solitary waves. *Journal of Fluid Mechanics 79*, 157–169.

Miles, J. (1977b). Resonantly interacting solitary waves. *Journal of Fluid Mechanics 79*, 171–179.

Novikov, S., S. Manakov, L. Pitaevskii, and V. Zakharov (1984). *Theory of Solitons. The Inverse Scattering Method*. Plenum, NY.

Olver, F. W. J., D. W. Lozier, R. F. Boisvert, and C. W. Clark (Eds.) (2010). *NIST Handbook of Mathematical Functions*. Cambridge University Press.

Osborne, A. (2010). *Nonlinear Ocean Waves and the Inverse Scattering Transform*, Volume 97 of *International Geophysics*. Academic Press.

Russell, J. (1844). Report on waves. In *Report of the 14th Meeting of the British Association for the Advancement of Science*, pp. 311–390. John Murray, London.

Satsuma, J. (1976). N-soliton solution of the two-dimensional Korteweg–de Vries equation. *Journal of the Physical Society of Japan 40*, 286–290.

Segur, H. and M. J. Ablowitz (1981). Asymptotic solutions of nonlinear evolution equations and a Painlevé transcendent. *Physica D 3*, 165–184.

Simula, T. P., P. Engels, I. Coddington, V. Schweikhard, E. A. Cornell, and R. J. Ballagh (2005). Observations on sound propagating in rapidly rotating Bose–Einstein condensates. *Physical Review Letters 94*, 080404.

Smyth, N. F. and P. E. Holloway (1988). Hydraulic jump and undular bore formation on a shelf break. *Journal of Physical Oceanography 18*(7), 947–962.

Song, Y. T., I. Fukumori, C. K. Shum, and Y. Yi (2012). Merging tsunamis of the 2011 Tohoku-Oki earthquake detected over the open ocean. *Geophysical Research Letters 39*, L05606.

Taylor, R. J., D. R. Baker, and H. Ikezi (1970). Observation of collisionless electrostatic shocks. *Physical Review Letters 24*(5), 206–209.

Wan, W., S. Jia, and J. W. Fleischer (2007). Dispersive superfluid-like shock waves in nonlinear optics. *Nature Physics 3*(1), 46–51.

Weidman, P. D., H. Linde, and M. G. Velarde (1992). Evidence for solitary wave behavior in Marangoni–Bénard convection. *Physics of Fluids A: Fluid Dynamics 4*(5), 921–26.

Whitham, G. B. (1965). Non-linear dispersive waves. *Proceedings of the Royal Society A: Mathematical Physical and Engineering Sciences 283*, 238–261.

Whitham, G. B. (1974). *Linear and Nonlinear Waves*. New York: John Wiley & Sons.

Wiegel, R. L. (1964). *Oceanographical Engineering*. Englewood, N.J.: Prentice-Hal.

Yeh, H., W. Li, and Y. Kodama (2010). Mach reflection and KP solitons in shallow water. *European Physical Journal Special Edition 185*, 97–111.

Zabusky, N. J. and M. D. Kruskal (1965). Interactions of solitons in a collisionless plasma and the recurrence of initial states. *Physical Review Letters 15*, 240–243.

Appendix A

Analyticity of KdV equation's eigenfunctions

The results in this appendix are not new, but are included for completeness.

To show the analyticity of the eigenfunctions, we will use integral equation for the eigenfunctions. It's convenient to define

$$M(x;\lambda) \equiv \phi(x;\lambda)e^{i\lambda x/\varepsilon} \qquad \bar{M}(x;\lambda) \equiv \bar{\phi}(x;\lambda)e^{i\lambda x/\varepsilon}, \tag{A.1a}$$

$$N(x;\lambda_r) \equiv \psi(x;\lambda_r)e^{i\lambda_r x/\varepsilon} \qquad \bar{N}(x;\lambda_r) \equiv \bar{\psi}(x;\lambda_r)e^{i\lambda_r x/\varepsilon}, \tag{A.1b}$$

so that

$$\begin{aligned} M(x;\lambda) &\sim 1, \qquad \bar{M}(x;\lambda) \sim e^{2i\lambda x/\varepsilon}, \qquad \text{as } x \to -\infty, \\ N(x;\lambda_r) &\sim e^{2i\lambda_r x/\varepsilon}, \qquad \bar{N}(x;\lambda_r) \sim 1, \qquad \text{as } x \to +\infty \end{aligned}$$

and

$$T(\lambda,\lambda_r)M(x;\lambda) \equiv \bar{N}(x;\lambda_r)e^{i(\lambda-\lambda_r)x/\varepsilon} + R(\lambda,\lambda_r)\bar{N}(x;-\lambda)e^{i(\lambda+\lambda_r)x/\varepsilon}. \tag{A.2}$$

We can use Green's functions to get Volterra integral equations for M and $\bar{N}$. To do this

we'll make the change of variables in (3.6a),

$$v(x;\lambda) = m(x;\lambda)e^{-i\lambda x/\varepsilon} \quad \text{and} \quad v(x;\lambda(\lambda_r)) = n(x;\lambda_r)e^{-i\lambda_r x/\varepsilon},$$

to get

$$\begin{aligned} m_{xx}(x;\lambda) - (2i\lambda/\varepsilon)m_x(x;\lambda) &= -u_0(x)m(x;\lambda)/(6\varepsilon^2), \\ n_{xx}(x;\lambda_r) - (2i\lambda_r/\varepsilon)n_x(x;\lambda_r) &= -[6c^2 + u_0(x)]n(x;\lambda_r)/(6\varepsilon^2). \end{aligned}$$

To solve, we consider the Green's functions defined by

$$G_{xx} - (2i\lambda/\varepsilon)G_x = -\delta(x) \quad \text{and} \quad H_{xx} - (2i\lambda_r/\varepsilon)H_x = -\delta(x);$$

using Fourier analysis then gives taking their Fourier transform gives

$$(-p^2 + 2\lambda p/\varepsilon)\hat{G} = -1, \qquad (-p^2 + 2\lambda_r p/\varepsilon)\hat{H} = -1,$$

and then taking the inverse Fourier tranform gives

$$G(x;\lambda) = \frac{1}{2\pi}\int_C \frac{e^{ipx}\,\mathrm{d}p}{p(p-2\lambda/\varepsilon)} \quad \text{and} \quad H(x;\lambda_r) = \frac{1}{2\pi}\int_C \frac{e^{ipx}\,\mathrm{d}p}{p(p-2\lambda_r/\varepsilon)},$$

where C is an appropriate contour. Note that $G(x;\lambda)$ has poles at $p = 0$ and $p = 2\lambda/\varepsilon$ and $H(x;\lambda_r)$ has poles at $p = 0$ and $p = 2\lambda_r/\varepsilon$. We close C in the lower-half p-plane for G (since we're interested in $x \to -\infty$ for M and $\bar{M}$) and in the upper-half p-plane for H (since we're interested in $x \to \infty$ for N and $\bar{N}$); thus,

$$G(x;\lambda) = \frac{\varepsilon}{2i\lambda}\left(1 - e^{2i\lambda x/\varepsilon}\right)H(x) \quad \text{and} \quad H(x;\lambda_r) = \frac{-\varepsilon}{2i\lambda_r}\left(1 - e^{2i\lambda_r x/\varepsilon}\right)H(-x),$$

where $H(x)$ is the Heaviside function. Therefore,

$$\begin{aligned} M(x;\lambda) &= 1 + \frac{1}{6\varepsilon^2}\int_{-\infty}^{\infty} G(x-\xi;\lambda)u_0(\xi)M(\xi;\lambda)\,\mathrm{d}\xi, \\ &= 1 + \frac{1}{12i\lambda\varepsilon}\int_{-\infty}^{x}\left(1 - e^{2i\lambda(x-\xi)/\varepsilon}\right)u_0(\xi)M(\xi;\lambda)\,\mathrm{d}\xi, \qquad \text{(A.3)} \\ \bar{N}(x;\lambda_r) &= 1 + \frac{1}{6\varepsilon^2}\int_{-\infty}^{\infty} H(x-\xi;\lambda_r)[u_0(x)+6c^2]\bar{N}(\xi;\lambda_r)\,\mathrm{d}\xi, \\ &= 1 - \frac{1}{12i\lambda_r\varepsilon}\int_{x}^{\infty}\left(1 - e^{2i\lambda_r(x-\xi)/\varepsilon}\right)[u_0(\xi)+6c^2]\bar{N}(\xi;\lambda_r)\,\mathrm{d}\xi. \qquad \text{(A.4)} \end{aligned}$$

These are Volterra integral equations. Note that $G(x-\xi;\lambda)$ is analytic in the upper half λ plane and $H(x-\xi;\lambda_r)$ is analytic in the lower half λ_r plane. As we'll show below, their iterates converge when

$$\int_{-\infty}^{\infty}\left|u(x) + 6c^2H(x)\right|(1+|x|^n)\,\mathrm{d}x < \infty, \qquad \text{(A.5)}$$

for $n \geq 1$. Hence $M(x;\lambda)$ is analytic in the upper half λ plane and $\bar{N}(x;\lambda_r)$ is analytic in the lower half λ_r plane; M is also continuous at $\lambda = 0$ and $\bar{N}$ is continuous at $\lambda_r = 0$ when $n \geq 2$.

The Volterra integral equations, (A.3) and (A.4), can be solved using the iterates:

$$M(x;\lambda) = 1 + \sum_{n=1}^{\infty} g_n(x;\lambda) \quad \text{and} \quad \bar{N}(x;\lambda_r) = 1 + \sum_{n=1}^{\infty} h_n(x;\lambda_r), \qquad \text{(A.6)}$$

where

$$g_n(x;\lambda) \equiv \int_{-\infty}^{\xi_n \leq \cdots \leq \xi_1 \leq x} G_\lambda(x-\xi_1)\cdots G_\lambda(\xi_{n-1}-\xi_n)u_0(\xi_1)\cdots u_0(\xi_n)\,\mathrm{d}\xi_n\cdots\mathrm{d}\xi_1,$$

$$\begin{aligned} h_n(x;\lambda) \equiv \int_{x\leq\xi_1\leq\cdots\leq\xi_n}^{\infty} & H_{\lambda_r}(\xi_1-x)\cdots H_{\lambda_r}(\xi_n-\xi_{n-1}) \\ & \times [u_0(\xi_1)+6c^2]\cdots[u_0(\xi_n)+6c^2]\,\mathrm{d}\xi_n\cdots\mathrm{d}\xi_1, \end{aligned}$$

$$G_\lambda(\xi) \equiv \frac{1 - e^{2i\lambda\xi/\varepsilon}}{12i\lambda\varepsilon} \quad \text{and} \quad H_{\lambda_r}(\xi) \equiv \frac{e^{-2i\lambda_r\xi/\varepsilon} - 1}{12i\lambda_r\varepsilon}, \qquad \xi \geq 0.$$

Adapting the proofs of Lemma 1 in (Deift and Trubowitz, 1979) and the first theorem in (Ablowitz et al., 1974) to our initial conditions gives that $M(x;\lambda)$ and $\bar{N}(x;\lambda_r)$ are analytic and continuous. For $\mathrm{Im}(\lambda) \geq 0$, we have that $|G_\lambda(\xi)| \leq 1/|6\lambda\varepsilon|$ since $\xi \geq 0$ and $|1 - e^{2i\lambda\xi/\varepsilon}| \leq 2$; thus

$$|g_n(x;\lambda)| \leq \frac{1}{|6\lambda\varepsilon|^n} \frac{\left(\int_{-\infty}^{x} |u_0(\xi)|\,\mathrm{d}\xi\right)^n}{n!}$$

and so

$$|M(x;\lambda)| \leq \exp\left\{\frac{1}{|6\lambda\varepsilon|}\int_{-\infty}^{x} |u_0(\xi)|\,\mathrm{d}\xi\right\} < \infty$$

for finite x. This estimate blows up for small λ, so for small λ we'll use that $|G_\lambda(\xi)| \leq \xi/(6\varepsilon^2)$ and so

$$\begin{aligned}
|g_n(x;\lambda)| &\leq \frac{1}{(6\varepsilon^2)^n} \int_{-\infty}^{\xi_n \leq \cdots \leq \xi_1 \leq x} (x - \xi_1)\cdots(\xi_{n-1} - \xi_n) \\
&\quad \times |u_0(\xi_1)| \cdots |u_0(\xi_n)|\,\mathrm{d}\xi_n \cdots d\xi_1, \\
&\leq \frac{1}{(6\varepsilon^2)^n} \int_{-\infty}^{\xi_n \leq \cdots \leq \xi_1 \leq x} (x - \xi_1)\cdots(x - \xi_n) \\
&\quad \times |u_0(\xi_1)| \cdots |u_0(\xi_n)|\,\mathrm{d}\xi_n \cdots d\xi_1, \\
&= \frac{1}{(6\varepsilon^2)^n} \frac{\left(\int_{-\infty}^{x} (x - \xi)|u_0(\xi)|\,\mathrm{d}\xi\right)^n}{n!},
\end{aligned}$$

which implies that

$$|M(x;\lambda)| \leq \exp\left\{\frac{1}{6\varepsilon^2}\int_{-\infty}^{x} (x - \xi)|u_0(\xi)|\,\mathrm{d}\xi\right\} < \infty$$

for finite x from (A.5). Thus, for $N = 1$ in (A.5), $M(x;\lambda)$ is analytic for $\mathrm{Im}(\lambda) > 0$ and is continuous for $\mathrm{Im}(\lambda) \geq 0$ when $\lambda \neq 0$; if $N = 2$ then $M(x;\lambda)$ is also continuous at $\lambda = 0$.

We can differentiate $M(x;\lambda)$ in (A.6) with respect to λ and this brings down a $(x-\xi)$ term; indeed, it can be shown that

$$\left|\frac{\partial^j}{\partial\lambda^j}G_\lambda(\xi)\right| \le \frac{2^j\xi^j}{6|\lambda|\varepsilon^{1+j}} \quad \text{and} \quad \left|\frac{\partial^j}{\partial\lambda^j}G_\lambda(\xi)\right| \le \frac{2^j\xi^{j+1}}{6(1+j)\varepsilon^{2+j}},$$

so

$$\left|\frac{\partial^j}{\partial\lambda^j}g_n(x;\lambda)\right| \le \frac{2^{nj}}{6^n|\lambda|^n\varepsilon^{n(1+j)}}\frac{\left(\int_{-\infty}^x (x-\xi)^j|u_0(\xi)|\,\mathrm{d}\xi\right)^n}{n!}$$

and

$$\left|\frac{\partial^j}{\partial\lambda^j}g_n(x;\lambda)\right| \le \frac{2^{nj}}{6^n(1+j)^n\varepsilon^{n(2+j)}}\frac{\left(\int_{-\infty}^x (x-\xi)^{j+1}|u_0(\xi)|\,\mathrm{d}\xi\right)^n}{n!}.$$

Therefore, $M(x;\lambda)$ is N-fold differentiable (with respect to λ) for $\mathrm{Im}(\lambda)\ge 0$ and $\lambda\neq 0$ (and finite x) and is $(N-1)$-fold differentiable at $\lambda=0$, where N is given in (A.5).

Likewise, it can be shown that: For $N=1$ in (A.5), $\bar{N}(x;\lambda_r)$ is analytic for $\mathrm{Im}(\lambda_r)<0$ and is continuous for $\mathrm{Im}(\lambda_r)\le 0$ when $\lambda_r\neq 0$. If $N=2$ then $\bar{N}(x;\lambda_r)$ is also continuous at $\lambda_r=0$. Moreover, $\bar{N}(x;\lambda_r)$ is N-fold differentiable (with respect to λ_r) for $\mathrm{Im}(\lambda_r)\le 0$ and $\lambda_r\neq 0$ (and finite x) and is $(N-1)$-fold differentiable at $\lambda_r=0$.

Moreover, following the identical techniques, if $u(x,t)$ satisfies

$$\int_{-\infty}^{\infty}|u(x,t)+6c^2H(x)|e^{d|x|}\,\mathrm{d}x<\infty, \qquad 0<d\in\mathbb{R},$$

then it can be shown that $M(x;\lambda)$ is analytic in $\mathrm{Im}(\lambda)>-d$ and $\bar{N}(x;\lambda_r)$ is analytic in $\mathrm{Im}(\lambda_r)<d$.